CHARACTERIZATION OF OXIDATION PRODUCT FILMS ON LEAD IN AQUEOUS MEDIA BY IN SITU RAMAN SPECTROSCOPY

TECHNICAL REPORT NUMBER 6

CONTRACT NUMBER: N00014-76-c-0889

SUBMITTED TO:

DEPARTMENT OF THE NAVY

OFFICE OF NAVAL RESEARCH

METALLURGY PROGRAM-CODE 471

PREPARED BY:

R. THIBEAU, C. BROWN AND R. HEIDERSBACH

DEPARTMENT OF OCEAN ENGINEERING

UNIVERSITY OF RHODE ISLAND

KINGSTON, RHODE ISLAND 02881

FEBRUARY 1979

CHARACTERIZATION OF OXIDATION PRODUCT FILMS ON LEAD IN AQUEOUS MEDIA BY IN SITU RAMAN SPECTROSCOPY

TECHNICAL REPORT NUMBER 6

CONTRACT NUMBER: N00014-76-c-0889

SUBMITTED TO:

DEPARTMENT OF THE NAVY

OFFICE OF NAVAL RESEARCH

METALLURGY PROGRAM-CODE 471

PREPARED BY:

R. THIBEAU, C. BROWN AND R. HEIDERSBACH

DEPARTMENT OF OCEAN ENGINEERING

UNIVERSITY OF RHODE ISLAND

KINGSTON, RHODE ISLAND 02881

FEBRUARY 1979

SECURITY CLASSIFICATION OF THIS PAGE (When Data Entered)

REPORT DOCUMENTATION PAGE

READ INSTRUCTIONS BEFORE COMPLETING FORM

1. REPORT NUMBER: Technical Report Number 6
2. GOVT ACCESSION NO.
3. RECIPIENT'S CATALOG NUMBER

4. TITLE (and Subtitle): Characterization of Oxidation Product Films on Lead in Aqueous Media by In Situ Raman Spectroscopy
5. TYPE OF REPORT & PERIOD COVERED: Technical Report, 1979
6. PERFORMING ORG. REPORT NUMBER

7. AUTHOR(s): R. Thibeau, C. Brown, R. Heidersbach
8. CONTRACT OR GRANT NUMBER(s): N00014-76-C-0889

9. PERFORMING ORGANIZATION NAME AND ADDRESS
Department of Ocean Engineering
University of Rhode Island
Kingston, Rhode Island 02881

10. PROGRAM ELEMENT, PROJECT, TASK AREA & WORK UNIT NUMBERS

11. CONTROLLING OFFICE NAME AND ADDRESS
Office of Naval Research
Department of the Navy
Arlington, Virginia 22217

12. REPORT DATE: February 1979
13. NUMBER OF PAGES: 153

14. MONITORING AGENCY NAME & ADDRESS (if different from Controlling Office)
173p.; TR-6

15. SECURITY CLASS. (of this report): Unclassified
15a. DECLASSIFICATION/DOWNGRADING SCHEDULE

16. DISTRIBUTION STATEMENT (of this Report)

This document has been approved for public release and sale; its distribution is unlimited.

17. DISTRIBUTION STATEMENT (of the abstract entered in Block 20, if different from Report)

18. SUPPLEMENTARY NOTES

19. KEY WORDS (Continue on reverse side if necessary and identify by block number)

Lead; lead oxide; Raman spectra; corrosion; corrosion products: oxidation; passivation; passive films; surface films

20. ABSTRACT (Continue on reverse side if necessary and identify by block number)

This report contains the manuscript of a dissertation by R. Thibeau, Ph.D. candidate in Chemistry at the University of Rhode Island.

Raman spectroscopy was used to determine the composition of surface films formed on lead by exposure to aqueous solutions of several different compositions. Spectra were recorded while the flat lead samples were completely immersed in solution, while the oxidative reactions were occurring, thus avoiding any changes which might be caused by removal from the aqueous environment.

cont.

DD FORM 1 JAN 73 1473 EDITION OF 1 NOV 65 IS OBSOLETE

S/N 0102-014-6601

LB

SECURITY CLASSIFICATION OF THIS PAGE (When Data Entered)

407 892

20. ABSTRACT (cont.)

Controlled potential exposures of lead in phosphate, carbonate, chloride, and sulfate solutions were conducted under various conditions of potential and pH. The results of spectroscopic identification of the compounds present in insoluble surface films were compared to theoretical Pourbaix diagrams for lead in simple solutions of the appropriate ions and to potentiodynamic polarization curves for the solutions used. Experimental results showed only partial agreement with theoretical predictions. The major reason for the lack of agreement seems to be the failure of calculations to include all of the species present in the solutions used.

Raman spectra of thin oxide films formed on Armco iron by high temperature oxidation were also obtained. For both iron and lead surface films, a minimum thickness of approximately 200 angstroms was found necessary to permit observation of a useable spectrum.

TABLE OF CONTENTS

LIST OF TABLES

LIST OF FIGURES

I. INTRODUCTION

In the first half of the nineteenth century, Faraday first used the term "passive metal" to describe a metal which was unreactive under conditions where, thermodynamically, it should oxidize (1). Observing that pure iron reacts 100,000 times more slowly with concentrated nitric acid than it does with dilute nitric acid, he proposed that some sort of invisible film protected, or passivated, the iron in the concentrated solution. The nature and composition of such a film were not known. Today, after over 130 years of study, we know a great deal about the conditions which will cause or prevent corrosion; however, we are still unsure about the nature and composition of thin passive films on metal surfaces exposed to water (2).

Whether exposed to water or air, all but the noble metals are almost invariably used under conditions where their oxides are thermodynamically stable relative to the metal and oxygen. It is the presence of thin surface films which slow or nearly stop the oxidation reactions and allow metal objects to exist without rapidly oxidizing to a useless state. A good definition for passivity is, therefore, "the loss of chemical reactivity under certain environmental conditions" (3).

Two major theories have been proposed to explain the protection of the underlying metal: the adsorption theory, which states that passivity is achieved by the formation of

a thin layer of adsorbed oxygen (4,5); and the oxide-film theory, which states that a monolayer or thicker film of insoluble oxide provides protection (5,6). Regardless of which theory is closer to the truth, there are three aspects of aqueous passive films generally agreed upon:

1) A film can be extremely thin, maybe less than a monolayer (7,8), and still provide protection.

2) Films contain considerable amounts of water (3,9).

3) Films are extremely delicate and are subject to change when removed from the metal or from the corrosive environment (3).

Although there are several experimental techniques which are useful in determining the rate of corrosion of a metal sample, determining the composition of the oxidation products is a difficult problem. A non-destructive analytical method is needed to identify the compounds present in an extremely thin crystalline or amorphous film on a metal surface while it is immersed in an aqueous solution. Unfortunately, at present, no one technique meets all of these requirements. There are several surface analytical methods such as Auger electron spectroscopy (AES), secondary ion mass spectrometry (SIMS), low energy electron diffraction (LEED), and electron spectroscopy for chemical analysis (ESCA) (10) which can examine films of monolayer thickness. These extremely sensitive methods require ultra high vacuum, which introduces the possibility of altering a surface film by removal of water. At the same

time, those techniques such as ellipsometry (11) and the many electrochemical methods, which can be used in situ, while a metal surface is in the reactive solution, cannot give information to conclusively identify the compounds present.

The use of vibrational Raman spectroscopy to characterize surface films on metal in aqueous media offers a unique compromise. Although not as sensitive to extremely thin films as the high vacuum techniques, it gives more information than the other methods, and it can be used in situ. Unlike the other in situ techniques mentioned above, it can identify insoluble corrosion products. The reasons for using Raman spectroscopy in the study of corrosion may be summarized as follows:

1) Because water is a weak Raman scatterer, spectra can be obtained from samples immersed in aqueous solutions (12). Aqueous surface films may be analyzed while avoiding any changes due to the drying required by most techniques.

2) Vibrational Raman spectroscopy can permit unambiguous identification of compounds present. It can differentiate between compounds and between polymorphs of the same compound (13,14).

3) Both crystalline and amorphous films will give Raman spectra. Passive films have been described as crystalline, amorphous (15), or a combination of crystalline and amorphous phases (16,17).

4) Spectra can be obtained from films as thin as 50 angstroms on metal substrates (18,19).

5) Since only vibrations due to chemical bonds are observed, there is no interference by the underlying metal.

6) Using visible light, Raman spectroscopy is non-destructive to most substances.

In recent years, Raman spectroscopy has been used for the study of surface species, both at solid-gas (20,21) and solid-liquid interfaces (22-29), because of the unique properties listed above. The applicability of this technique to the study of aqueous corrosion has been demonstrated by identifying oxide and chloride surface layers on lead (12).

A brief review of the theory and use of vibrational Raman spectroscopy for surface analysis is presented in Appendix I. More detailed discussions of surface film spectroscopy may be found in the papers by Greenler (18,19). Several books explain the theory and applications of Raman spectroscopy at length (30-34).

I.A. Pourbaix Diagrams

In the study of aqueous corrosion, the potential-pH, Pourbaix, diagram (35) is of considerable value. By calculating the relative stabilities of possible metal and solution species, the lowest energy species for any given

conditions of potential and solution pH can be specified and displayed on a two-dimensional diagram, as shown in Figure 1. The diagram identifies thermodynamically stable compounds for any set of conditions.

Pourbaix diagrams have found wide application in corrosion research (36-38) because they predict whether immunity, passivation, or corrosion of a metal will occur under specific conditions, assuming that this behavior depends on the nature of a surface film. In the lead-water Pourbaix diagram of Figure 1, lead is predicted to be immune to oxidation at low potentials (Pb is thermodynamically stable), corroding at potentials in the Pb^{++}, PbO, and Pb_3O_4 regions (because these forms have appreciable solubility), and passive in the PbO_2 region (because it is essentially insoluble).

The important, but unanswered, question is how accurate are calculations based on free energy relationships in describing the actual behavior of a metal in a solution. Experimental investigations of some Pourbaix diagrams conducted using electrochemical polarization techniques have shown some agreement and some disagreement with the theoretical predictions (36,37,39-42). Electrochemical techniques cannot determine the composition of a surface film as required to thoroughly investigate the relationship between the diagram and actual passive films. Raman spectroscopy is uniquely suited to identify the species present in an insoluble film in situ, under conditions where

passivity is predicted by thermodynamics.

I.B. Lead

There are several reasons for choosing lead for an electrochemical and Raman investigation of the Pourbaix diagram:

1) Lead electrodes have been studied extensively (43-46) because of their use in storage batteries so their electrochemical reactions are generally understood.

2) Throughout history, lead has been used for construction and decorative coverings because of its resistance to corrosion. Today this property gives lead considerable use in the chemical industry (3,47). While it is well known that the corrosion resistance is due to thin surface films, these have only been examined in detail in sulfuric acid solutions (48-60) and, to a lesser extent, in hydrochloric acid (61-64).

3) The oxidation products of lead are generally good Raman scattering species because of the presence of lead atoms, the large number of electrons tending to give large polarizability.

4) Oxidation of lead in aqueous media can make thick protective or non-protective surface films (35). Films of varying thicknesses are necessary because the thickness required to give a useful Raman spectrum is

not well defined.

5) Lead exhibits several oxidation states, and its oxides can exist as different polymorphs (35,65): thus, it is typical of the commonly used metals.

Previous research on the aqueous corrosion products of lead has involved calculation of the lead-water Pourbaix diagram (35), the lead-water-chloride diagram (66), and the lead-water-sulfate diagram (67,68). The theoretical predictions for the sulfate system have been investigated experimentally using electrochemical methods (56) and X-ray diffraction (49,69). The experimental findings showed that exposure in sulfuric acid solutions formed a multilayer surface film consisting of oxides and sulfates. The corrosion product layers consist of several different compounds, a condition that could not be predicted by the Pourbaix diagram. A recent brief analysis of the chloride diagram using Raman spectroscopy (12) found that the compound $3PbO \cdot PbCl_2$, which was considered in calculating the diagram, probably exists as $3Pb(OH)_2 \cdot PbCl_2$, which was not considered. The ability of Pourbaix diagrams to describe the behavior of lead in aqueous media has, therefore, not been proven because of shortcomings in calculation of the diagrams.

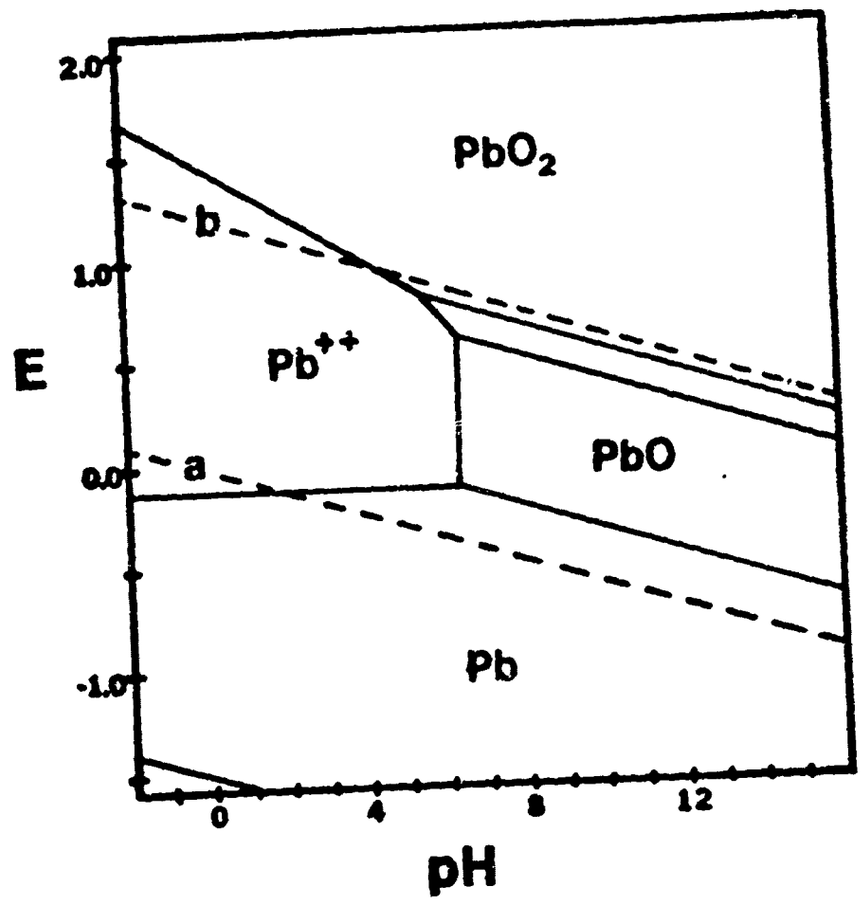

Figure 1. Pourbaix diagram of the lead-water system, M. Pourbaix, Atlas of Electrochemical Equilibria in Aqueous Solutions, NACE, Houston (1974).

II. EXPERIMENTAL

II.A. Raman Spectrometer

Raman spectra were recorded with a Spex Industries Model 1401 double monochromator using a photon counting system. A simplified optical schematic of this type of spectrometer is shown in Figure 2. A Coherent Radiation Laboratories Model CR-3 argon ion laser is located beneath the monochromator, and the laser beam is directed by a mirror to the bottom of the sample container. Both the 488.0 and 514.5 nm. wavelength lines were used. With either line, the power at the sample was approximately 500 mW. Some of the light scattered by the sample is collected by the lens (L), positioned 90 degrees from the vertical laser beam, and is focused onto the entrance slits of the monochromator. Light entering the slits is collimated by a mirror and dispersed by the first grating. The light, now dispersed according to frequency, is directed by a second collimating mirror and a plane mirror to the intermediate slits. The narrow frequency band of light which has passed through the first monochromator then enters a second, identical monochromator where it is dispersed again to maximize rejection of stray light and narrow the frequency band. The light which leaves the exit slits is incident on the photocathode of a photomultiplier tube, the detector. Each photon reaching the photomultiplier is converted to an electrical pulse which is amplified and counted by an Elscint, Inc. counting system. The number of counts (number of photons) detected

per selected time interval is converted to an analog signal which drives the pen on a strip chart recorder. A frequency range is scanned by turning the two gratings in the monochromator simultaneously so that the frequency of light reaching the photomultiplier is changed. The Raman spectrum recorded is thus a plot of light intensity vs. frequency, where the frequency of interest is actually the difference from the excitation frequency.

For all Raman spectra, the metal sample was held at an angle of twenty degrees from vertical to optimize observation of Raman scattered light. As explained in detail by Greenler and Slager (18), the angle between the sample surface and the incident beam controls how strongly the electric vector of the incident light may interact with molecules in a surface film. The angle also affects the amount of stray light entering the monochromator. The sample must be positioned so that the specularly reflected exciting radiation is not collected by the focusing lens; only scattered light should reach the entrance slits (70). For example, an incident angle of 45 degrees would direct the full intensity of the laser beam into the monochromator, making observation of the weak Raman lines nearly impossible. In consideration of both of these effects, the 20 degree alignment shown in Figure 4 gives the strongest Raman spectrum. The same angle was also found to give the best spectra of pellets, so all pellet spectra were obtained with the surface of the pellet at a 20 degree angle from the

vertical laser beam.

Before using Raman spectra to identify compounds present in surface films, spectra of pure compounds were required for reference. Orthorhombic PbO, $PbCl_2$, and $PbBr_2$ were purchased from Alfa Products, Inc.; basic lead carbonate, $(PbCO_3)_2 \cdot Pb(OH)_2$, from Mallinckrodt Chemical Works, Inc.; Pb_3O_4 and PbO_2, from Allied Chemical, Inc.; and $PbSO_4$, from J. T. Baker Chemical Company, Inc. Reagent grade samples of these compounds were placed in 1.5 mm. diameter glass capillary tubes and their spectra recorded. Some lead species decomposed in the laser beam or gave weak spectra so these were pressed into pellets of the lead compound alone or of the compound mixed with potassium bromide. In all cases, pellets yielded stronger spectra than the powders.

II.B. Preparation Of Lead Samples

The lead used in aqueous exposures was supplied by Alfa Products, Inc., Danvers, Mass., as 1 mm. thick foil of two types: 99.9995% and greater than 99% purity. Both types were used interchangebly and seemed to give identical results. In order to clean the lead of its surface oxide layer prior to an aqueous exposure, one of three different methods was used:

1) immersion in dilute nitric acid solution for five minutes to dissolve the surface, giving soluble lead nitrate,

2) polishing with emery paper followed by immersion in warm, concentrated ammonium acetate solution for five minutes, or

3) immersion in warm, concentrated ammonium acetate solution for five minutes.

Polishing with abrasive silicon carbide paper was discontinued because electron micrographs such as that shown in Figure 3 revealed that SiC particles from the polishing remained embedded in the sample surface. Since the particles tend to disrupt the surface, the polishing was stopped and immersion in concentrated ammonium acetate solution alone was used for most exposures. All three sample preparation methods gave very similar lead surfaces; all gave the same shiny silver appearance and no differences in exposures or in resulting spectra were observed. After cleaning by one of these methods, the lead sample was washed with distilled water, dried and polished lightly with KIMWIPES, and immediately placed in the selected solution.

II.C. Simple Immersion Exposures

Some lead exposures were conducted by simply immersing lead samples, which had been cleaned by the methods detailed above, in reactive solutions and allowing them to react at whatever equilibrium potential they assume. No electrical connections were made and no attempt was made to control the potential. A lead strip, 5 X 1 cm., was clamped to the side

of a Pyrex beaker of solution as shown in Figure 4. The solutions and conditions used for this type of exposure are detailed in Table I. All solutions were made from reagent grade components and distilled water.

Simple immersion exposures were conducted with either air saturated or deaerated solutions. For air saturated conditions, laboratory air was pumped into the solution through a fritted glass cylinder for thirty minutes before and throughout the period of exposure. To achieve deaerated conditions, dry nitrogen was bubbled through the solution for thirty minutes before and during exposures. Samples remained in solution for periods of one or more days before being analyzed in the Raman spectrometer.

II.D. Conditions For Electrochemical Exposures

The conditions for potentiostatic electrochemical exposures were chosen using two sources, calculated Pourbaix diagrams (71), and potentiodynamic polarization curves. The two sources were used together to provide both a theoretical, thermodynamic basis and an experimental basis for choosing exposure conditions.

Solutions were selected to give pH's in as many different regions of the Pourbaix diagrams as possible. The compositions of the solutions used for controlled potential exposures are listed in Table II. Care was also taken to insure that potentials were chosen so that samples were

exposed in every region of the diagram calculated to be present at that pH.

Potentiodynamic polarization curves were recorded for each solution used to see if the behavior of lead in a solution corresponds to the Pourbaix diagram and to select exposure potentials where this experimental technique indicates the formation of different species. The current vs. potential curves were run between -0.76 V versus the standard hydrogen electrode, SHE, and +1.24 V.

A block diagram of the apparatus for measuring polarization curves is shown in Figure 5. An Elscint Model RBA-2b automatic baseline advance device drove the WL-1 potentiostat at a scan rate of 40mV/min. The outputs of the potentiostat, the potential and resulting current, were plotted on an MFE 815 Plotmatic X-Y recorder. Polarization curves were recorded with a reduction cycle first so the sample would have a clean, reduced surface when the oxidation cycle, of greater interest, was begun. In this way, no surface species which might alter the initial oxidation processes were thought to be present.

II.E. Potentiostatic Exposures

Lead samples were exposed to aqueous solutions for periods varying from 6 minutes to 24 hours at controlled potentials. At or near the end of the exposure period a Raman spectrum of the metal surface was recorded. This was

done in a manner very similar to that used for simple immersion exposures, without removing the sample from the solution or disconnecting it from the potentiostat.

The electrochemical cell shown in Figure 6 was used, in the sample compartment of the spectrometer, to permit the recording of Raman spectra while the sample was undergoing oxidation in an aqueous solution. The cell is typical of electrochemical cells in most respects (72); the auxiliary electrode is platinum mesh and the potential is maintained (by a potentiostat) relative to a saturated calomel electrode which is connected to the solution by a glass Luggin capillary positioned 1-2 mm. from the working electrode surface. The unusual aspect of this cell is the shape and position of the working electrode. It consists of a flat lead sample held close to the bottom and one side of the cylindrical glass cell at an angle of 20 degrees from vertical so that it is in an excellent position for observation of Raman spectra.

Two different types of sample holder were used during this research. The first and simplest, shown in Figure 7, consists of a hollow glass tube into the end of which was sealed a 1 X 5 cm. lead strip attached to a copper wire. The back and edges of the strip and the opening of the glass tube were coated with beeswax to allow only a measured area of the sample to come in contact with the solution. The connection between the copper wire and the lead was made inside the tube so no copper reached the solution. Sample

strips for this type of holder were bent to give the proper 20 degree angle with the laser beam.

The alternate type of sample holder used was a larger device made of Teflon which holds a 2.8 X 5.7 cm. flat, rectangular sample. This size was chosen because, after in situ examination by Raman spectroscopy, the sample can be removed from the holder, dried, and it will fit the sample holder of a Wilks Scientific Corporation Model 9 multiple specular reflection attachment for infrared reflection-absorption analysis (71). The sample holder, shown in Figure 8, allows only one face of the sample to come in contact with the solution and holds it at the proper angle for Raman examination.

Two potentiostats were used, a Wenking Model LT73 and the WL-1, a device constructed in our laboratory. Both are very similar, consisting mainly of a voltage feedback circuit utilizing negative feedback. Both can supply potentials ranging from +2.0 V to -2.0 V relative to the reference electrode. The LT73 can supply a maximum of 1.0 amperes and the WL-1, 1.5 amperes. Currents of this magnitude were observed, under some conditions, due to the large samples used. Taking advantage of the current to voltage conversion circuitry present in the potentiostats, current was recorded versus time on a strip chart recorder throughout the potentiostatic exposures.

In preparation for a controlled potential exposure the electrochemical cell, Figure 6, was filled with one liter of

the appropriate solution and positioned in the sample compartment of the Raman spectrometer. Three of the cell's necks were sealed with rubber stoppers, one held the thermometer, and the fifth neck contained the gas dispersion tube. For thirty minutes before introduction of the sample, the solution was stirred and purged of reactive dissolved gasses by bubbling nitrogen through it. The gas purge and stirring were continued throughout the controlled potential oxidation.

After thirty minutes of purging, the platinum mesh auxiliary electrode and the Luggin capillary were placed in the cell. The Luggin probe was connected to a beaker of the deaerated solution containing the saturated calomel reference electrode by Tygon tubing. The lead electrode, cleaned as described previously and mounted in the sample holder, was positioned in the cell. The three electrodes were then connected to the potentiostat terminals and the specified voltage was applied.

The exposures were conducted for various lengths of time, more time being required for some films to become thick enough to give a good Raman spectrum than others. The cell was in a thermostatically controlled room so the solution temperature was maintained at 25±2 degrees.

After oxidation, without disturbing the electrochemical cell, an in situ Raman spectrum of the sample surface was recorded. This required only turning on the Raman instrument and possibly adjusting the position of the cell

to focus scattered light on the entrance to the monochromator. If the spectrum observed was weak or nonexistent, the potentiostatic exposure was continued so the surface film might become thicker and give more intense Raman scattering.

Once an in situ Raman spectrum of sufficient intensity to characterize the surface film had been recorded, the lead working electrode was disconnected from the potentiostat, removed from the solution, and thoroughly washed with distilled water. After drying at room temperature, the sample was returned to the spectrometer and a Raman spectrum of the dry surface was obtained. By examining the sample both in the solution and in the dry condition, any changes due to removal of water from the film should have been observed.

To confirm the Raman findings and to answer some questions about the surface films formed electrochemically, some samples were examined by X-ray diffraction. The diffraction patterns were recorded using a General Electric 11GJ1 X-ray unit with a copper target.

Some samples were examined by scanning electron microscopy on a Hitachi Scanscope SSM-2 with a Tektronix C-27 oscilloscope camera. Samples were cut into small pieces, about 6 X 6 mm., to fit into the SEM sample chamber and they were examined uncoated. Some samples were analyzed with an AMR 1000 SEM and an EDAX 707A X-ray energy dispersive analyzer.

To measure the thickness of a corrosion product film on a lead surface, special samples were prepared. A thin layer of gold was vacuum deposited on a glass microscope slide then a layer of lead was deposited on the gold using a Hitachi Model HUS-4GB vacuum evaporator. The gold allowed electrical contact to be made with the lead and provided a nonreactive reflecting surface when the lead was completely oxidized. During deposition, part of the gold was masked by another microscope slide so that a sharp step equal in height to the lead thickness was created, as shown in Figure 9. The height of the step was measured before and after potentiostatic oxidation by a Taylor-Hobson Taylstep-1, a stylus type profile instrument with vertical resolution better than 10 angstroms.

The vacuum deposited samples could not fit the sample holders used for in situ Raman spectroscopy so they were clamped in position during exposure and removed as soon as the oxidation period was completed. No in situ spectra were attempted due to the difficulty of positioning the samples, only spectra of the dried samples were measured.

II.F. Iron Exposures

Several oxides of iron are readily available as reagent grade powders. Ferrous oxide, FeO, was purchased from Pfaltz and Bauer, Inc., Fe_3O_4, from Amend Drug and Chemical Company, and α-Fe_2O_3, from Alfa Products, Inc. Pure FeOOH

is not available so two polymorphs were synthesized.

Crystalline α-FeOOH was precipitated by hydrolysis of 0.1M ferric oxalate solution at the initial pH of 6.5 (adjusted by the addition of 1M $NaHCO_3$ solution) (73,74). The solution was held at 100°C for 45 minutes and allowed to cool. The resulting precipitate was washed with distilled water, separated from the solution by centrifugation, and dried at room temperature.

Hydrolysis of a ferrous chloride solution formed γ-FeOOH. A solution of 20g. $FeCl_2 \cdot 4H_2O$ in 500 ml. of water was added to 100 ml. of 2M hexamethylenetetramine solution, giving a blue-green $Fe(OH)_2$ precipitate. To this was added 100 ml. of 1M $NaNO_2$ solution and the mixture was held at 60° C for three hours (75,76). After cooling, the rust-colored precipitate was removed by filtration, washed with water, and dried at 100° C.

Raman spectra were recorded with the compounds in KBr pellets. The identity and purity of the synthesized compounds were confirmed by their infrared absorption spectra (71).

Armco iron samples were mechanically polished and washed with distilled water to give a clean surface. For high temperature exposures the samples were placed in a preheated laboratory tube furnace for specified time periods. Upon completion of an exposure, a sample was cooled to room temperature and a Raman spectrum of its surface was recorded in the manner used for dry lead samples.

TABLE I

Conditions for Simple Immersion Exposures

CONDITION	SOLUTION COMPOSITION	OXYGEN CONTENT
a	2M HCl	deaerated
b	0.1M HCl	deaerated
c	0.1M HCl	air saturated
d	0.1M HBr	air saturated
e	2.3M HBr	deaerated
f	0.01M NaOH	deaerated
g	0.01M NaOH	air saturated
h	0.5M NaOH	air saturated

TABLE II

Solutions Used for Controlled Potential Exposures

SOLUTION	pH	COMPOSITION
1	7.0	0.063 M KH_2PO_4, 0.037 M NaOH
2	10.0	0.041 M $NaHCO_3$, 0.018 M NaOH
3	1.1	0.1 M HCl
4	7.0	0.063 M KH_2PO_4, 0.037 M NaOH, 0.1 M KCl
5	10.0	0.041 M $NaHCO_3$, 0.018 M NaOH, 0.1 M KCl
6	1.0	0.1 M H_2SO_4
7	6.5	0.1 M K_2SO_4
8	11.0	0.1 M K_2SO_4, 0.004 M KOH

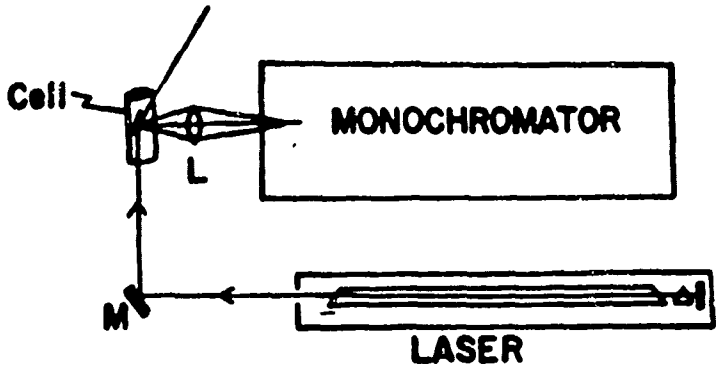

SIDE VIEW

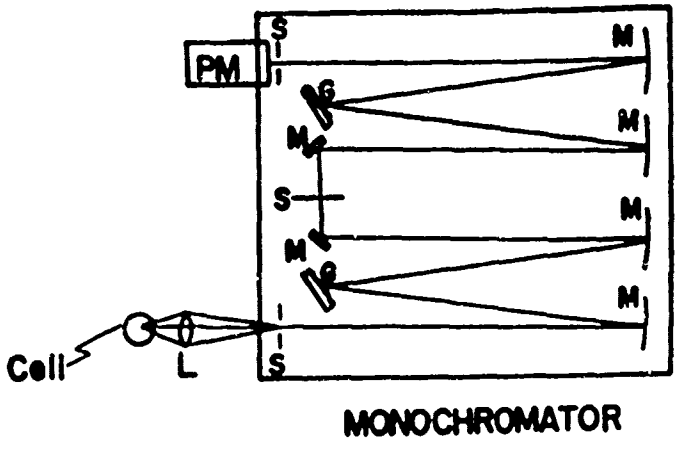

TOP VIEW

Figure 2. Schematic drawing of a laser Raman spectrometer. Mirrors are labelled M, gratings, G, slits, S, and lens, L.

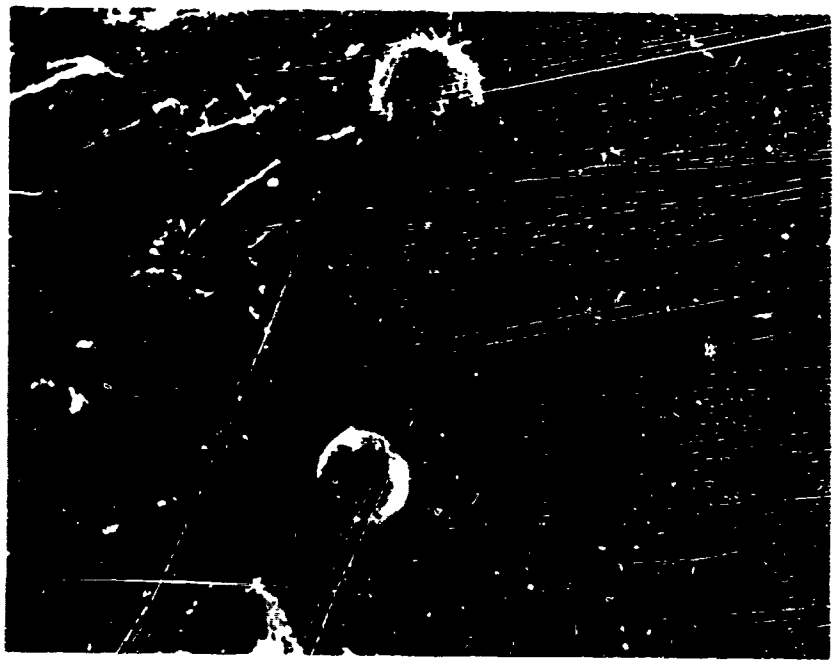

Figure 3. Scanning electron micrograph of a lead surface exposed in pH 7, phosphate buffer at -0.11V vs. SHE for 19 hours. Magnification 2000X. Black particle consists of SiC, white balls contain phosphate.

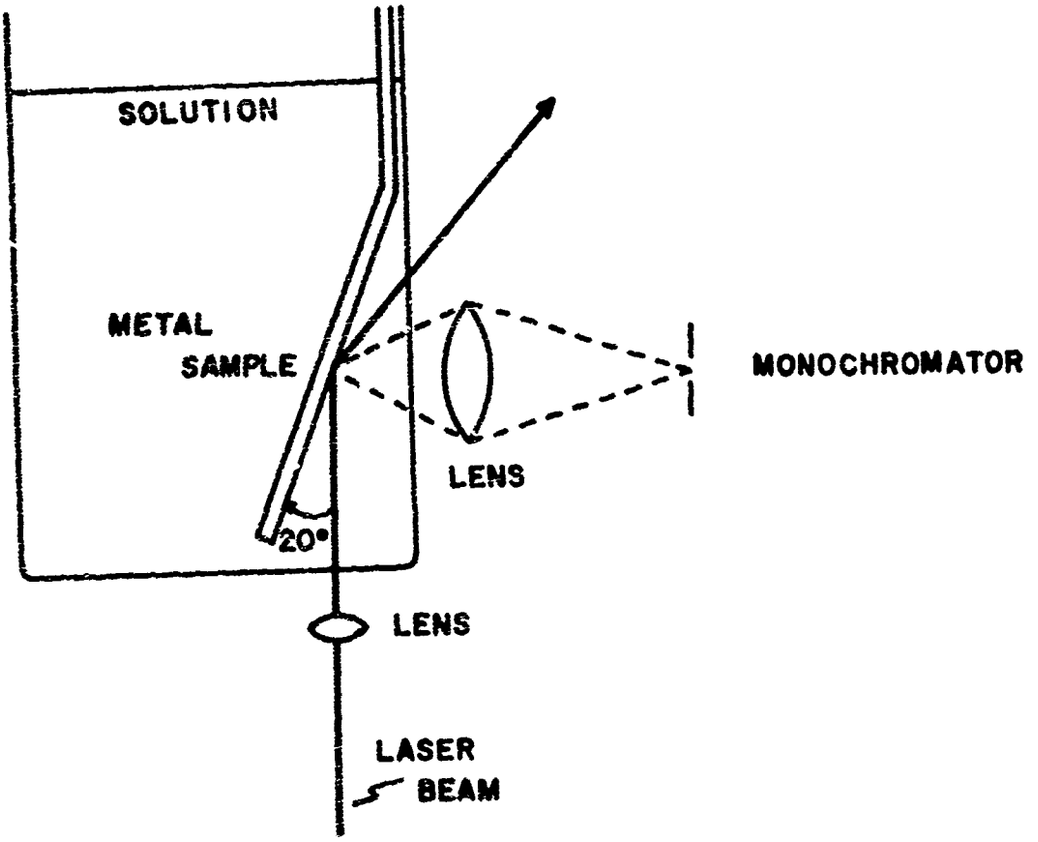

Figure 4. Sample arrangement used for recording in situ Raman spectra of simple immersion sample surfaces.

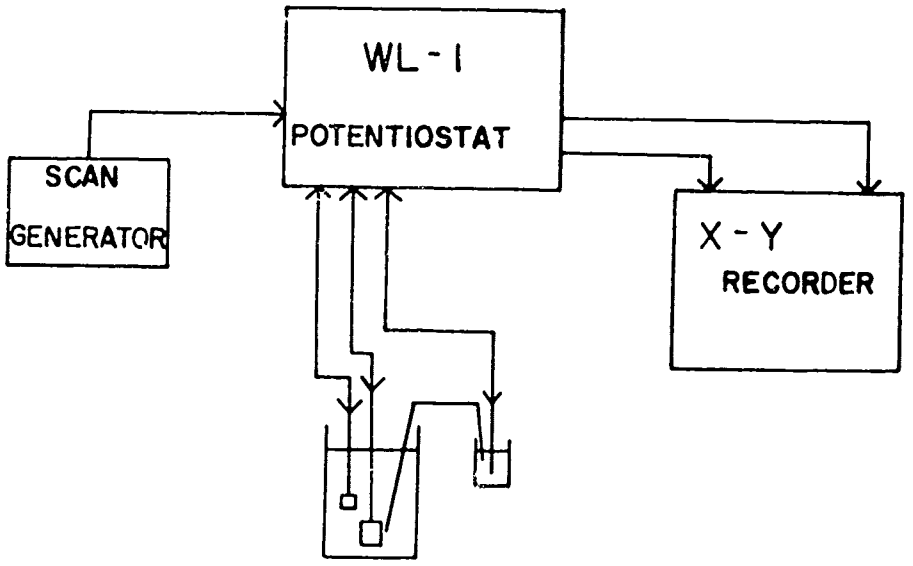

Figure 5. Block diagram of the equipment used to record polarization curves.

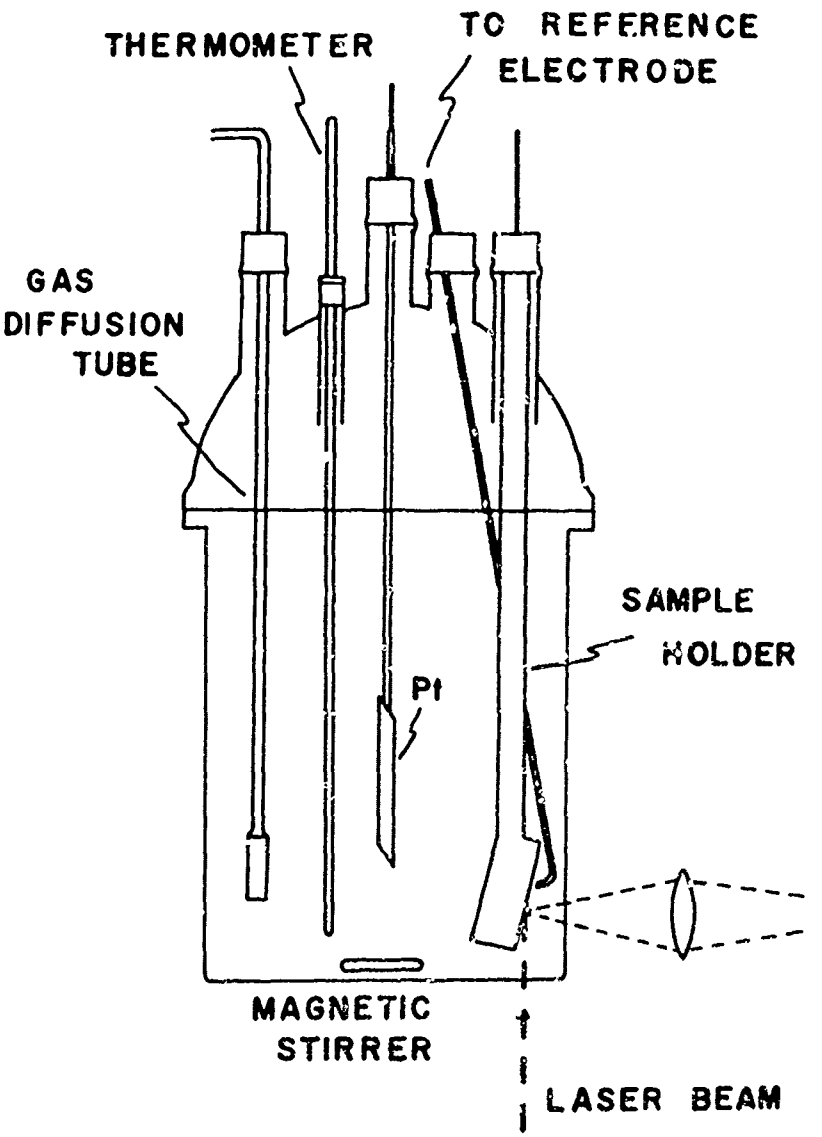

Figure 6. Drawing of the electrochemical cell used for in situ Raman spectroscopy.

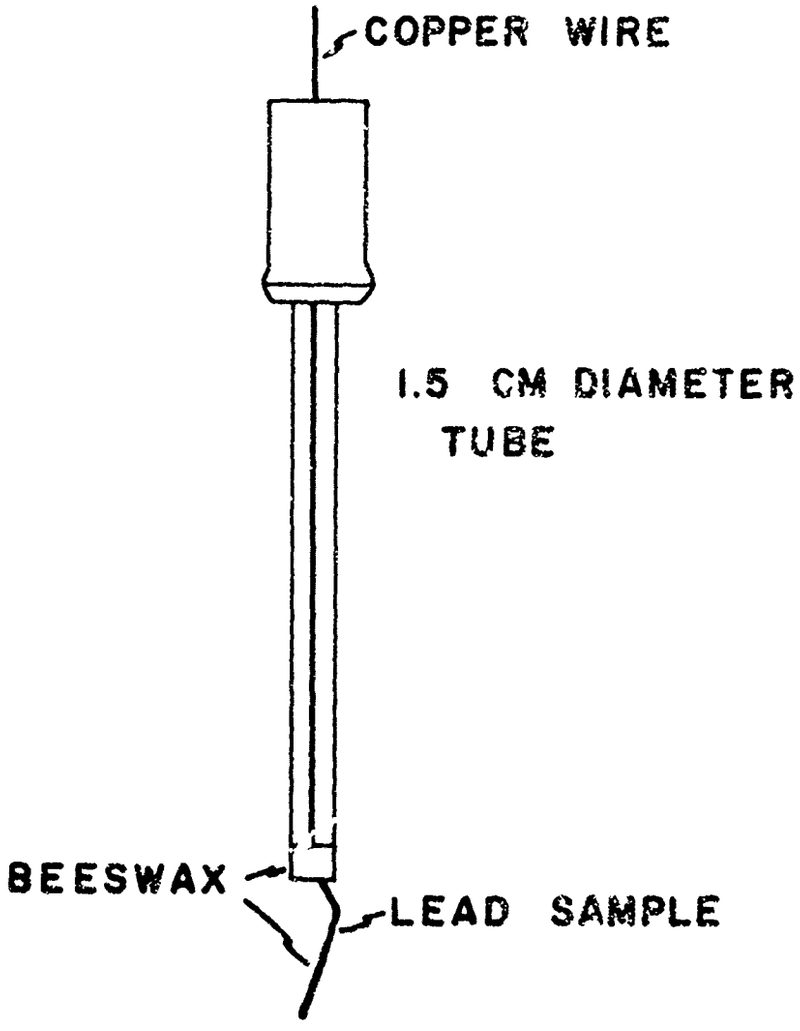

Figure 7. Drawing of glass sample holder.

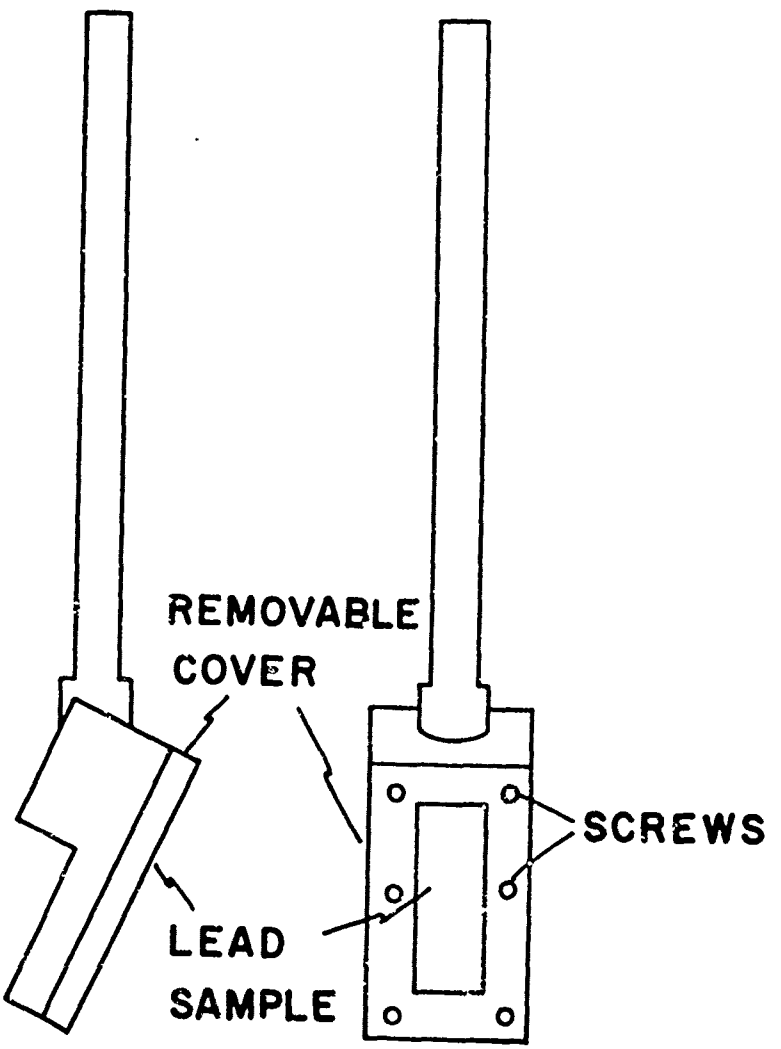

Figure 8. Drawing of TEFLON sample holder.

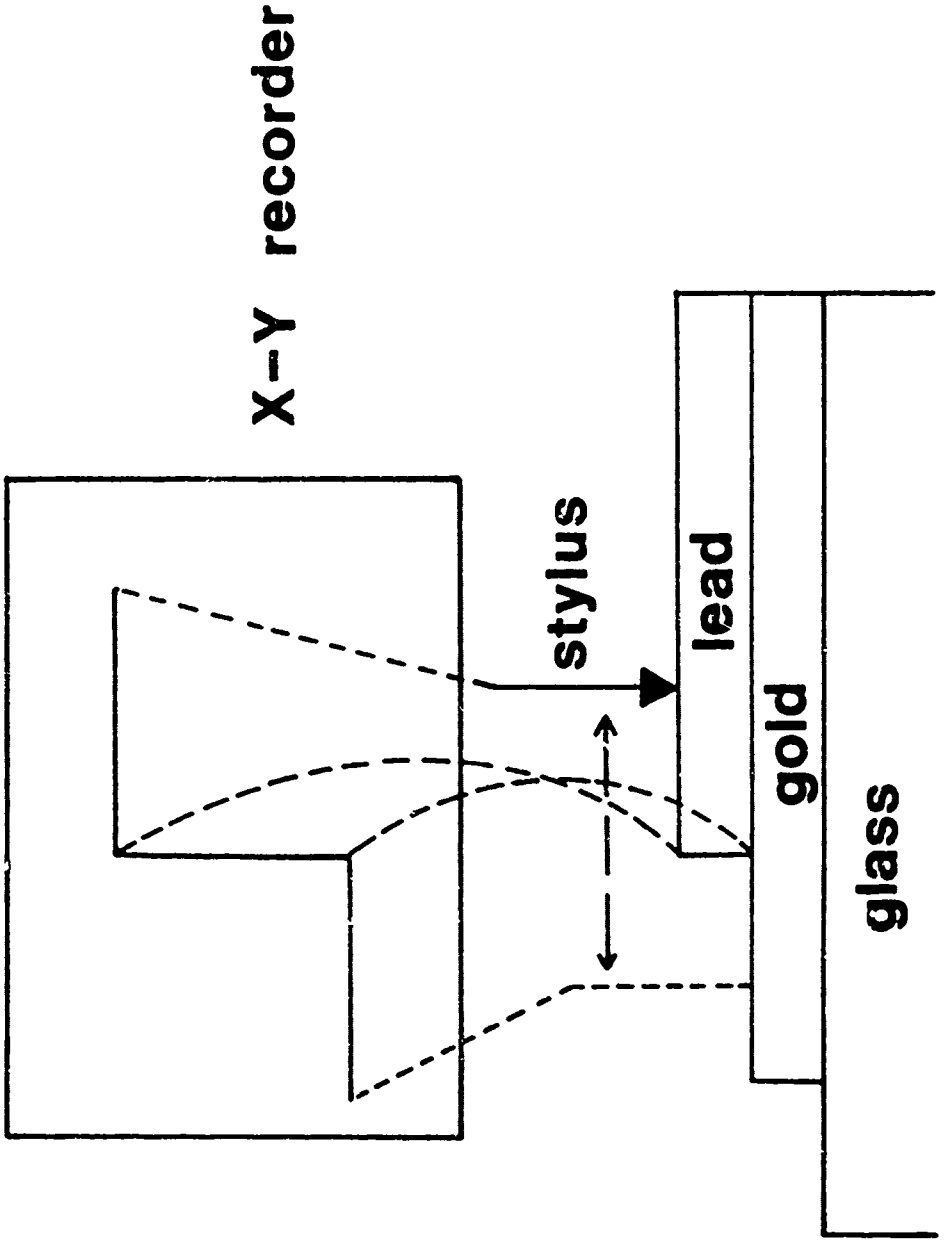

Figure 9. Vapor deposited lead film on glass for film thickness measurements by a stylus instrument.

III. RESULTS AND DISCUSSION

III.A. Reference Spectra.

In order to use Raman spectra to identify the compounds present in surface films on lead, spectra of possible lead compounds were needed for reference and comparison. Raman spectra of several compounds are available in the literature, but some other important species have not been previously examined. One of the reasons for using lead in this research was that, since it has a large polarizability (i.e., loosely held electrons), its compounds were expected to give strong Raman spectra. Because lead is a heavy element, most vibrations of its compounds are very low in frequency, but Raman instrumentation allows bands as close to the exciting line as 20 cm^{-1} to be observed without difficulty. As demonstrated by the lead chloride spectrum of Figure 10, lead compound spectra were found to be typically strong and low in frequency.

Identification of lead halides using Raman spectroscopy is very easy and conclusive. Eight of the ten Raman bands observed in the spectrum of single crystal lead chloride (77) may be seen in the spectrum of the powder in a capillary tube. Since the crystal structures of lead chloride and lead bromide are identical, their Raman spectra are extraordinarily similar. Due to the presence of the heavier bromine atom, $PbBr_2$ has the same bands as $PbCl_2$, but shifted to lower frequencies (78).

Raman spectra of the two polymorphic forms of PbO are

available in the literature (13,14,79), and they demonstrate that the two forms are easily distinguishable. Spectra of samples sold as litharge, or tetragonal PbO, and massicot, or orthorhombic PbO, were recorded. They indicated that both of the samples were actually orthorhombic PbO.

As shown in Figure 11, spectra of PbO can be slightly different for different sample preparations. The spectrum of PbO powder in a capillary tube is not the same as that of the same compound in a pressed KBr pellet. Although both are primarily spectra of orthorhombic PbO, the pellet spectrum shows impurity bands at 84, 149, and 344 cm^{-1}, i.e., the positions of the three strong bands of tetragonal PbO. The grinding required in the pellet making process apparently transforms some of the orthorhombic oxide to the lower energy, tetragonal form. The crystal structures of the two oxides are very similar. The orthorhombic form is a slightly distorted version of the tetragonal, which is the thermodynamically stable form at temperatures below 488° C (80,81). Orthorhombic PbO is stabilized by the presence of small quantities of various impurity ions (81,82), allowing it to remain indefinitely without reverting to the tetragonal form. It is likely that small amounts of impurities stabilize the reagent grade PbO so that it can remain in the orthorhombic form until intensive grinding brings about the transformation.

The Raman spectrum of the most common carbonate of lead, hydrocerrusite, $(PbCO_3)_2 \cdot Pb(OH)_2$, has not previously been

published. The spectrum, shown in Figure 12, quickly confirms the presence of carbonate with the very strong 1051 cm^{-1} band, the C-O symmetric stretch characteristic of carbonates. The other bands specify the type of carbonate, i.e., $(PbCO_3)_2 \cdot Pb(OH)_3$.

The mixed oxide Pb_3O_4, minium, decomposed in the laser beam and a spectrum could not be obtained. By making a KBr pellet containing approximately equal amounts of Pb_3O_4 and KBr, the excellent spectra shown in Figure 13 were recorded. This was the only lead compound to show marked differences when using different excitation frequencies. The two spectra of Pb_3O_4 in Figure 13 were recorded under identical conditions, but the bands in the spectrum recorded with the 514.5 nm. exciting line are two to three times as intense as those in the 488.0 nm. spectrum. The change in spectral intensity is an example of pre-resonance enhancement of the Raman transitions due to exciting the molecules with a frequency near an electronic absorption band (30-32,83,84).

The other oxide of lead, lead dioxide, presents a problem for vibrational spectroscopy. There are no infrared absorption bands at wavelengths above 240 cm^{-1} (85), and no Raman bands were observed using either powder or pellet samples. When exposed to the laser, the black compound rapidly decomposed, the exposed portion becoming pale yellow in color. A spectrum of a PbO_2 pellet which had been exposed to the 514.5 nm. laser line for an hour is shown in Figure 14. The spectrum identifies the compound as

orthorhombic PbO. Clearly the intense laser beam transformed the PbO_2 into orthorhombic PbO.

In the aqueous corrosion of a metal it is entirely possible that the insoluble oxide layer may consist primarily of one compound with one or more impurities present. In order to determine the minimum concentration of an impurity substance required for detection by Raman spectroscopy, spectra of mixtures of the lead compounds were recorded. The minimum detectable concentrations were found to vary widely. From the spectrum of lead chloride containing 0.95% (by weight) orthorhombic lead monoxide shown in Figure 15, it is clear that 1% or greater proportion of PbO in lead chloride should be easily visible. The strong PbO bands at 143 and 292 cm^{-1} which do not coincide with chloride bands are easily seen. This spectrum shows that small amounts of oxide should be detectable in a lead chloride film. The opposite mixture, a small amount of PbCl mixed with a large amount of PbO, showed that the Raman spectrum of PbO is considerably stronger than that of lead chloride. No bands due to the chloride could be seen in mixtures containing up to 16% $PbCl_2$. As shown in Figure 16, these mixtures gave spectra of orthorhombic PbO alone, with no hint of the impurity. It is probable that the yellow PbO dominates the spectra of mixtures because its electronic absorption band, extending to approximately 450 nm. (86,87), is much closer to the excitation frequencies used than that of colorless lead chloride. Pre-resonance

Raman enhancement of the PbO spectrum can account for the intensity of the bands. Since there is considerable variation in spectral intensity from one compound to another, it has not been possible to specify any single concentration which is the minimum detectable concentration for which a useful Raman spectrum can be obtained. The minimum concentrations for the lead compounds examined varied from approximately 0.5 to 30 percent.

III.B. Simple Immersion Oxidation.

In order to develop the equipment and technique for recording in situ Raman spectra of lead surfaces oxidized in aqueous solutions, clean lead strips were simply immersed in reactive solutions and allowed to corrode freely. After exposure periods of from one to thirty-four days, spectra of the relatively thick surface films which had formed were recorded using the arrangement shown in Figure 3.

A lead strip was immersed in a deaerated 2.3 molar hydrobromic acid solution and allowed to react for eight days. At that time a thick gray film, crystalline in appearance, had formed on the surface. The in situ Raman spectrum of the surface, shown in Figure 17, clearly indicates that it consists of $PbBr_2$. The six strongest bands in the spectrum of pure lead bromide are present in the spectrum of the film. Furthermore, the band shapes and frequencies in spectra of the film and of the powder are

identical.

The sample was allowed to continue reacting undisturbed in the solution, and the crystalline surface film developed into white, needle-like crystals one to two centimeters in length. After a total immersion time of 34 days, the sample was removed and dried at room temperature. The white crystals were scraped off and ground into powder to simplify the measurement of a Raman spectrum. The spectrum was identical to that of the surface film. It is clear that the Raman spectrum of a thick film is identical to that of a bulk sample; Raman scattering from a powder is not significantly different from scattering from a film.

Lead samples were exposed to dilute hydrochloric acid solutions with the expectation that they would react more rapidly with chloride than with bromide ions. Although at least four days of immersion were required to form a lead bromide surface layer thick enough to give a good spectrum, lead in HCl solution formed a dark gray coating which was sufficiently thick to give a lead chloride spectrum after eighteen hours of exposure The in situ Raman spectra of sample surfaces which had been reacting in air saturated 0.1 molar hydrochloric acid for varying lengths of time are shown in Figure 18. While the thin film of the eighteen hour exposure is difficult to identify, as the films became thicker, the spectra became more and more like that of the powder shown in Figure 10. These exposures were conducted in aerated solutions; however, samples exposed in

deoxygenated HCl solutions gave identical spectra. As demonstrated by the spectra of Figure 19, the only effect of the presence or absence of oxygen is apparently in the rate of the reaction; a $PbCl_2$ film became thick enough to give a good spectrum much sooner when the solution contained dissolved oxygen. The presence of dissolved oxygen makes the solution more corrosive to lead (88), increasing the amount of dissolved Pb^{++} ions present. Since the formation of lead chloride probably depends only on its solubility product, increasing the amount of Pb^{++} present has the effect of increasing the amount of $PbCl_2$ which is precipitated. The same effect was noted in hydrobromic acid exposures, i.e., lead bromide appears to form more rapidly under air saturated conditions.

Lead immersed in a basic solution (0.01 M NaOH) under deaerated conditions was oxidized to tetragonal PbO as the spectrum of Figure 20 indicates. The spectrum differs considerably from that of the orthorhombic form, and it agrees completely with single crystal spectra of the tetragonal form published previously (13); there is no difficulty in determining which polymorph of PbO is present.

In air saturated exposures to sodium chloride solutions, a different product formed. Instead of a dull, gray PbO coating, a thick, white substance appeared on both the sample and glass container surfaces. The white precipitate was identified as basic lead carbonate by its spectrum; both the sample surface and the material scraped from the side of

the container gave identical spectra. Figure 21 shows a spectrum of the dried sample surface and one of reagent grade basic lead carbonate, $(PbCO_3)_2 \cdot Pb(OH)_2$. No spectra were recorded in situ because the precipitate on the container prevented light from reaching the sample.

Since they were found only on the lead surface, the nature of the reactions forming the lead halides could not be determined from these experiments, although it is assumed that they are precipitated from dissolved ions. They could be formed by a solid state reaction at the lead surface. It is evident from the nature of the precipitate that the basic lead carbonate was formed from dissolved carbon dioxide/carbonate species reacting with lead ions in solution. Lead and lead monoxide have appreciable solubility in alkaline solutions (35,47), so the presence of dissolved carbonate controls which compound is form When little or no carbonate is present, as in a o aerated solution, lead is oxidized to tetragonal PbO, but when dissolved carbon dioxide is present, as it is in air saturated exposures, it reacts with lead icns to form the insoluble carbonate.

It is not known if PbO formed in the aerated solution. No indication of PbO bands was seen in the Raman spectra of the surface, but the oxide may have been present under a layer of basic lead carbonate thick enough to prevent detection of the oxide. It has been estimated that light is scattered from a surface layer with a thickness on the order

of the wavelength of the light (89), in this case approximately 500 nm. Although accurate measurement of the thickness of the carbonate coatings could not be made, the layer was estimated to be nearly a millimeter thick, several orders of magnitude greater than the light causing Raman scattering could penetrate.

A summary of the spectral results of the simple immersion exposures is presented in Table III. In addition to identification of the compounds comprising the surface films, the immersed samples were used to develop the apparatus and technique used for the electrochemically oxidized lead sample analysis, the more important part of this research.

III.C. Lead - Water Pourbaix Diagram

As mentioned in the experimental section, both calculated Pourbaix diagrams and potentiodynamic polarization curves were used to determine the exposure conditions required to thoroughly investigate the behavior of lead in water. The simplified Pourbaix diagram available in the literature (35) is shown in Figure 1. It designates theoretical conditions of stability for Pb, Pb^{++}, tetragonal PbO, Pb_3O_4, and PbO_2. Because more recent and, presumably, more accurate thermodynamic data has become available in the years since the calculation of that diagram, it was desirable to recalculate the diagram using the recent data.

The slightly altered lead - water Pourbaix diagram resulting from applying new free energy values (90) to the same chemical reactions and equilibria used by Pourbaix (35) is shown in Figure 22. The revised values for free energy used are presented in Table IV. Although the values do not differ from previous ones by large amounts, they do cause considerable changes in the diagram since they affect the slopes of the equilibrium lines. The most obvious difference is the appearance of a region where Pb_2O_3 is predicted to be stable.

The Pourbaix diagram of Figure 22 was used to select the pH values of interest. No acid solutions were chosen because they were predicted to form no insoluble species, only lead or plumbous ions appear in the acid region of the diagram. It was felt that any acid chosen to achieve a low ph would have a strong effect on the behavior of the lead. Dissolved Pb^{++} ions either remain in solution or precipitate as salts of the anions present in the acid. No meaningful lead - water reactions can be examined in the acid region with the presence of anions.

In neutral and basic solutions, insoluble lead oxides are predicted to be stable so solutions of pH 7 (phosphate) and ph 10 (bicarbonate) were selected for controlled potential exposures. These buffer solutions, the compositions of which are listed in Table II, were similar to those used in the past for electrochemical investigations of Pourbaix diagrams for other metals (42,91). It was hoped

that the presence of dissolved buffer species would not affect the equilibria of the diagram, that the surface films which formed would be results of lead - water reactions only, with no interference from the dissolved ions of the phosphate or carbonate species.

The potentials for potentiostatic exposures were chosen so that they were representative of the various regions of the Pourbaix diagram and, also, so that they represented each of the regions which appeared in potentiodynamic polarization curves. Polarization curves were recorded for lead in the solutions of interest between -0.76 V and +1.24 V vs. SHE. This potential range was chosen to examine the behavior of lead throughout the Pourbaix diagram. Since the purpose of the research was to study aqueous corrosion, potentials where water is stable were the only ones of interest. To permit the formation of relatively thick films which were expected to allow some comparison with potentiostatic exposures, the polarization curves were recorded during slow potential scans, 40 mV/minute.

Anodic polarization curves for lead in the pH 7 and pH 10 solutions are shown in Figure 23. From the Pourbaix diagram it is apparent that lead is thermodynamically stable within part of the region of water stability. The lowest oxidative wave of each curve seems to correspond, approximately, to the potential of the Pb/PbO transition. At lower potentials, net current flow was in the reducing direction, as is likely where lead is stable, and at higher

potentials current flowed in the direction of oxidation, certainly indicating that an oxidation product was formed. The upper waves, at +1.05 V in pH 7 and at +0.88 V in pH 10, roughly correspond to the predicted Pb_2O_3/PbO_2 transition potentials. It is in agreement with the Pourbaix diagram that the potentials of the transitions are higher in neutral than in basic solutions. In the pH 10 polarization curve, the oxidative wave going off scale at 1.20 V undoubtedly represents oxygen evolution, although the potential is considerably higher than the calculated oxygen evolution line, 'b' in Figures 1 and 22. The other, smaller, waves seen in the polarization curves of both solutions are not immediately explained by the Pourbaix diagram. They could be due to formation of the intermediate oxides Pb_3O_4 or Pb_2O_3, formation of some species which involve the buffer solution, or due to some kinetic effect. Positions of polarization curve waves depend on sweep rate and concentration of reactants as well as on sample material and solution composition (92). Clearly, the polarization curves and Pourbaix diagrams alone cannot adequately describe the oxidation of lead in the buffer solutions. To find whether the waves of the polarization curves actually identify the same transitions predicted in the Pourbaix diagram, the composition of the surface films must be analyzed by Raman spectroscopy.

III.C.I. Immunity Region.

Potentiostatic exposures of lead samples were conducted in each of the various potential regions identified by Pourbaix diagrams and polarization curves. At low potentials lead is calculated to be thermodynamically stible, or immune to oxidation. Electrochemical exposures confirmed the prediction.

In the pH 7, phosphate solution exposure at a potential of -0.62 (V vs. SHE) resulted in a very small reducing current, and the samples remained silver and shiny in appearance throughout the exposures. Raman spectra could not be observed from the surfaces either in sclution or after drying. From all indications, no surface film was formed.

Exposure at -0.16 V also gave no spectrum. In the Pourbaix diagram -0.16 V is in the immunity region, but it lies above the first oxidative wave of the polarization curve. Current remained extremely small for that exposure, 0.06 mA/cm^2, but it was in the oxidizing direction. Possibly lead is oxidized under these conditions, as the polarization curve indicates, but the film may be very protective. The -0.16 V exposure apparently did not exhibit the immunity predicted by the calculations of the Pourbaix diagram.

The results of exposures at low potentials in pH 10 solution were slightly different. At -0.80 V the sample remained shiny, net current flow was in the reducing

direction, and no spectrum could be observed, the same immunity results as in the phosphate buffer. At a potential of -0.42 V, however, while the sample remained relatively shiny, current flow was in the oxidizing direction and the surface gave a weak Raman band at 1050 cm^{-1}, indicating the presence of carbonate. Infrared reflection-absorption spectroscopy, which is more sensitive to carbonate films of this type, confirmed that the compound on the surface was basic lead carbonate (71). From the spectroscopic results it may be inferred that the oxidative wave at -0.36 V is not necessarily an indication of a Pb to PbO transition but it seems to be related to the appearance of the basic carbonate.

III.C.2. PbO Region.

According to the Pourbaix diagram of Figure 22, the region of tetragonal PbO stability exists between -0.16 V and +0.62 V at pH 7 and between -0.34 V and +0.42 V in pH 10 solution. All potentiostatic exposures conducted in this region formed tetragonal PbO. They all formed relatively thick, non-protective surface films which were identified by their Raman spectra. The physical appearances of the films varied over the range of potentials. At lower potentials the surfaces appeared gray, and oxidation currents were moderate, becoming constant at values near 0.05 mA/cm^2. At higher potentials the currents were higher and the color of

the surfaces became blacker. The black lead oxide is known to be a light colored lead monoxide layer with some elemental lead dispersed on the surface, the oxide/water interface (80). At the lower potentials where oxidation is slower, a smaller amount of elemental lead seemed to be present. As the potential was raised and the rate of oxidation increased, the color of the surfaces indicated that the films contained more lead. Although the films had different physical appearances, the Raman spectra of films formed throughout the PbO region were identical, as shown by the spectra of Figure 24.

Lead samples exposed throughout the PbO region also exhibited similar current behavior with time. A typical plot of current versus time during such an exposure is shown in Figure 25. All exposures which resulted in the formation of tetragonal PbO showed similar current behavior with only small differences in the magnitude of current. The current decreased rapidly for approximately thirty seconds, rose rapidly to a maximum after approximately one minute of exposure, and then it gradually decreased, reaching a relatively steady value after about ten minutes. The initial drop in current can be attributed to the rapid oxidation of the clean lead surface, forming an initial oxide layer. The cause of the current maximum after a minute of oxidation is not so certain. It may indicate the initiation of another process, perhaps the initial current decrease is due to the surface being covered by one species

which, after formation of a thin layer, is transformed to another species. The current behavior could also be explained by the simultaneous occurrence of two competing processes, such as a solid state reaction and a dissolution or precipitation process. If the rate of one process depended on the concentration of dissolved lead or the presence of an oxide film at the surface, it could have changed greatly in the first minute of oxidation, as lead was dissolved and an oxide film began to grow. A significant change in the relative rates of two competing reactions could account for the temporarily high current obseved.

Since the same current behavior was observed in both phosphate and bicarbonate buffer solutions, it is unlikely that dissolved anions cause it. Since spectra of the surface films indicated the presence of only tetragonal PbO, it may be assumed that only the reactions forming PbO or dissolved lead ions are involved. Spectra of lead surfaces were recorded only after the current maximum had been reached; therefore, information as to the state of the surface before the maximum was not obtained. The instrumentation used to record Raman spectra is not designed for rapid scanning of a spectrum. A minimum of three minutes is required to scan the spectral region of interest, so the one minute period between the initiation of a potentiostatic oxidation and the current maximum is not enough to permit the recording of a spectrum, without even

considering the time needed to adjust the sample position and optics to direct light scattered from the sample into the monochromator. It should be pointed out that the purpose of this research was to identify the compounds comprising surface films under conditions of relatively long term oxidation, not to examine the initial phases of oxide film formation, which would require different instrumentation and experimental methods.

After in situ Raman spectra were recorded, each sample was thoroughly washed with distilled water and allowed to dry at room temperature. Raman spectra of the dried sample surface were then recorded to detect any possible change in the surface film which might have occurred due to drying and to make sure that the spectra of the surface species were due to insoluble compounds and not adsorbed or solution species which could be removed by washing. All samples that gave tetragonal PbO spectra in solution gave identical spectra when dry. The similarity between wet and dry sample spectra is shown in Figure 26. In this investigation, in situ spectra were generally found to have approximately half the intensity of dry ones due to the difficulty of focusing light scattered in the large electrochemical cell onto the entrance slits of the monochromator, and because of losses due to reflection and scattering from the glass cell and the solution. The difference in spectral intensities was not enough to be significant, although it meant that thinner films could be identified from spectra of dry samples. The

spectra of dried samples showed slightly better signal to noise ratios, but all Raman bands of dry samples were also detected from samples in solution. One drawback encountered when obtaining spectra of dried samples was the increased intensity of grating ghosts. Due to the greater amount of light directed into the monochromator by dry samples, more light was available to be diffracted improperly by the gratings.

In general, when any lead sample was exposed to the laser, the current increased very slightly, no more than one percent, probably because the intense radiation disrupted the double layer at the point of incidence. However, it was found that the oxidation current of a lead sample covered with tetragonal PbO increased sharply when the laser beam was incident on the surface. When lead electrodes with a tetragonal PbO coating were exposed to laser radiation of either 488.0 or 514.5 nm. wavelength, the oxidation current increased suddenly and markedly. An example of such behavior is shown in the current vs. time curve of figure 27. Similar current behavior has been observed when lead was oxidized in sulfuric acid solutions (54), because of the photoconductivity of tetragonal PbO on Pb/PbO electrodes.

When a lead sample being oxidized in the PbO region was exposed to the laser beam, three effects were observed: the current increased markedly, the spot of laser incidence became brownish in color, and bubbles appeared at that spot. The potential and thickness of the oxide layer affected the

occurrence of these effects. Each became more pronounced with higher potentials and thicker films. The formation of bubbles at the point of laser incidence caused considerable difficulty in obtaining in situ spectra. A bubble complicates the geometry of light scattering at the solution/sample interface. Bubbles scatter large amounts of light away from the direction desired for examination in the spectrometer, thus weakening the observed Raman spectrum greatly. An example of the degradation of a spectrum by bubble formation is shown in Figure 28. The bubbles disappeared when the potential was removed. The only difference in recording the spectra of Figure 28 was in potential. Bubbles were generated by the laser when the potential was applied; when the potential was removed and the electrode could assume its rest potential, the bubbles were no longer present.

Laser incidence caused the oxide films to turn brown if the sample was irradiated while at a potential higher than the Pb/PbO transition. The scanning electron micrograph in Figure 29 shows the change in the surface due to the laser. After the applied potential was removed the lead electrode assumed a rest potential at the value of the lowest oxidative wave of the polarization curve, and no further color change was observed. The brown spot remained brown, but irradiation of any part of the remaining gray or black surface film caused no change in color, just as it caused no further bubble formation.

Apparently the reactions due to the laser beam are potential dependent, indicating that the process is photochemical in nature, not thermal decomposition as is often seen with laser irradiation (83). It is very difficult to envision any thermal process resulting in the decomposition of PbO which could be potential dependent. The photoelectrochemical process described by Pavlov, Zanova, and Papazov (54) in which PbO is transformed to brownish PbO_2 with the formation of oxygen gas and a resulting high photocurrent seems to fit the observed behavior. Although the experimental setups were different, Pavlov, et. al., used a lead electrode covered with a transparent lead sulfate outer layer over tetragonal PbO exposed to a tungsten lamp, results of irradiated potentiostatic exposures are very similar. A summary of the process proposed by Pavlov follows.

The basic process involves the reaction of PbO with light of wavelengths shorter than 650 nm. The energy of light at this wavelength corresponds to 1.9 eV, the bandgap energy for tetragonal PbO (93). Interaction with light can promote an electron into the conduction band of the oxide leaving the PbO layer with electron holes in the semiconductor lattice,

$$PbO + h\nu \rightarrow PbOh^{+} + e^{-} \qquad (1$$

Electron holes are represented by h^{+} in Equation (1. The holes move through the PbO due to the electric field imposed across it until they collect at structural defects, which

are plentiful in PbO. The holes interact with defects, represented by d, creating

$$h^+ + PbOd \rightarrow PbOd^+ \quad (2$$

charged $PbOd^+$ centers containing Pb^{3+} ions which are unstable. These quickly interact with another hole to form a more stable Pb^{4+} structure.

$$h^+ + PbOd^+ \rightarrow PbOd^{2+} \quad (3$$

There is very little difference between the tetragonal PbO lattice and that of PbO_2 (80,94), so the $PbOd^{2+}$ is essentially lead dioxide with an oxygen vacancy. Reaction with water can easily eliminate the vacancy to complete the process.

$$PbOd^{2+} + H_2O \rightarrow PbO_2 + 2H^+ \quad (4$$

The reaction of the PbO species with OH^- ions from the solution has been proposed to explain the formation of oxygen (54) through a two step pathway,

$$PbOh^+ + OH^- \rightarrow PbO + OH(ad) \quad (5$$

$$PbOd^{2+} + 2OH^- \rightarrow PbOd + 2OH(ad) \quad (6$$

The first step is the formation of adsorbed OH radicals which may combine to liberate oxygen gas at the oxide/solution interface.

$$2OH(ad) \rightarrow 1/2\ O_2 + H_2O \quad (7$$

The proposed mechanism agrees very well with the observed results. The formation of bubbles, the change to a brown color, characteristic of Pb^{4+}, and the current behavior are all explained. The scanning electron micrograph of Figure 29 shows that the surface was radically

changed by the laser. The surface of PbO which was not exposed to laser radiation was very rough, and it appeared black. The area irradiated by the 488.0 nm. line, however, was much smoother. The micrograph of that area, shown in Figure 30, shows a relatively smooth film with only a few of the flake-like features which completely covered the unexposed parts of the sample.

It must be pointed out that no differences in the oxide films due to laser irradiation were detected by Raman spectroscopy. In all cases strong tetragonal PbO spectra were recorded from all parts of each sample. As stated previously, no spectra of lead dioxide were obtained so the presence of Pb^{++} species was undetectable. Apparently enough tetragonal PbO was present after irradiation, either mixed with lead dioxide or in another layer, to give the strong lead monoxide spectra observed.

The flake-like surface was not necessarily an indication of tetragonal PbO, since PbO spectra were recorded from areas without flakes. The flakes may consist of PbO or of elemental lead (80) and, due to the surface roughness, give the samples a black color. Whatever species or characteristic they represent is destroyed by laser irradiation at potentials above the Pb/PbO transition. If they are due to tetragonal PbO their disappearance can be explained by the theory of Pavlov (54) discussed above, but, if they are characteristic of elemental lead, then their disappearance must be explained by some other reaction

mechanism which is not known.

III.C.3. Higher Oxide Region.

Potentiostatic exposures were conducted at potentials as high as +1.24 V giving no indication of the presence of higher oxides. Raman spectra and X-ray diffraction patterns found that tetragonal PbO was the only compound present.

Potentiostatic exposures gave no correspondence with the polarization curves. Exposures at potentials above and below the oxidative waves observed at +1.05 V in pH 7 and +0.88 V in pH 10 all formed lead monoxide. No differences were observed. Sample surfaces rapidly blackened during exposure, and oxidation currents were similar to those found throughout the PbO region, 0.1 to 0.4 mA/cm^2.

A summary of the results of exposures in the pH 7 and pH 10 buffer solutions is presented in Table V. The relationship of these experimental results to the calculated Pourbaix diagram is shown in Figure 31. There is excellent agreement with the Pourbaix diagram in all regions except those of the higher oxides.

The reasons for the lack of agreement at higher potentials is not known, but three possibilities should be considered: 1) There may be some kinetic effects in the formation of higher oxidation state lead compounds which cannot be accounted for in the equilibrium calculations of the diagram. 2) The oxygen which begins to evolve at the lead

surface at high potentials (the cause of high current in pH 10 exposures at +1.24 V) may complicate the reactions and make PbO the stable compound under the experimental conditions achieved. 3)The Raman technique examines the surface of the sample, in this case a PbO surface layer, not the surface of the lead metal. Conceivably a thin film of lead dioxide or some other compound could exist at the lead surface, beneath a thick PbO film. This higher oxide might not be detected by X-rays if it were only a small fraction of the total oxide layer. The presence of a layer of PbO_2 is unlikely, however, because such a layer would be protective, thus restricting the flow of current through the sample electrode. Exposures in the PbO_2, Pb_3O_4, and Pb_2O_3 regions resulted in oxidation currents as high or higher than those at lower potentials which resulted in PbO.

III.D. Lead-Water-Chloride Pourbaix Diagram

The Pourbaix diagram for the lead-water-chloride system was calculated in the same manner as for the nil chloride system (71). The reactions considered for the potential region below +0.2 V (vs. SHE) were the same as those used by Appelt (66). Using the more recent thermodynamic data available for some species (90) and extending the diagram to higher potentials gives a more complete and probably more accurate picture of the behavior of lead in chloride solutions. The free energy values used which differ from

those of Appelt's diagram are listed in Table VI.

The positions of equilibria between species on the diagram depend strongly on chloride concentration. A concentration of 0.1 molar was chosen as a reasonably high ionic level which would be likely to affect oxide film formation, but which would not be so high that the solutions would differ greatly from those used in the nil chloride exposures. The calculated lead-water-chloride Pourbaix diagram for a chloride ion activity of 0.1 is shown in Figure 32.

There are two somewhat confusing regions of the diagram, the $PbCl_2$ and the $3PbO \cdot PbCl_2$ regions. In acid solutions the plumbous ion, Pb^{++}, is the stable species at potentials above -0.20 V. The concentration of Pb^{++} in solution is limited by the solubility of lead chloride. The species Pb^{++}, Cl^-, and lead chloride all exist together, bound by the solubility relationship:

$$Pb^{++} + 2Cl^- \rightarrow PbCl_2 \qquad (8$$

$$K = [Pb^{++}][Cl^-]^2 = 10^{-4.6} \quad (95) \qquad (9$$

In neutral and basic solutions, the insoluble phase $3PbO \cdot PbCl_2$ has been considered, but there is some doubt that such a compound exists. It may actually be $3Pb(OH)_2 \cdot PbCl_2$ (12).

Solutions were chosen which allowed electrochemical exposures under acidic, neutral, and basic conditions. The composition of each solution is detailed in Table II. The pH 7 and pH 10 solutions were identical to those used for

nil chloride oxidations except that enough potassium chloride was added to these buffer solutions to make them 0.1 molar in chloride. For an acid pH, no suitable buffer solution could be found, so 0.1 M hydrochloric acid solutions were used. It was found that the pH of acid solution changed by no more than 0.2 pH units during a twenty-four hour exposure.

Potentiodynamic polarization curves were recorded for lead in the three chloride solutions selected for exposures. The curves, shown in Figure 33, seem to have a definite relation to the Pourbaix diagram of Figure 32. The lower oxidative wave occurs at the approximate potential of the predicted $Pb/PbCl_2$ or $Pb/3PbO \cdot PbCl_2$ transitions, and the wave at +0.96 V in pH 10 corresponds roughly to the $3PbO \cdot PbCl_2/PbO_2$ transition. The waves at +0.17 V in pH 7 or at -0.07 V in pH 10, however, cannot be explained by the Pourbaix diagram.

The difference between polarization curves of lead in solutions with and without chloride present is surprising. The pH 10 polarization curve of Figure 33 is very similar in overall appearance to the nil chloride pH 10 curve shown in Figure 23. The presence of 0.1 M chloride seems to have little effect on the oxidation of lead in the bicarbonate buffer solution; the strong waves are found at approximately the same potentials and are of roughly the same magnitudes in both solutions.

The polarization curve in pH 7 chloride solution is

markedly different from that of the nil chloride one. The polarization curves were recorded in precisely the same manner with and without chlorides. The presence of 0.1 M Cl^- was expected to increase the conductivity of the solution and the reactivity of the lead causing stronger oxidative waves than in the same solution without chlorides. As seen in the polarization curves, the opposite effect occurred. Current remained very low in the presence of chloride. Polarization curves gave indication that something different occurs in the phosphate buffer solution when chlorides are present, but they give no hint as to what occurs. The only conclusion which can be reached is that the lead was oxidized more slowly when 0.1 M Cl^- was present in the pH 7 buffer than when it was not.

The exposure conditions selected using the Pourbaix diagram in Figure 32 and polarization curves in Figure 33, and the resulting surface film spectra are summarized in Table VII. The current values listed are those measured after current became relatively constant.

III.D.1. pH 1 Exposures.

In dilute hydrochloric acid, lead is stable at low potentials while it is oxidized to lead chloride at higher potentials (12,62). The potential of the Pb to lead chloride transition is calculated to be -0.20 V, and it is indicated at -0.08 V on the polarization curve. The low

potential reductive feature of the curve is undoubtedly due to the evolution of hydrogen.

In the region where immunity is predicted (exposures at -0.30 V and lower), net current flow was in the reducing direction and samples remained clean in appearance. In situ Raman spectra gave no indication of film formation. Lead seems to be immune to corrosion in this potential region.

After washing and drying samples exposed in the immunity region of the Pourbaix diagram, both Raman and infrared reflection spectra (71) indicated the presence of orthorhombic PbO on the lead surface. It is unlikely that the oxide was formed by oxidation of the lead under the generally reducing conditions observed, but the PbO was probably the result of dissolved lead being redeposited on the sample surface.

It has been suggested (69) that orthorhombic PbO is formed from the plumbous ion by the reaction:

$$Pb^{++} + H_2O \rightarrow PbO + 2H^{+} \qquad (10$$

Since lead is somewhat soluble in 0.1 M HCl, sufficient quantities of Pb^{++} to form an orthorhombic PbO surface coating go into solution when lead is exposed for several hours at potentials near the upper limit of the immunity region.

No Raman bands of orthorhombic PbO were found in the in situ spectra, whereas dry samples gave rather strong spectra, as shown in Figure 34. Samples were clean and shiny during controlled potential exposures, but acquired a

light gray, crystalline surface appearance upon drying. This may indicate that the oxide was formed during washing and drying of the sample surface, not during the potentiostatic exposure. Possibly Pb^{++} ions were too low in concentration to form a surface film while the potential was held in the immunity region but, when the applied potential was removed so the sample could be washed and dried, the lead surface may have rapidly oxidized. The mechanism of oxidation could be that of reaction 10, or some other, similar mechanism.

The Raman spectra of lead oxidized at potentials of +0.14 V and higher indicated the presence of a $PbCl_2$ surface layer. A typical surface film spectrum from the chloride region is shown in Figure 35. The spectrum is identical to that of pure lead chloride powder with bands at 62, 88, 126, 156, and 178 cm^{-1} (77,78). Oxidation currents in the chloride region were extremely high, approximately 10 mA/cm^2, and the samples quickly became covered with light gray, crystalline coatings.

In the potentiostatic exposures which formed lead chloride, a gray substance was deposited on the platinum mesh counter electrode (cathode). After removing the cathode from the solution it was allowed to dry at room temperature and the adherent gray material was scraped off of the platinum. Raman spectra of the dry material identified it as orthorhombic PbO, as shown in Figure 36. The presence of the oxide on the cathode, far from the lead

electrode, is proof that it was formed by deposition of dissolved species (such as Pb^{++} ions) in the solution. Since the formation of orthorhombic PbO seems to depend only on its solubility, not on any electrochemical reaction, it could be formed in other solutions. Due to the high rate of lead dissolution, as evidenced by the very high oxidation currents observed in the lead chloride region, a large amount of Pb^{++} was present to permit formation of thick orthorhombic PbO deposits. It is likely that lead chloride was formed at the lead anode and PbO at the platinum cathode because of the relative solubilities of the two species.

III.D.2. pH 7, 0.1 M Chloride Exposures.

According to the Pourbaix diagram of Figure 32, potentiostatic oxidation of lead in a pH 7, 0.1 M chloride solution should result in immunity at potentials below -0.26 V, formation of $3PbO \cdot PbCl_2$ between -0.26 V and +0.75 V, and formation of lead dioxide at higher potentials. The predicted compounds were not found experimentally.

In the region where immunity is predicted, i.e., below -0.26 V, the Pourbaix diagram, polarization curve, and spectroscopic results were all in agreement. Potentiostatic exposure resulted in a reducing current, the samples remained shiny and silver in color, and no Raman bands were observed from wet or dry samples.

Above the potential where lead is the stable species,

i.e., -0.34 V according to the polarization curve of Figure 33, current flow, although small, was in the oxidizing direction. The sample surfaces darkened quickly when electrochemical exposures were begun and became dark gray in color after a few hours. An insoluble oxidation product film was formed.

In situ Raman spectra of sample surfaces indicated that, at potentials between -0.11 V and +0.18 V, orthorhombic PbO was formed. At +0.18 V both orthorhombic and tetragonal PbO were observed and at higher potentials the films consisted of tetragonal PbO alone, as shown by the spectra of Figure 37.

No explanation has been found to explain why the two polymorphs of lead monoxide should be found at different potentials. The tetragonal form is thermodynamically favored under all conditions at room temperature (80). It is likely that a weak wave at approximately +0.16 V on the polarization curve indicates a PbO (orthorhombic) to PbO (tetragonal) transition, but such a transition is not reflected in the Pourbaix diagram which is based solely on thermodynamic equilibria.

There were no differences observed, other than spectral ones, between the exposures which formed orthorhombic PbO and those which resulted in tetragonal PbO films. In both cases the visual appearances were similar and, although the oxidation currents for exposures which resulted in orthorhombic PbO were slightly higher than for the others,

the differences were not large.

The effect of chloride ion concentration was investigated by conducting exposures at -0.01 V in the pH 7 buffer solution with two different KCl concentrations: 0.01 M and 0.1 M. In 0.01 M chloride solution, the oxidation product was tetragonal PbO, i.e., the same compound observed in nil chloride exposures under similar conditions. In 0.1 M chloride, orthorhombic PbO was formed. These results indicate that the presence of chloride ions is the factor which allows the formation of the thermodynamically unstable orthorhombic PbO layer. The presence of small amounts of impurities can stabilize the orthorhombic structure (81,82) at temperatures far below the 488°C transition to the tetragonal form (80). Although the effect of chloride on PbO stability has not been studied, it is reasonable that small amounts on the order of parts per million (too little to be detected by Raman spectroscopy) could prevent the transition to the tetragonal structure.

At higher potentials no other insoluble species was observed, all exposures formed tetragonal PbO. The polarization curve, showing no transitions at potentials above +0.16 V, agrees with the Raman results. These disagree with the Pourbaix diagram which predicts the formation of lead dioxide at high potentials.

Throughout a wide range of potentials in pH 7 chloride solutions, PbO was observed. No exposures resulted in $3PbO \cdot PbCl_2$ formation, the compound expected from Pourbaix

diagram cal ations. If such a compound had been formed, Raman spectra should have been able to identify it. Spectra of that compound, or the closely related species $(PbOH)_n Cl_n$ and $[Pb_8(OH)_{12}]_n Cl_{4n}$ (12,96) are very different from the PbO spectra recorded in this research. If any chloride had been present in the surface layer, it should have been detectable by X-ray energy dispersive analyzer. Examination of the exposed samples found only lead. This agrees with the formation of PbO because oxygen cannot be detected by the analyzer.

III.D.3. pH 10, 0.1 M Chloride Exposures.

According to the Pourbaix diagram, the results of potentiostatic exposures should be the same in pH 10 chloride solutions as in pH 7 but, experimentally, they are not. The polarization curves in the two solutions are quite different, and some significant differences were found by Raman spectroscopy. The differences are due, in part, to the composition of the pH 10 buffer used. They are also due to the nature of soluble lead species in basic solutions.

The pH 10 buffer gave slightly different results from those predicted in the immunity region. As seen in nil chloride exposures, lower potentials resulted in immunity while those in the region of lead stability in the Pourbaix diagram, but above -0.42 V, gave oxidizing currents and formed a thin film of basic lead carbonate. The large

oxidative wave at -0.35 V on the pH 10 polarization curve in Figure 33 apparently corresponds to a transition from lead to basic lead carbonate stability. Raman spectra of films resulting from exposure in this region consisted only of a weak band at 1050 cm^{-1} as shown in the poor quality spectrum of Figure 38. Reflection-absorption infrared spectra were required to identity the compound which comprised the invisible surface film as basic lead carbonate (71).

The experimentally determined composition of films formed electrochemically at higher potentials had no correlation with the predictions of the Pourbaix diagram. The compounds $3PbO \cdot PbCl_2$ and PbO_2 were predicted but neither was found. Spectroscopic results did show excellent agreement with the polarization curves, however. At potentials between the waves at -0.07 V and +0.96 V tetragonal PbO was found. No trace of the predicted chloride or of orthorhombic PbO was detected.

There seems to be a simple explanation for the appearance of orthrhombic PbO in acid and neutral solutions but not in basic media. The orthorhombic PbO is formed by deposition from a solution containing plumbous ions by reaction 10. The plumbous ion is present only in solutions with pH'S of 9.34 or less. At that pH the dissolved lead species, Pb^{++} and $HPbO_2^-$, are in equilibrium and, in more basic solutions, HPbO predominates (35). The Pb^{++} ions required for formation of orthorhombic PbO are not present in pH 10 solutions. Tetragonal PbO, however, is probably

formed at the lead surface, using no dissolved lead species, by the reaction:

$$Pb + H_2O \rightarrow PbO + 2H^+ + 2e^- \quad (11$$

Although the transition to a higher oxidation state predicted by the Pourbaix diagram would occur at approximately +0.50 V and result in PbO_2 formation, the transition found occurred at the +0.96 V wave of the polarization curve and resulted in formation of a thick layer of minium, Pb_3O_4. The Pb_3O_4 film appeared thick and flaky and it had a light brown color. The composition of the film was confirmed by comparison of its Raman spectrum with that of the pure compound as shown in Figure 39.

The discovery of a Pb_3O_4 film was rather surprising. It is a relatively unstable compound which has only been found in corrosion product films as an intermediate layer covered by a gray or black PbO_2 film (69). In the present investigation no PbO_2 was found. Since no Pb_3O_4 was found in nil chloride exposures, it appears that the presence of chloride ions permits the formation of Pb_3O_4 alone.

Several differences between 0.1 M chloride and nil chloride exposures were found. The most obvious differences were the formation of orthorhombic PbO and Pb_3O_4 films because of the presence of chloride ions. The other effect noted was the considerably lower current generally found during chloride exposures. The presence of a small amount of chloride seems to have the effect of making the solution less corrosive to lead. This finding agrees with others on the passivation of lead which found that increasing the concentration of dissolved chloride helped achieve

passivation more easily (62).

Study of the potentiostatic oxidation of lead in chloride solutions showed that changes in surface film composition agree very well with potentiodynamic polarization curves. There was very little agreement with the calculated Pourbaix diagram. Every wave of the polarization curves corresponded to a change in the surface layer that was detectable by Raman spectroscopy, but the changes had little relation to the predictions of the Pourbaix diagram.

In calculating the diagram, the presence of dissolved substances other than lead, oxide, or chloride species was not considered. The presence of buffer solution ions may account for the discrepancies between experimental results and those predicted by the Pourbaix diagram. In dilute hydrochloric acid, a relatively simple solution containing no unaccounted for ions, the Pourbaix diagram, polarization curve, and spectroscopic results were in agreement. The complexity of including all the species of buffer solutions makes calculation of the equilibria involved in a Pourbaix diagram an extremely complicated process but one which might give results more closely related to experimental findings.

III.E. Lead-Water-Sulfate Pourbaix Diagram

The behavior of lead in sulfuric acid solutions has been thoroughly studied because of the importance of lead-acid

storage batteries. Much less research has been conducted on lead in neutral and basic sulfate solutions. Pourbaix diagrams for lead in aqueous sulfate solutions have been calculated (56,67,68), and some efforts have been made to experimentally verify the theoretical predictions, although experimental sulfate exposures have been confined to the acid and neutral regions of the diagram (56,69).

The Pourbaix diagram for the lead-water-sulfate system was calculated using the relationships used by Ruetschi and Angstadt (56) but employing more recent free energy values (90). The different thermodynamic data, summarized in Table VIII, caused only small changes in the positions of the $PbO \cdot PbSO_4$ equilibria lines. A sulfate ion activity of 0.1 was used for the calculations (71) resulting in the Pourbaix diagram shown in Figure 40.

Electrochemical exposures in sulfate solutions were not carried out in buffer solutions. The solutions chosen, the compositions of which are detailed in Table II, were simple solutions of the desired pH which were 0.1 molar in sulfate. Those used gave pH values of approximately 1, 6.5, and 11 to allow observation of the reactions of lead over a wide portion of the Pourbaix diagram. Measurement of solution pH before and after potentiostatic exposures showed that the pH of the unbuffered solutions remained fairly constant, not changing by more than 0.6 after as long as twenty-four hours.

The polarization curves recorded for lead in the sulfate

solutions of interest are shown in Figure 41. They are rather similar, each has a strong wave at approximately -0.25 V as its major point. These waves mark the transition from reduction to oxidation, the upper limit of potential of the immunity region. In accordance with the Pourbaix diagram, the potential of such a transition decreases as pH increases. The oxidative wave was observed at -0.23 V in pH 1, -0.27 V in pH 6.5, and -0.30 V in pH 11. The positions of these waves are in general agreement with the Pb to $PbSO_4$ and Pb to $PbO \cdot PbSO_4$ transitions of the Pourbaix diagram.

III.E.1. pH 1, 0.1 M Sulfate Exposures.

In the 0.1 M sulfuric acid solutions used to attain acidic conditions, lead is stable at low potentials while it is oxidized to lead sulfate at higher potentials (56-58). After formation of a sulfate surface film thick enough to hinder reactions of lead with solution species, layers of PbO or basic lead sulfates develop under the sulfate film at potentials of +0.32 V and higher (52,56,57). While the formation of underlying layers was not considered in the calculation of the Pourbaix diagram (71), the very weak wave at +0.34 V on the polarization curve may indicate the start of formation of another compound beneath the sulfate film.

Potentiostatic exposures of lead in 0.1 M sulfuric acid formed surface films whose compositions agreed well with X-ray diffraction work by Pavlov and Iordanov (52). Raman

spectroscopic results indicated three ranges of potential: immunity, lead sulfate, and a lead sulfate - lead monoxide region. A summary of the experimental results of exposure in sulfate solutions is presented in Table IX.

At potentials below -0.26 V lead appeared to be immune to oxidation. No insoluble surface layer was detected by in situ Raman spectroscopy, samples remained clean and shiny, and current flow was in the reducing direction. When samples exposed in this region were washed and allowed to dry a non-uniform, light gray surface coating appeared. Spectra of dry samples indicated that parts of their surfaces were covered with orthorhombic PbO and parts with $PbSO_4$. The appearance of these compounds, just like the appearance of orthorhombic PbO in the immunity region exposures in 0.1 M hydrochloric acid, probably results from precipitation of dissolved lead ions. In the reducing conditions of this region it is unlikely that any lead would be directly oxidized at the electrode surface during the potentiostatic exposure. The formation of PbO and lead sulfate is probably a result of the sample removal, washing, and drying process.

At potentials higher than the -0.23 V wave of the polarization curve, net current flow was in the oxidizing direction and spectra showed that lead sulfate was formed. Oxidation at -0.26 V and -0.02 V resulted in $PbSO_4$ films.

Exposure at potentials higher than the wave at +0.34 V gave surface films identified as tetragonal PbO and $PbSO_4$,

in agreement with the findings of earlier research (51,52). A spectrum of the film in this potential region is compared with one of a purely $PbSO_4$ film and with the Raman spectrum of reagent grade $PbSO_4$ (97) powder in Figure 42. The spectra of sulfate compounds are dominated by the very strong sharp band at 979 cm^{-1}, the S-O symmetric stretch (98).

Although it was not possible to measure the relative amounts of PbO and lead sulfate in the surface films from Raman spectra, just as it was impossible to identify film thickness, observation of strong tetragonal PbO spectra gave an indication of the thickness of film analyzed by this technique. Ruetschi (57) developed a model for the $PbO/PbSO_4$ two phase film formed by oxidation of lead in sulfuric acid solutions. He assumed that a surface film with a thickness on the order of a micron was needed before any underlying tetragonal PbO could form (56). Electrochemical measurements and calculations based on ion diffusivity in the films determined that a twenty-four hour exposure of lead in 4.2 M sulfuric acid in the range of +0.2 to +1.1 V would give a film consisting of one micron of lead sulfate covering one micron of tetragonal lead monoxide. The ability to record a strong spectrum of the underlying layer of PbO gives indication that Raman spectroscopy can examine the entirety of films with thicknesses on the order of a micron.

The ability of laser light to penetrate the surface

sulfate film was also demonstrated by current vs. time plots such as that shown in Figure 43. The increase in oxidation current due to laser radiation was identical to behavior observed for surface films which consisted solely of tetragonal PbO.

The commencement of PbO formation may be indicated by the current plateau of the i vs. t curve shown in Figure 44. Exposures which gave spectra of tetragonal PbO and $PbSO_4$ together all had a current plateau or maximum after a period of exposure ranging from 0.5 to 1.5 hours. Observation of such current behavior was interpreted to indicate the beginning of a new electrochemical reaction, the formation of PbO, by Ruetschi and Angstadt (56). This interpretation may be correct, but it was not confirmed by Raman spectra. At potentials above +0.34 V spectra indicated the presence of both PbO and $PbSO_4$ on the lead surfaces. None of the exposures in that region gave any spectra of $PbSO_4$ alone, even with spectra recorded after as little as twenty minutes of oxidation, before the current plateau occurred. The Raman method was unable to find any film which consisted of lead sulfate alone, before formation of the oxide began.

III.E.2. pH 6.5, 0.1 M Sulfate Exposures.

The lead-water-sulfate Pourbaix diagram predicts that, in a pH 6.5, 0.1 M sulfate solution, lead should be stable at potentials below -0.3 V, PbO_2 should exist above +0.5 V,

and $PbSO_4$ should be found at potentials in between. The lower transition was observed in the polarization curve for lead in the 0.1 M potassium sulfate used, but no transition to PbO_2 was observed. The polarization curve shows a weak wave at +0.06 V which does not correspond to any feature of the Pourbaix diagram.

As in other solutions, potentiostatic exposures resulted in films whose compositions were in better agreement with the polarization curve than with the Pourbaix diagram. Exposure at potentials below the -0.27 V wave resulted in immunity. Current flow was in the reducing direction, the surface remained clean and shiny, and no Raman spectrum was obtained in solution or in air. Higher potentials resulted in oxidation of the lead electrode and formation of insoluble surface films. Up to +0.24 V, films consisted of lead sulfate and, above that, tetragonal lead monoxide covered the sample surfaces.

The formation of lead sulfate was in agreement with the Pourbaix diagram, but the $PbSO_4$ gave slightly different spectra from the sulfates examined previously. As shown in Figure 46, the sulfate film gave an exceptionally strong 451 cm^{-1} band, the band associated with the O-S-O bending vibration (98). Infrared reflection spectra of the films also showed a band at 451 cm^{-1} (71). Such a vibration is not infrared active in normal sulfate compounds. The unusual intensity of the 451 cm^{-1} band is assumed to be due to a distortion of the normal lead sulfate lattice.

The broad wave at +0.06 V is near the potential where film composition changed from lead sulfate to PbO, and it may be due to such a transition. Lead monoxide films produced were black in color and gave no evidence of the presence of sulfate. No waves were observed at higher potentials and Raman spectra indicated no change to the PbO_2 predicted by the Pourbaix diagram.

An exposure was conducted in the pH 7, phosphate, buffer solution to which was added enough potassium sulfate to make the solution 0.1 M in sulfate. Oxidation at +0.24 V formed a dark layer of tetragonal PbO. The composition was determined from the Raman spectrum. Another exposure at +0.24 V in 0.1 M potassium sulfate, but without the phosphate buffer, resulted in the formation of lead sulfate. As expected, the presence of buffer species can complicate the system and give different results from those of the simple systems considered in the thermodynamic calculations.

III.B.3. pH 11, 0.1 M Sulfate Exposures.

Oxidation of lead in 0.1 M sulfate solutions at a pH of 11 was predicted to form a basic lead sulfate, $PbO \cdot PbSO_4$, at potentials between -0.45 V and +0.50 V and lead dioxide at higher potentials. The solution used, 0.1 M potassium sulfate with enough KOH added to make the initial pH 11, resulted in a polarization curve with only one clear oxidation feature. The experimentally observed wave, or

group of waves, at approximately -0.30 V represents the transition from lead stability to the formation of an oxidized species. The oxidative change seen above +0.80 V in Figure 41 could represent a transition to a higher oxidation state, but it seems to be due to the decomposition of water to evolve oxygen.

Potentiostatic exposures were conducted throughout the potential range where water is stable. As expected, exposure at low potentials gave extremely low current flow in the reducing direction and no Raman bands were observed. Below the -0.30 V wave of the polarization curve lead is immune to oxidation.

All exposures at higher potentials resulted in the formation of tetragonal PbO surface films. An oxidation at -0.34 V, a potential higher than the first lobe of the oxidative wave, resulted in a film which gave a strong tetragonal PbO spectrum. Although the wave at -0.30 V seems to be made up of three seperate waves, all exposures at potentials above -0.45 V, where the current recorded in the polarization curve first became oxidative, formed tetragonal PbO.

Although the composition of the films was identified as PbO, spectra recorded in solution were somewhat misleading. In situ spectra, as shown in Figure 46, contained the strong bands of tetragonal PbO but also the 980 cm^{-1} band characteristic of the S - O symmetric stretch and a broad band in the 450 cm^{-1} region. Except for the broadness of

the 450 cm^{-1} band, these spectra look like a mixture of PbO and lead sulfate. Upon washing the samples thoroughly, however, those bands characteristic of sulfate disappeared. Dry sample spectra indicated only tetragonal PbO. The sulfate bands, which can be distinguished from those of $PbSO_4$ by the broad 450 cm^{-1} band (lead sulfate has two sharp bands in that region, 439 and 451 cm^{-1}), are due to the sulfate of the solution. The bulk sulfate solution gave the same sulfate spectrum. The change in the spectrum caused by washing the samples was evidence that spectra of both wet and dry samples were needed to distinguish solution or adsorbed species from those compounds which were actually part of an insoluble surface film.

The possibility that the surface layer might consist of $PbO \cdot PbSO_4$ as predicted by Pourbaix diagram calculations was investigated. Although spectra of the sample surfaces identified tetragonal PbO, no Raman spectra of the basic sulfate are available. Infrared reflection spectra confirmed that tetragonal PbO was the compound present (71). Comparison with published infrared spectra of $PbO \cdot PbSO_4$ (99) showed no trace of that compound.

The oxidation currents recorded during potentiostatic exposures and potentiodynamic polarization curve measurements confirmed that lead sulfate forms more protective surface films than does PbO. In 0.1 M sulfate solutions, all of which had approximately the same conductivity and ionic strength, conditions which caused the

formation of PbO resulted in net current flow 5 - 10 times greater than that observed when $PbSO_4$ was formed. The smallest differences were noted in pH 6.5 exposures, a pH near the minimum of PbO solubility (35), but even in those conditions oxide films allowed measurably higher current flow than sulfate films. The ability of sulfates to form an insoluble, passivating film on lead is well known. Because of its behavior in sulfate-containing solutions, lead equipment is used extensively in the manufacture of sulfuric acid (47).

III.F. Film Thickness Studies

Potentiostatic exposures of vacuum deposited lead samples were conducted so that the thickness of the resultant films could be measured and their spectra recorded. While films of organic compounds on silver mirrors have shown that Raman spectra of films as thin as 50 angstroms can be recorded (18,19), no studies of the sensitivity of this technique for examining inorganic oxide films on a metal substrate have been conducted.

A vacuum deposited lead sample was exposed to a pH 7, phosphate, buffer solution at +0.20 V for 45 minutes. Stylus measurement found the oxide film thickness to be 1620±40 angstroms. The Raman spectrum of the PbO film is shown in Figure 47. The spectrum identified the film composition as orthorhombic PbO.

Because lead sulfate films tended to be rough, consisting of fairly large crystals (50-53,71), accurate direct measurement of sulfate film thickness was difficult. The thickness of the lead sample was measured before oxidation, and the value found was multiplied by 4.12 to give an estimate of the thickness if all of the lead were oxidized to lead sulfate. The factor, 4.12, was an average ratio of $PbSO_4$ film to Pb thickness measured for several exposed samples.

A lead sulfate film, estimated to be 2140±60 angstroms thick, was formed by oxidation at +0.80 V in 0.1 M sulfuric acid for 15 minutes. The spectrum of Figure 48 shows that the strong sulfate bands are clearly visible, although grating ghosts are nearly as strong as the Raman bands. Exposure of solid lead electrodes under the same conditions formed a film consisting of both lead sulfate and tetragonal PbO, but the vacuum deposited sample showed no trace of PbO. Presumably the thin sulfate film was not thick enough to provide a diffusion barrier to allow the formation of an underlying PbO layer.

Both the 1620 angstrom PbO and the 2140 angstrom lead sulfate films gave reasonably strong spectra, with bands much stronger than the background noise. It is estimated that a film approximately one tenth as thick would still give spectra with signal to noise ratios of two or more, the ratio considered necessary for observation of a band. Films of these compounds as thin as 200 angstroms should be

observable by the Raman technique. When considering minimum film thickness it must be remembered that Raman scattering intensities can vary greatly from one compound to another so the 200 angstrom value may not be useful for films of other compounds.

Single spectrometer scans were used to record all spectra. Greater sensitivity to very thin films could be attained by averaging the results of multiple scans. Signal averaging of more than one scan of the spectral region of interest should increase the signal to noise ratio observed and reduce the minimum detectable thicknesses (100).

III.G. Iron Exposures

Some research was conducted to investigate the feasibility of using Raman spectroscopy for the study of iron corrosion. The work was conducted in two phases. Since Raman spectra of very few oxides of iron are available in the literature, recording reference spectra of the compounds expected as corrosion products was the initial phase. After spectra of the important iron oxides were recorded, the second phase, using spectroscopy to identify the surface compounds formed by high temperature oxidation of iron was begun.

As demonstrated by spectra of PbO, in addition to identifying specific compounds, vibrational Raman spectra can easily identify different crystalline forms of the same

compound. This ability is a valuable asset in the study of iron oxidation because nearly all of the oxides of iron can exist as two or more polymorphs. The spectra of the two most common forms of FeOOH are shown in Figure 49. Although their chemical compositions are the same, different crystal structures and, therefore, different bonding and symmetry cause very different Raman spectra. The strong bands at 397 (alpha form) or 252 cm^{-1} (gamma form) immediately identify the two oxyhydroxides; no other iron oxide has been found to have bands at these positions.

The Raman bands observed from bulk samples of iron oxides are listed in Table X. The spectrum of alpha ferric oxide is identical to that of the single crystal, the only previously published iron oxide spectrum (101). As shown in Figure 50, the spectra recorded from FeO and Fe_3O_4 samples are the same. The samples consisted of two distinct compounds, as confirmed by their X-ray diffraction patterns, but the spectra are identical. It may be that the vibrations which cause Raman bands in Fe_3O_4 are due to Fe - O bonds which are nearly identical to those of FeO, but a more likely explanation is that the FeO, which is unstable at temperatures below 570°C (102), was decomposed by the laser.

The problem of sample decomposition is a common one when opaque samples are examined using relatively intense laser excitation. Visible light is strongly absorbed by black FeO, and heating due to the absorption of the excitation

beam may transform it into Fe_3O_4 and Fe, the stable species at room temperature. Both Fe_3O_4 and FeO are black and presented problems with decomposition in the laser beam. After a period of exposure spectral intensity decreased and the surface of a pellet of either compound was visibly changed. The spot of laser incidence became much lighter in color.

Decomposition due to the excitation beam was a less serious problem with the red-brown compounds, α- and γ-FeOOH and ferric oxide. The use of relatively low intensity excitation, either by lowering the power of the laser or by placing neutral optical density filters in the beam, allowed the recording of much higher quality spectra of these compounds than were obtained from the black species.

As an example of the ability of Raman spectroscopy to characterize corrosion product films on iron surfaces, polished Armco iron plates were oxidized in air in a laboratory oven and examined. Spectra resulting from oxidation at 250°C are shown in Figure 51. The Raman spectra identify the surface films as Fe_3O_4 and α-Fe_2O_3. The Fe_3O_4 bands at 616 and 663 cm^{-1} can be seen in all three spectra, while at first only the strongest Fe_2O_3 bands could be seen. After 217 hours of exposure all seven bands of α-Fe_2O_3 were visible. Bands due to both compounds increased in intensity throughout the exposures, indicating that both the Fe_3O_4 and α-Fe_2O_3 layers were thickening.

After oxidation of iron under conditions similar to

those reported here, Poling (103) found an oxide film thickness of approximately 500 angstroms for a 50 hour exposure at 250°C. If the 50 hour spectrum in Figure 51 results from a 500 angstrom thick oxide film, an α-Fe_2O_3 film of 100 - 200 angstroms is probably the minimum necessary before spectra useful for identification could be observed with a single scan. For thinner films the bands would probably not be discernable above the noise.

An iron sample was oxidized in air at 700°C for twenty hours and quenched in water in an effort to retain the FeO, which should have formed, without allowing it to transform to a more stable compound as it does during slow cooling below the 570°C transition temperature (103). The Raman spectrum of the sample surface shown in Figure 52 identified only α-Fe_2O_3, with no indication of FeO or Fe_3O_4. It is well documented that exposure at 700°C forms FeO (104), so the spectrum of Figure 52 must be taken as evidence that FeO does not give a Raman spectrum.

Apparently the only Raman bands seen from FeO are from its decomposition product, Fe_3O_4. In a KBr pellet, heat transfer away from the point of laser incidence is very poor, so absorption of laser light can heat the local area and decompose it to Fe_3O_4 and Fe. A thin film of FeO on an iron surface, however, has the iron to conduct heat away from the point of incidence. The FeO film need not be decomposed by the excitation necessary to record a Raman spectrum. Therefore, although present on the surface, no

FeO was detected in the spectrum of Figure 52.

A clean iron sample was suspended in boiling 0.01 M NaOH solution for 168 hours and then removed. It gave the spectrum shown in Figure 53. The spectrum confirmed that the thick black surface coating consisted of Fe_3O_4, in agreement with work which used other analysis techniques (103). The relatively poor quality of the spectrum is due to the poor Raman scattering characteristics of Fe_3O_4, not because of the nature of the film. After 168 hours of exposure, the black surface layer was very thick, probably hundreds of microns.

TABLE III

Results of Simple Immersion Exposures

CONDITION	EXPOSURE PERIOD, DAYS	SPECTRUM OBSERVED
a	7	$PbCl_2$
b	12	$PbCl_2$
b	15	$PbCl_2$
b	19	$PbCl_2$
c	2	$PbCl_2$
c	3	$PbCl_2$
c	7	$PbCl_2$
c	9	$PbCl_2$
d	14	$PbBr_2$
e	8	$PbBr_2$
e	34	$PbBr_2$
f	20	tetragonal PbO
f	26	tetragonal PbO
g	4	$(PbCO_3)_2 \cdot Pb(OH)_2$
h	5	$(PbCO_3)_2 \cdot Pb(OH)_2$

TABLE IV

Free Energy Data Used to Calculate the Lead - Water Pourbaix Diagram

SPECIES	STANDARD FREE ENERGY OF FORMATION (cal/mole)	
	NBS (90)	Pourbaix (35)
Pb^{++}	-5,830	-5,810
PbO (orthorhombic)	-44,910	-45,050
PbO (tetragonal)	-45,160	-45,250
PbO_2	-51,950	-52,340
Pb_3O_4	-143,700	-147,600

TABLE V

Results of Potentiostatic Exposures

in Nil Chloride Buffer Solutions

SOLUTION	VOLTS vs. SHE	EXPOSURE PERIOD, HRS.	CURRENT mA/cm² (a)	SPECTRUM OBSERVED
1	-0.62	17	0.002(b)	none
1	-0.62	19	0.001(b)	none
1	-0.16	20	0.006	none
1	-0.12	18	0.061	tetr. PbO
1	+0.06	2.8	0.112	tetr. PbO
1	+0.48	21		tetr. PbO
1	+0.58	3		tetr. PbO
1	+0.67	2	0.310	tetr. PbO
1	+0.74	23.5	0.397	tetr. PbO
1	+1.08	1.5	0.310	tetr. PbO
1	+1.08	18	0.294	tetr. PbO
2	-0.80	20.5	0.139(b)	none
2	-0.42	18	0.024	carbonate(c)
2	-0.28	4		tetr. PbO and carbonate(c)
2	-0.26	21	0.014	tetr. PbO
2	-0.03	17	0.046	tetr. PbO
2	+0.02	23		tetr. PbO
2	+0.24	17	0.054	tetr. PbO
2	+0.34	2	0.455	tetr. PbO
2	+0.46	2.5	0.210	tetr. PbO

SOLUTION	VOLTS vs. SHE	EXPOSURE PERIOD, HRS.	CURRENT mA/cm² (a)	SPECTRUM OBSERVED
2	+0.75	0.75		tetr. PbO
2	+0.75	18		tetr. PbO
2	+0.84	1.5	0.115	tetr. PbO
2	+0.94	0.1	0.175	tetr. PbO
2	+0.94	17.5	0.091	tetr. PbO
2	+1.24	17	1.20	tetr. PbO

Notes

(a) Final or steady current

(b) Current flow in reducing direction

(c) Basic lead carbonate

TABLE VI

Free Energy Data Used to Calculate

the Lead - Water - Chloride Pourbaix Diagram

SPECIES	STANDARD FREE ENERGY OF FORMATION (cal/mole)	
	NBS (90)	Appelt (66)
OH^-	-37,594	-37,595
Cl^-	-31,372	-31,350
$PbCl_2$	-75,080	-75,040
$3PbO \cdot PbCl_2$	-224,686	-225,000

TABLE VII

Results of Potentiostatic Exposures

in 0.1 M Chloride Solutions

SOLUTION	VOLTS vs. SHE	EXPOSURE PERIOD, HRS.	CURRENT mA/cm² (a)	SPECTRUM OBSERVED
3	-0.46	16.5	0.011 (b)	none (c)
3	-0.30	2.25	0.120 (b)	none (c)
3	+0.14	3	7.30	$PbCl_2$
3	+0.69	2.5	6.80	$PbCl_2$
3	+1.09	17	10.0	PbCl
4	-0.62	3	(b)	none
4	-0.11	17	0.020	ortho. PbO
4	-0.01	2	0.022	ortho. PbO
4	+0.18	18	0.019	ortho. PbO and tetr. PbO
4	+0.49	17		tetr. PbO
4	+0.68	18	0.012	tetr. PbO
4	+0.99	18	0.022	tetr. PbO
4	+1.08	1.5	0.380	tetr. PbO
5	-0.42	17	(b)	none
5	-0.26	3.1	0.007	carbonate (d)
5	-0.01	2	0.014	tetr. PbO
5	+0.08	22	0.012	tetr. PbO
5	+0.49	17		tetr. PbO

SOLUTION	VOLTS vs. SHE	EXPOSURE PERIOD, HRS.	CURRENT mA/cm² (a)	SPECTRUM OBSERVED
5	+0.74	17	0.034	tetr. PbO
5	+1.07	18	0.028	Pb_3O_4

Notes

(a) Final or steady current

(b) Current flow in reducing direction

(c) Some orthorhombic PbO observed on dried sample surface

(d) Basic lead carbonate

TABLE VIII

Free Energy Data Used to Calculate

the Lead - Water - Sulfate Pourbaix Diagram

SPECIES	STANDARD FREE ENERGY OF FORMATION (cal/mole)	
	NBS (90)	Ruetschi and Angstadt (56)
SO_4^{2-}	-177,970	-177,340
HSO_4^-	-180,690	-179,940
Pb_3O_4	-143,700	-147,600
$PbSO_4$	-194,360	-193,890
$PbO \cdot PbSO_4$	-246,700	-243,200

TABLE IX

Results of Potentiostatic Exposures

in 0.1 M Sulfate Solutions

SOLUTION	VOLTS vs. SHE	EXPOSURE PERIOD, HRS.	CURRENT A/cm² (a)	SPECTRUM OBSERVED
6	-0.46	19.5	73 (b)	none (c)
6	-0.26	18	19.7	$PbSO_4$
6	-0.02	4	13.3	$PbSO_4$
6	+0.48	17.5	15.7	tetr. PbO and $PbSO_4$
6	+0.80	20	12.8	tetr. PbO and $PbSO_4$
6	+1.24	2.5	48.4	tetr. PbO and $PbSO_4$
7	-0.46	21	9.4 (b)	none
7	-0.16	19	1.7	$PbSO_4$ (d)
7	+0.24	1.7	4.2	$PbSO_4$ (d)
7	+0.84	20	6.3	tetr. PbO
7	+0.94	3	19.6	tetr. PbO
8	-0.51	18		none (e)
8	-0.34	18.5	24.2	tetr. PbO
8	-0.25	2.2	109	tetr. PbO
8	-0.08	3.5	121	tetr. PbO
8	+0.34	1.7	256	tetr. PbO
8	+0.74	2.5	125	tetr. PbO
8	+1.09	2	243	tetr. PbO

Notes

(a) Final or steady current

(b) Current flow in reducing direction

(c) Dry sample spectrum indicated lead sulfate and orthorhombic PbO

(d) Band at 45[illegible] normal intense

(e) Dry sample spectrum indicated orthorhombic PbO

TABLE X

Frequencies of Iron Oxide Raman Bands

COMPOUND		BAND POSITIONS, cm^{-1}
α-FeOOH	goethite	298 397 414 474 550
γ-FeOOH	lepidocrocite	252 380
FeO	wustite	616 663
Fe_3O_4	magnetite	616 663
α-Fe_2O_3	hematite	227 245 293 298 414 501 612

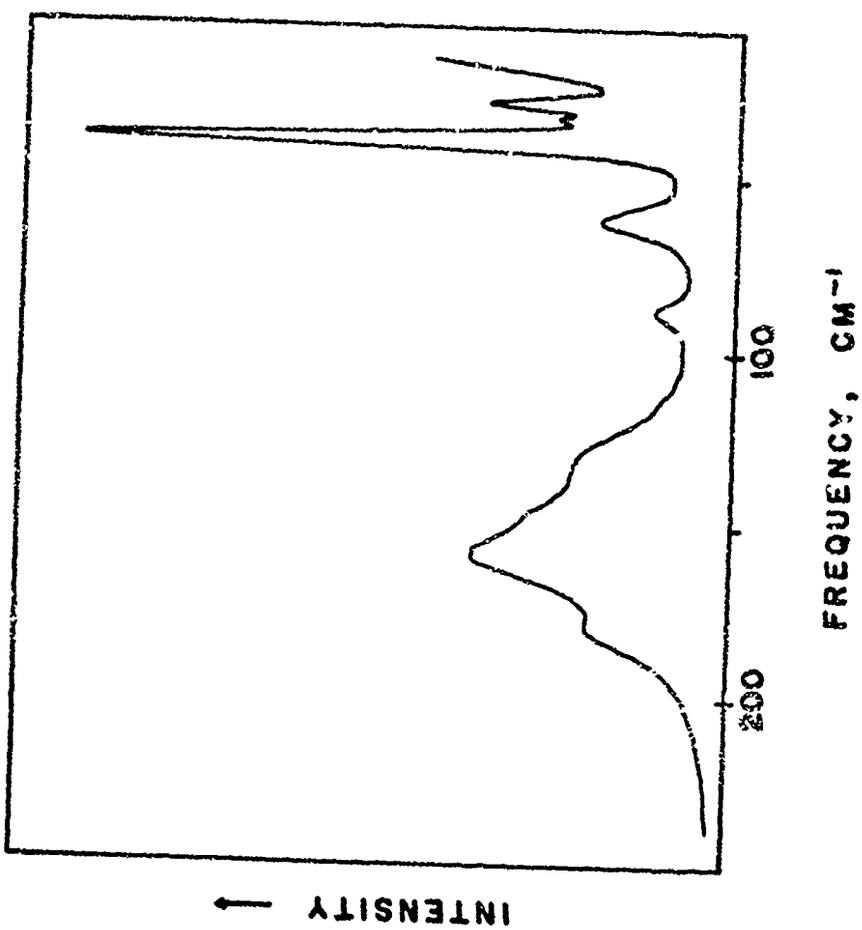

Figure 10. Raman spectrum of reagent grade lead chloride powder.

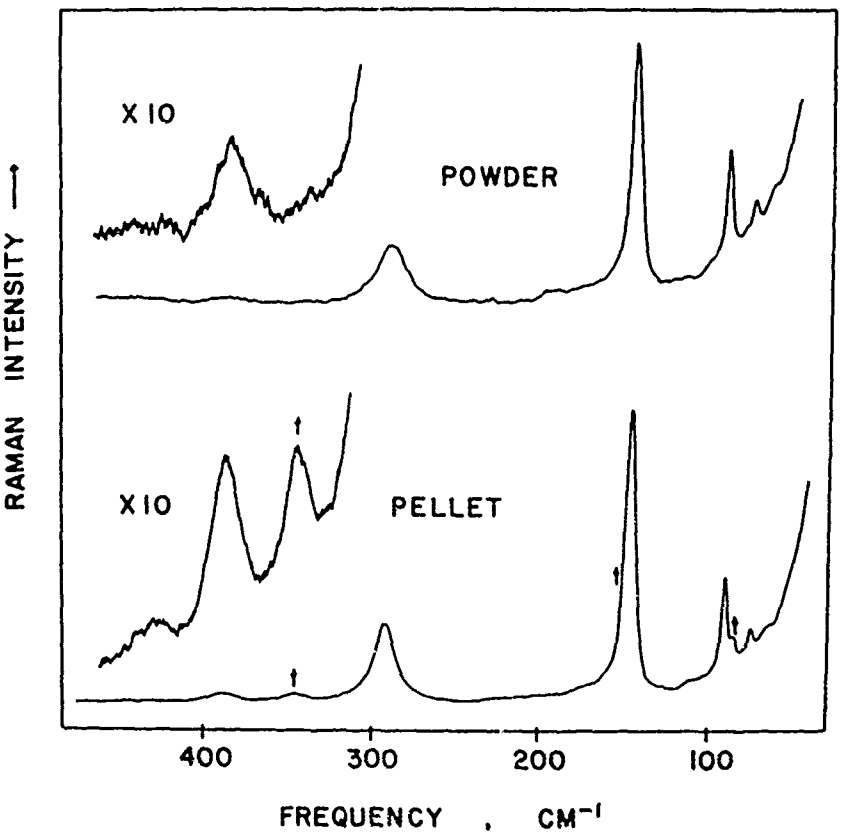

Figure 11. Raman spectra of orthorhombic PbO powder and of the same powder after being made into a KBr pellet, demonstrating that the pellet making process causes a transformation to tetragonal PbO.

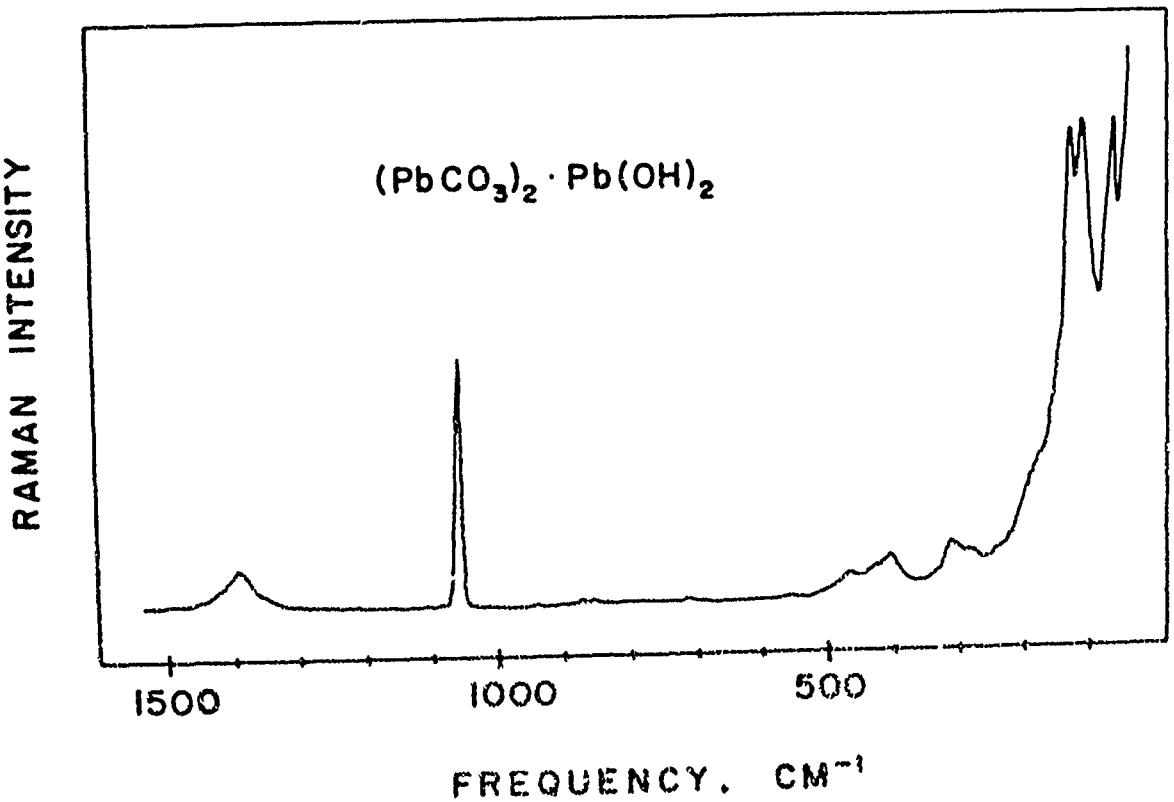

Figure 12. Raman spectrum of reagent grade basic lead carbonate.

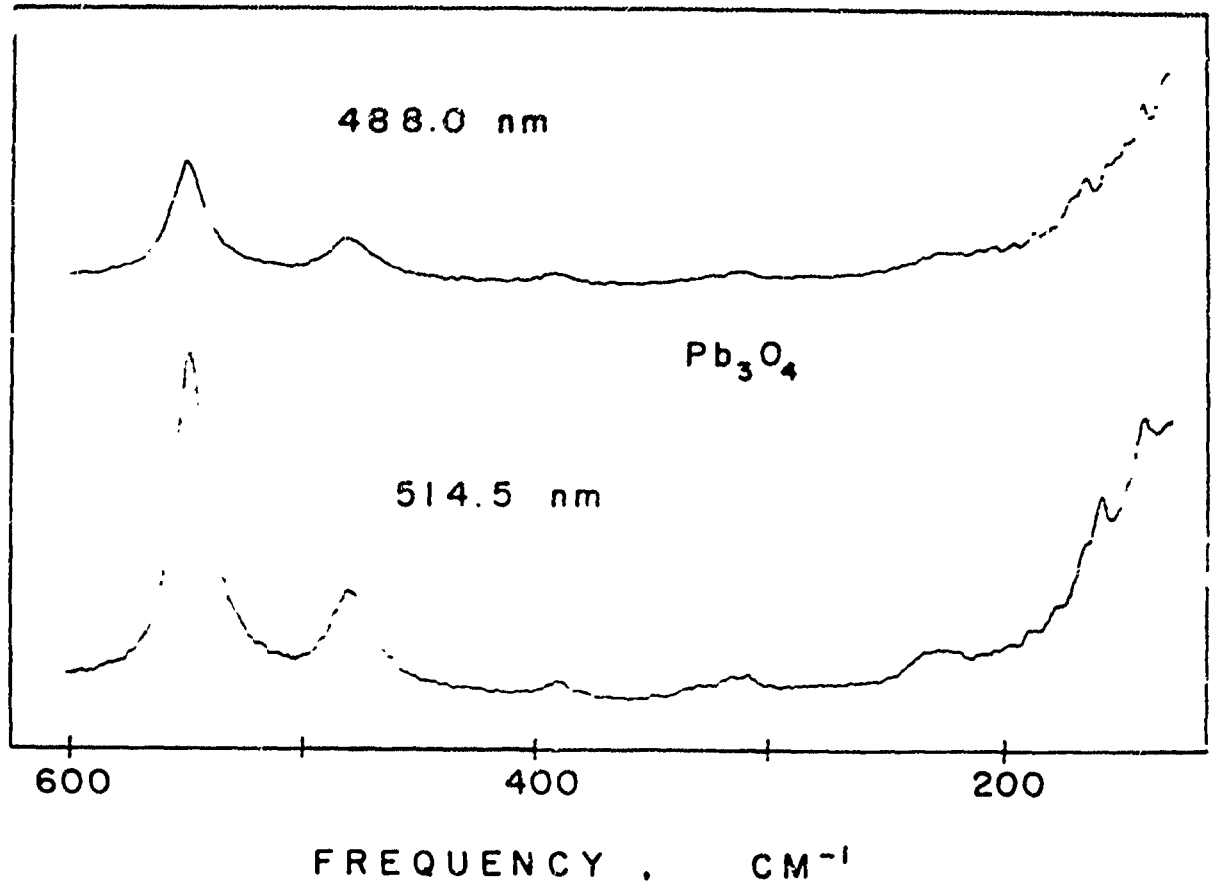

Figure 13. Raman spectrum of Pb_3O_4 in a KBr pellet using 488.0 and 514.5 nm. laser lines.

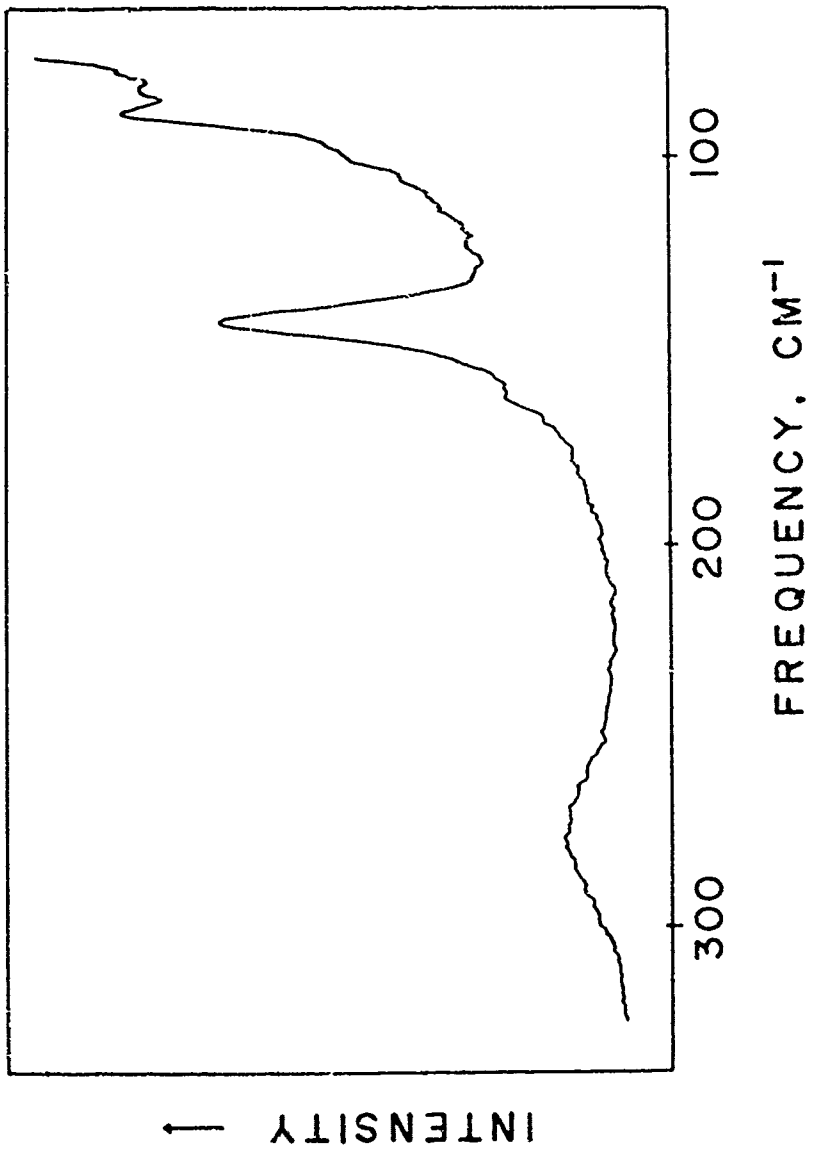

Figure 14. Raman spectrum of a lead dioxide, KBr pellet after exposure to the 514.5 nm. laser line for one hour.

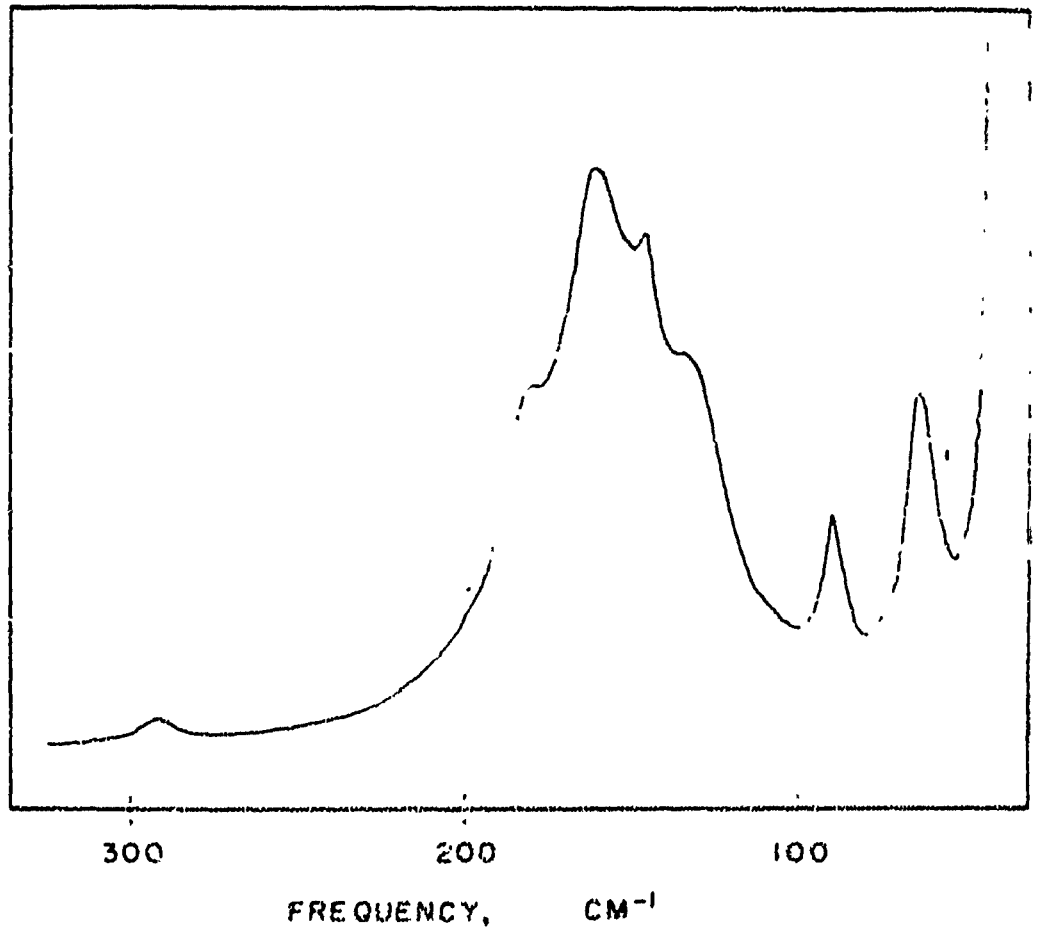

Figure 15. Raman spectrum of lead chloride powder containing 0.95% orthorhombic PbO by weight.

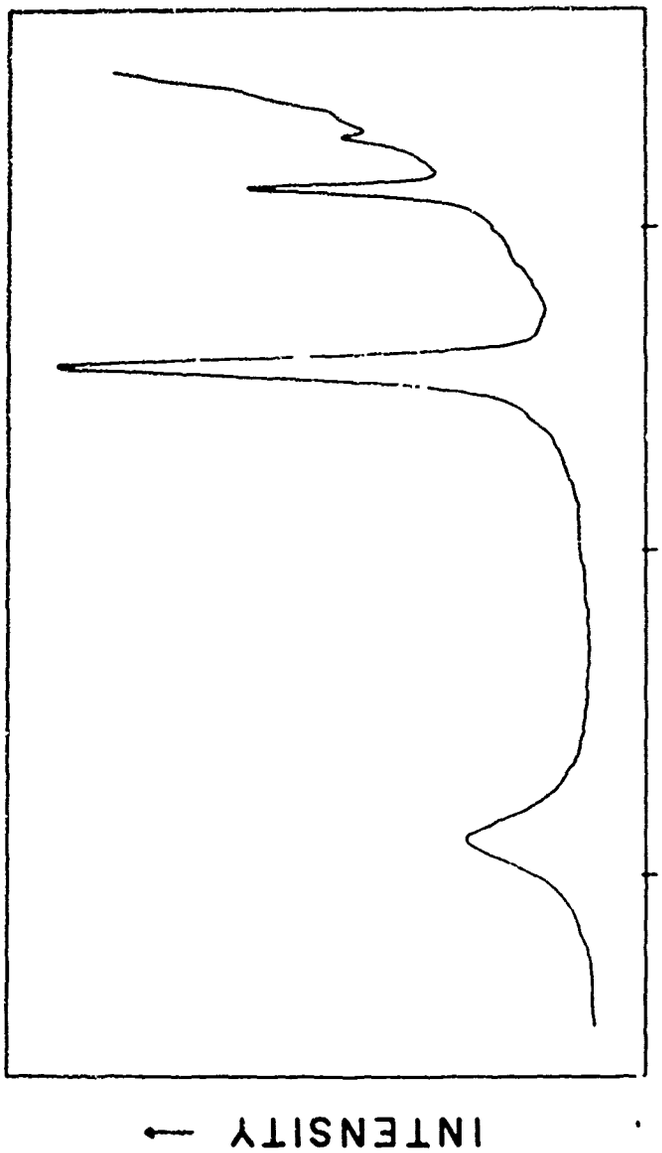

Figure 16. Raman spectrum of orthorhombic PbO powder containing 16% lead chloride by weight.

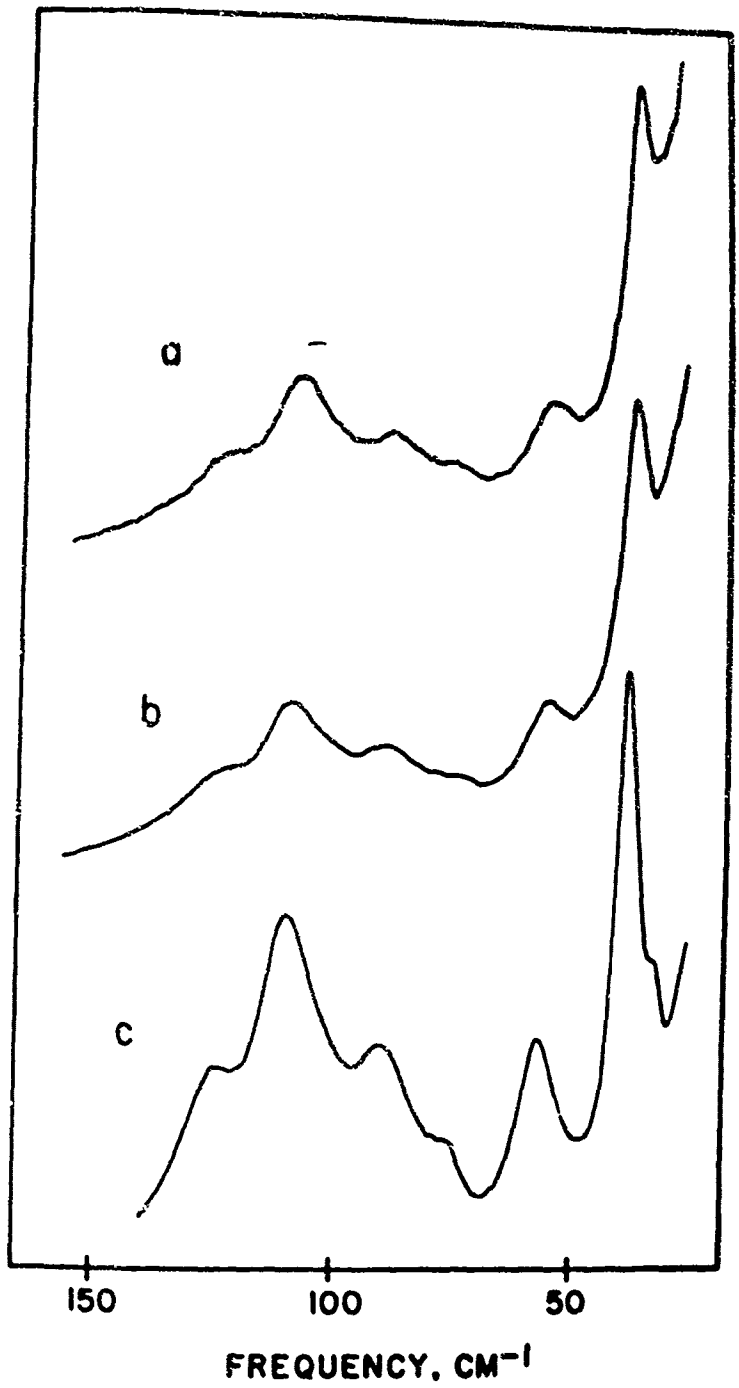

Figure 17. Raman spectra of a) the surface of lead foil immersed in deaerated 2.3M HBr solution for 8 days, b) lead bromide powder from crystals formed on lead in 2.3M HBr after 34 days, c) reagent grade lead bromide powder.

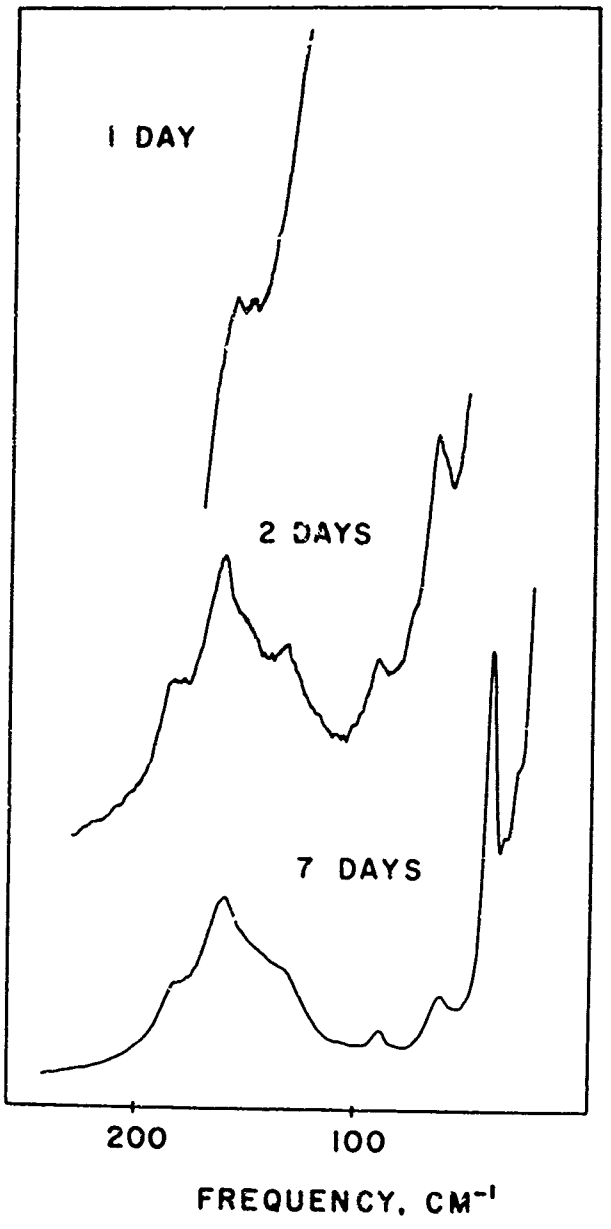

Figure 18. Raman spectra of the lead chloride film on a lead surface exposed to air saturated 0.1M HCl solution for 1, 2, and 7 days.

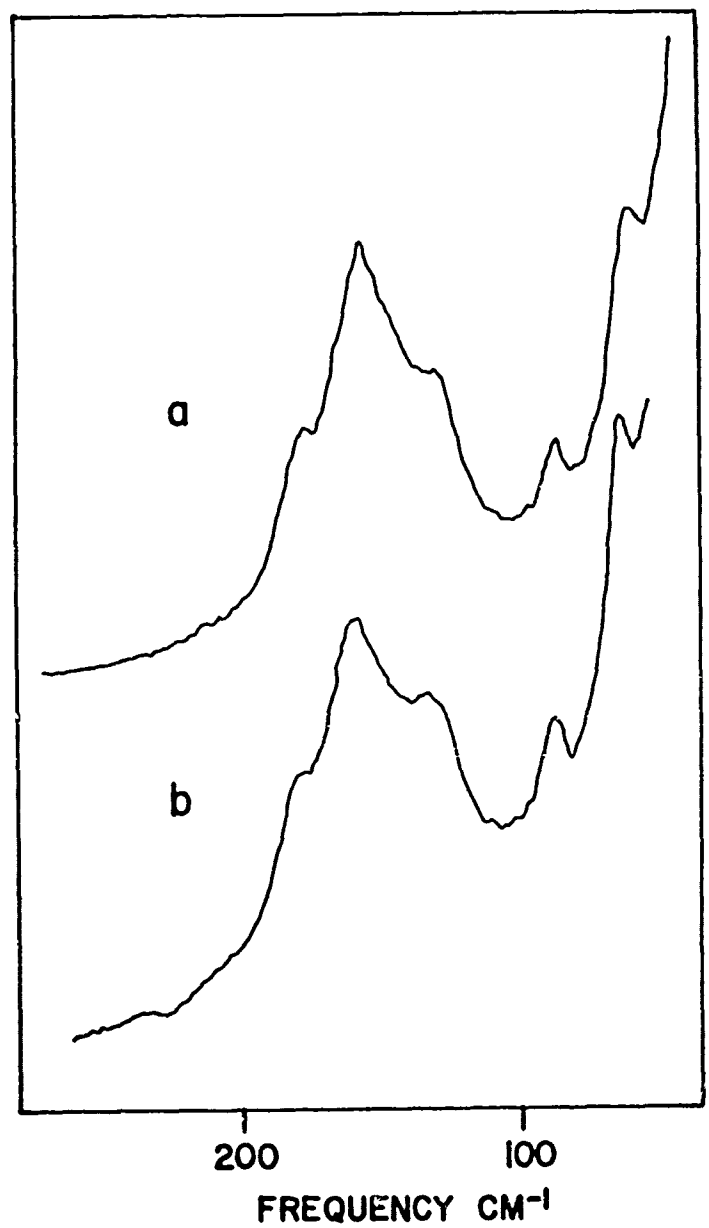

Figure 19. Raman spectra of a) lead sample immersed in air saturated 0.1M HCl solution after 3 days of exposure, b) a lead sample exposed to air saturated 0.1M HCl solution for 3 days then dried in air.

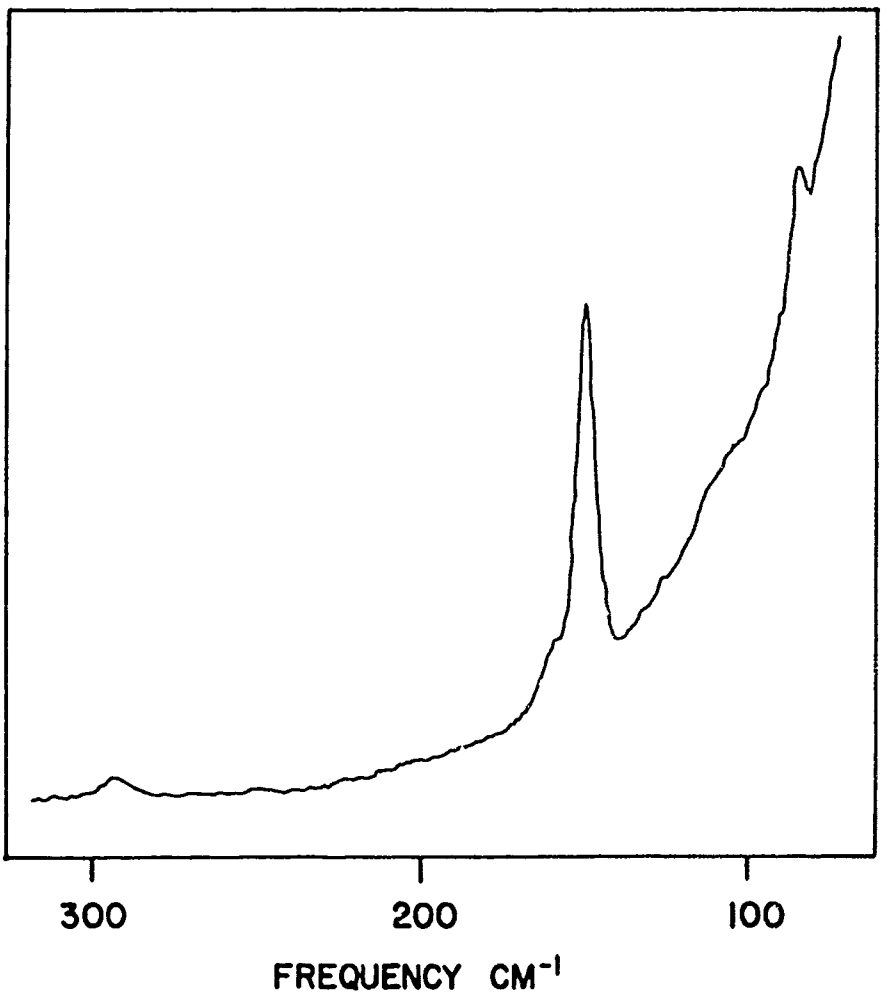

Figure 20. Raman spectrum of the PbO film on a lead surface in deaerated 0.01M NaOH solution for 26 days.

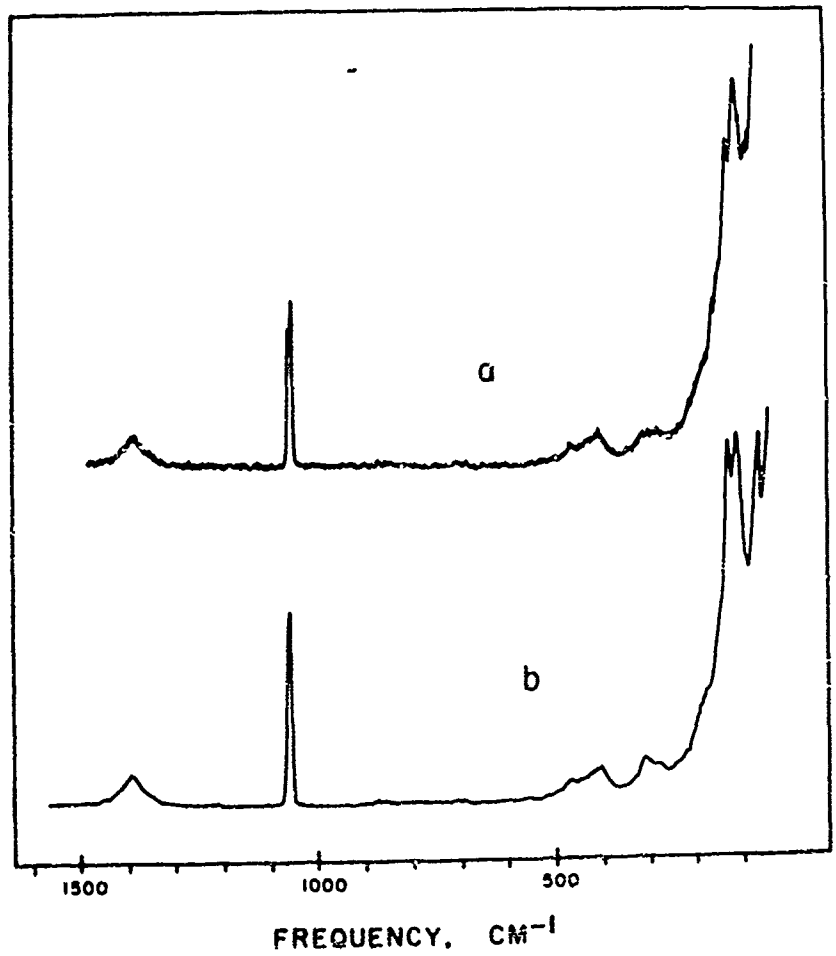

Figure 21. Raman spectra of a) a lead sample which was immersed in air saturated 0.01M NaOH for 4 days, then dried, b) a KBr pellet of basic lead carbonate.

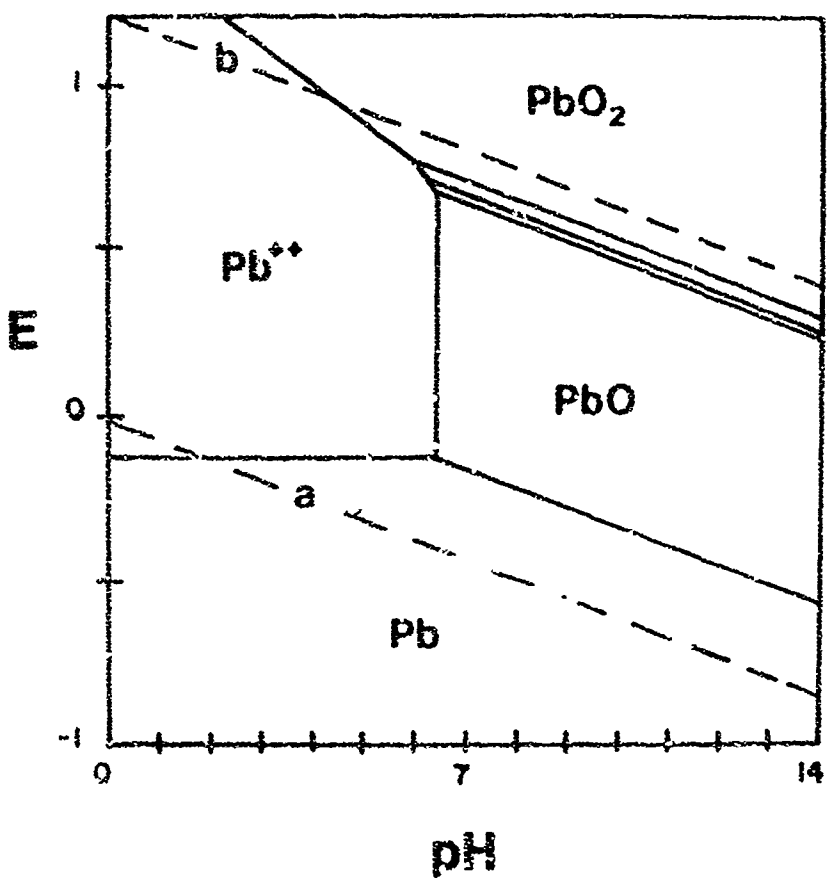

Figure 22. Pourbaix diagram of the lead-water system calculated with the most recent thermodynamic data (90).

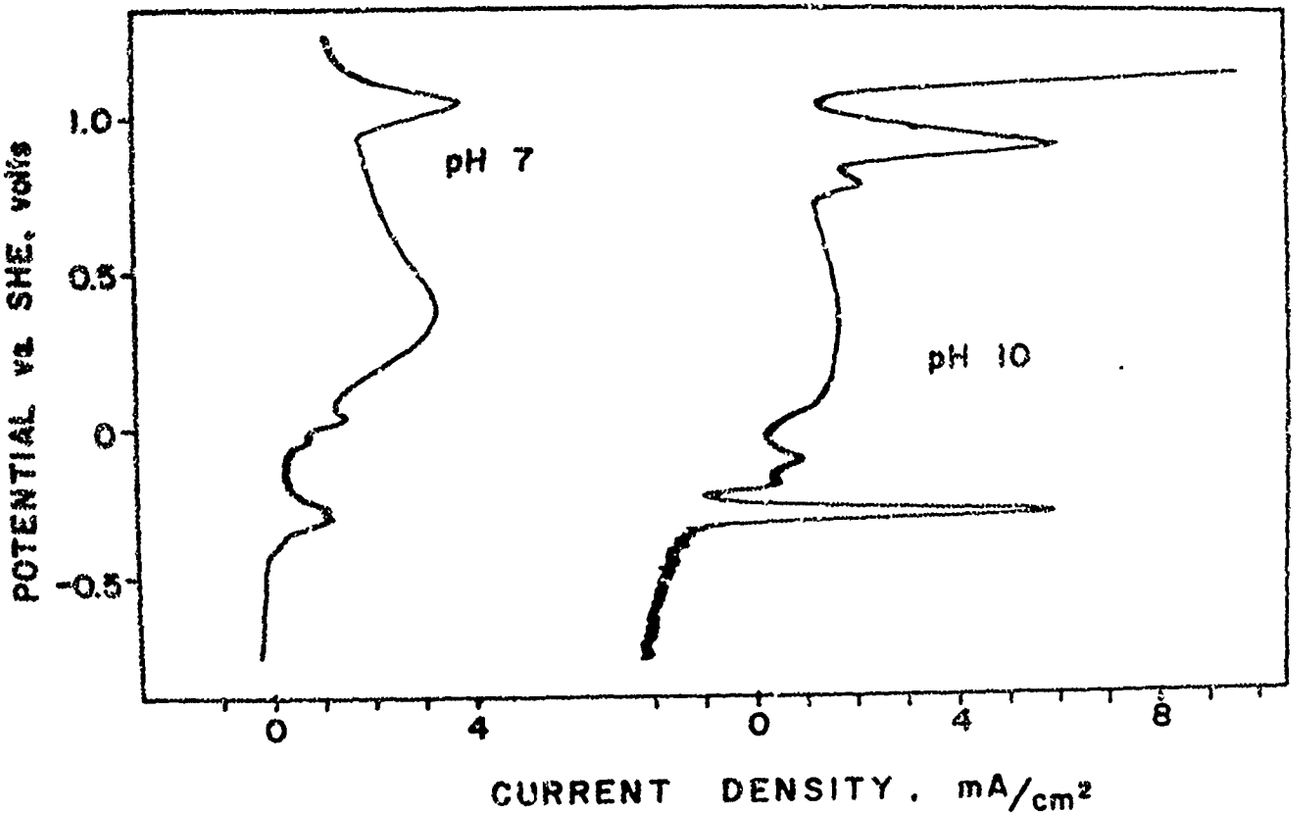

Figure 23. Anodic polarization curves for lead in pH 7 and pH 10 buffer solutions, scan rate 40 mV per min.

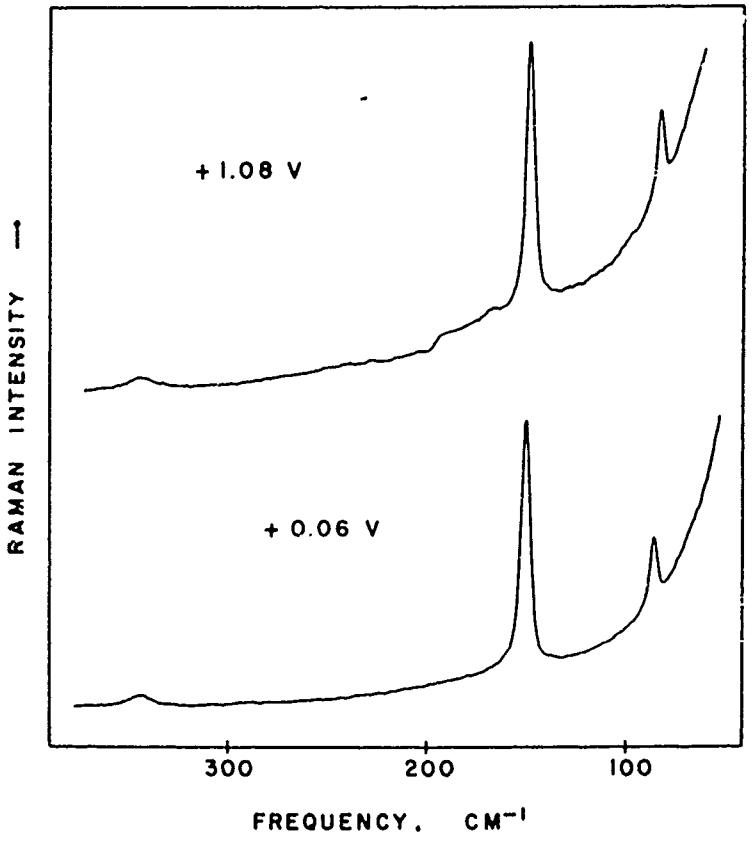

Figure 24. In situ Raman spectra of lead in pH 7 buffer at +1.08V after 1.5 hours of exposure, and at +0.06V after 2.5 hours.

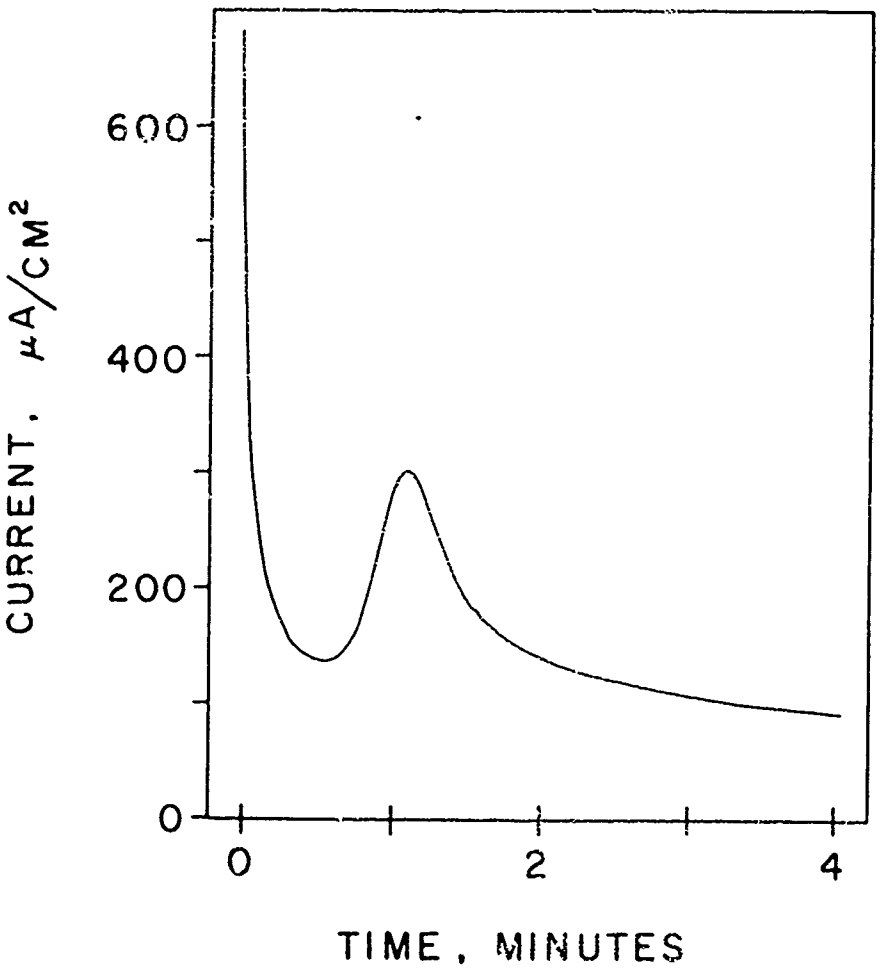

Figure 25. Current-time behavior of lead in pH 10 buffer solution at +0.94V.

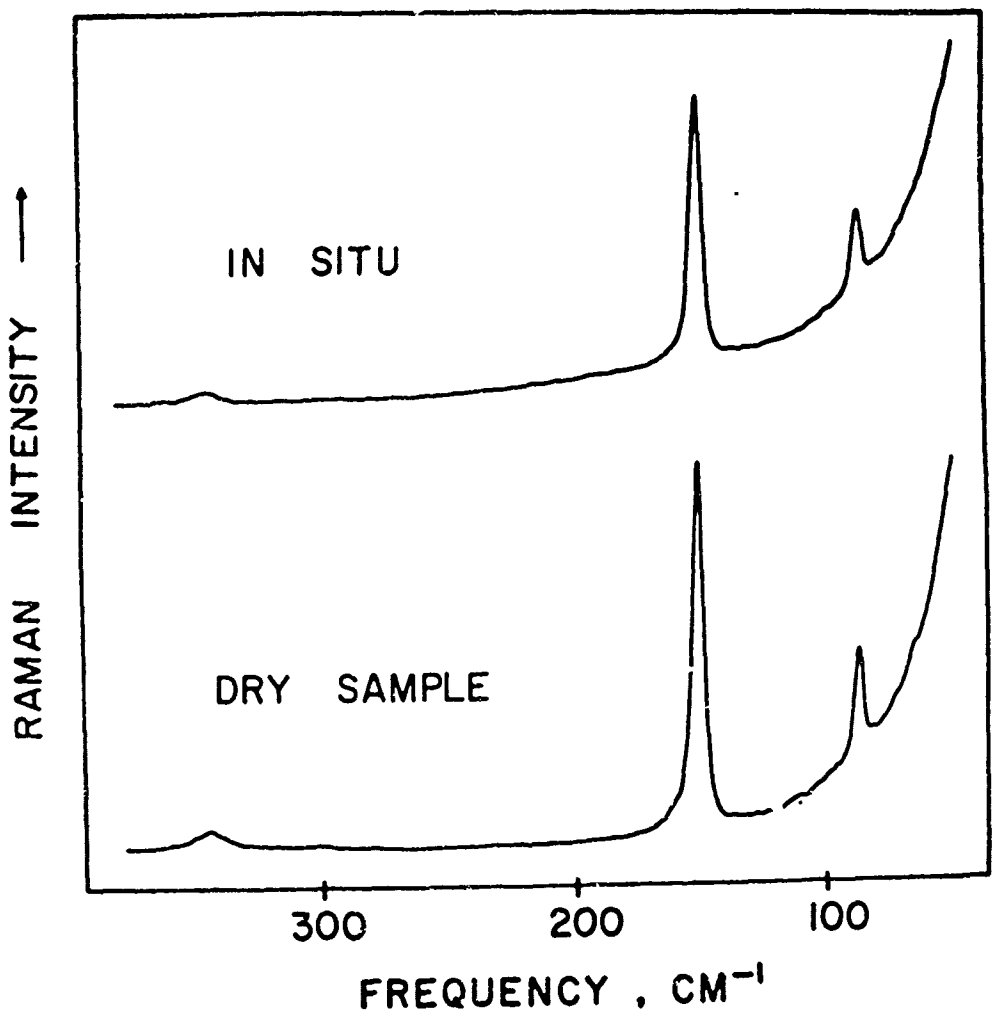

Figure 26. Raman spectra of a lead surface in pH 7 solution at +0.06V after 2.8 hours of exposure, and of the same sample after washing with distilled water and drying.

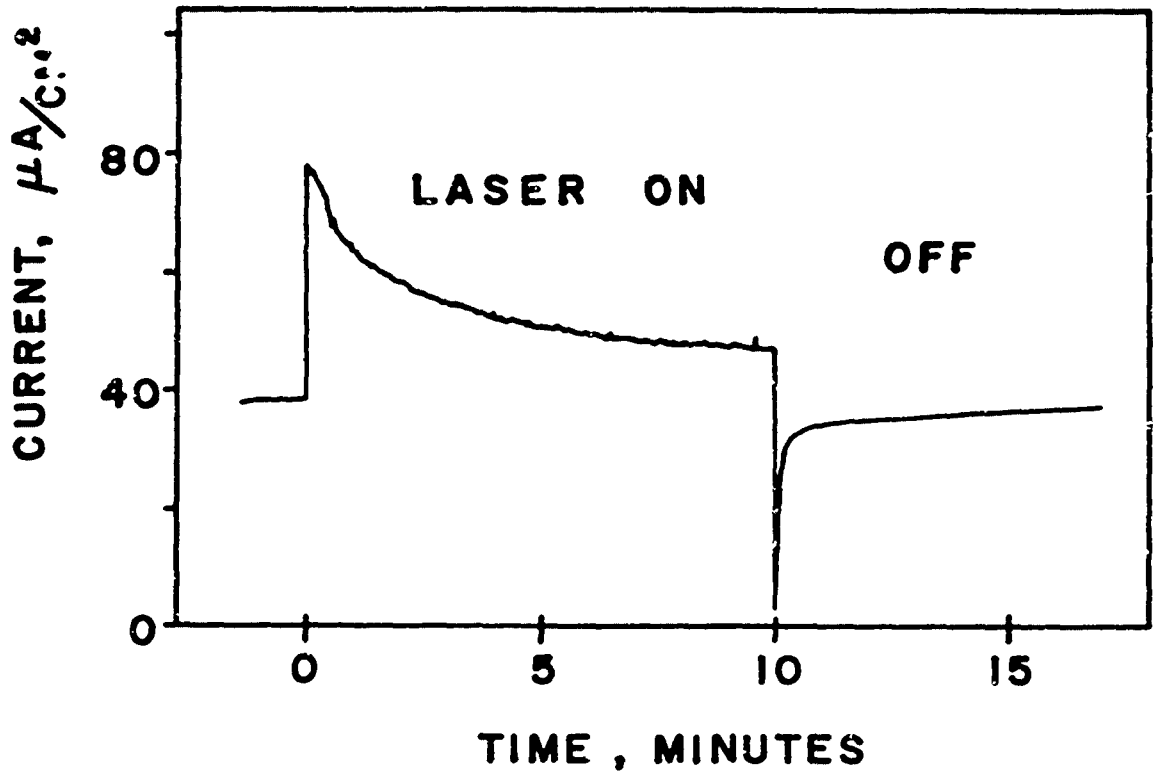

Figure 27. Current behavior of lead with a tetragonal PbO surface film when exposed to the 488.0 nm. laser line. The sample was exposed for 18 hours in pH 10 solution at +0.24V and exposed to the laser beam for one hour.

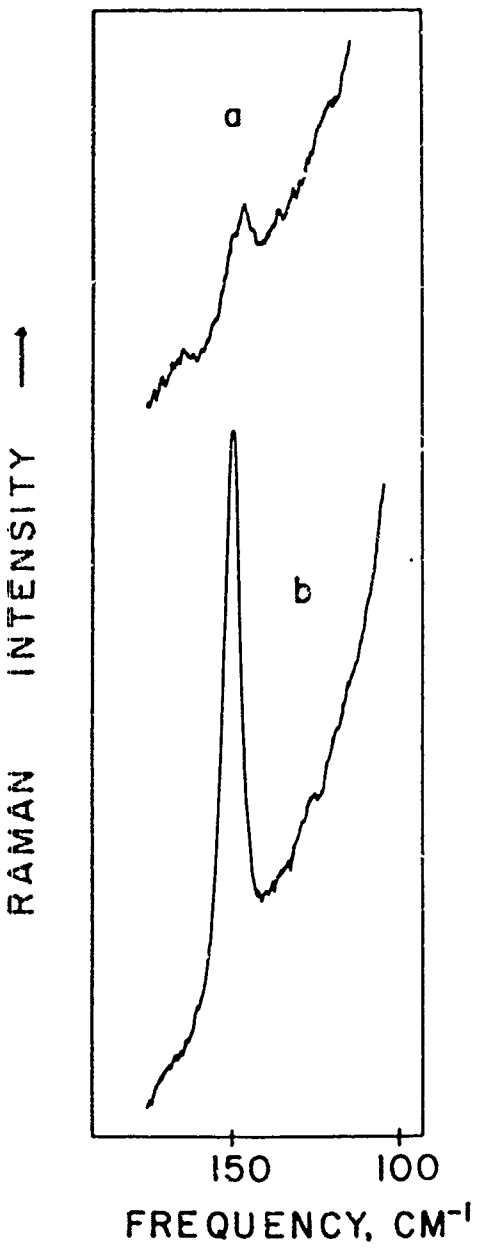

Figure 28. Raman spectra of lead exposed to the pH 10 buffer solution at +0.34V for 3 hours a) potential applied, b) potential not controlled.

Figure 29. Scanning electron micrograph of a lead sample which had been irradiated by the 488.0 nm. laser line during oxidation at +0.34V in pH 10 solution. The darker area on the left is the irradiated portion. Magnification: 5000X. Spectra indicated that the surface film was tetragonal PbO.

Figure 30. Spot of a lead sample which was irradiated by the 488.0 nm. laser line during oxidation in pH 10 solution at +0.34V. Magnification: 5000X.

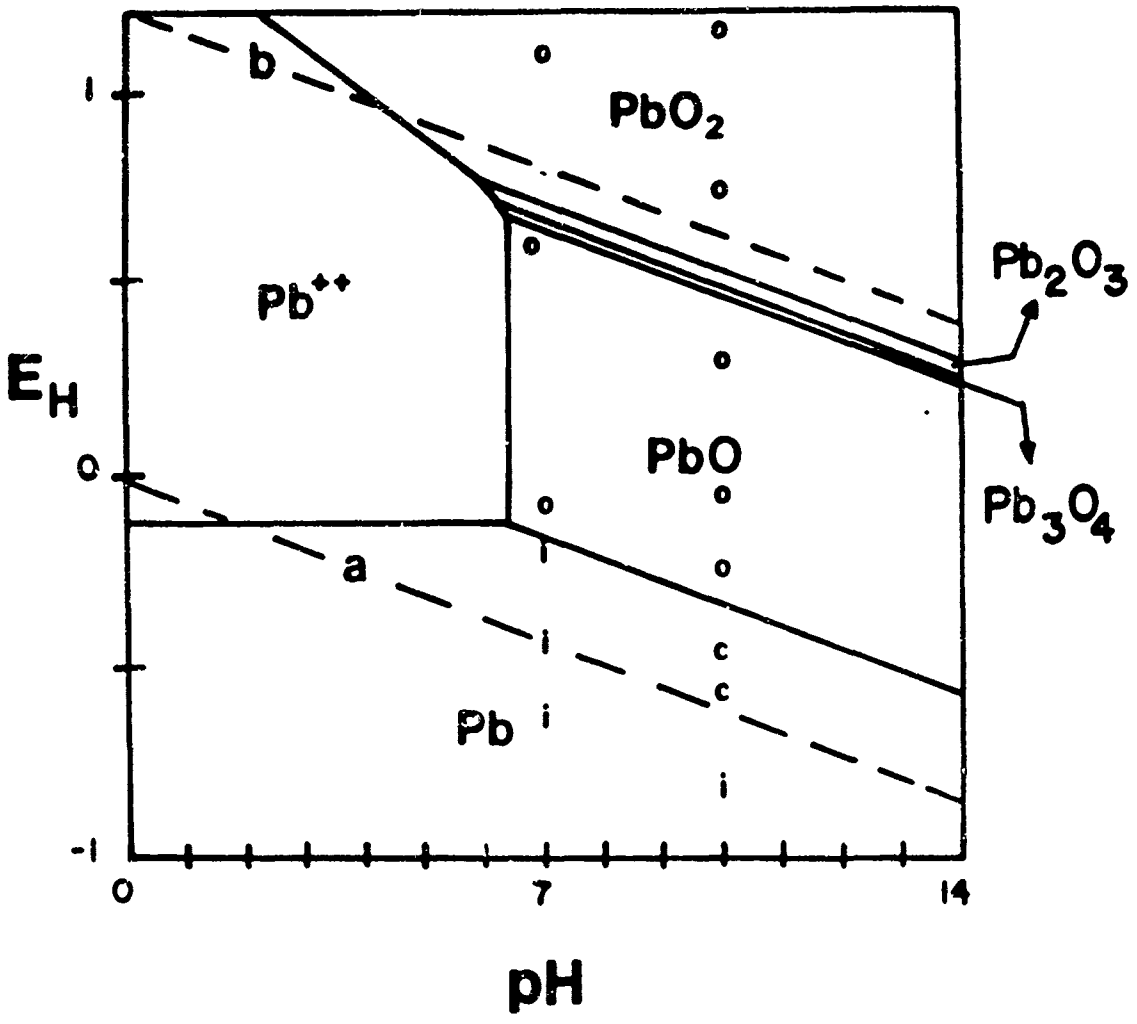

Figure 31. Pourbaix diagram for the lead-water system calculated with recent thermodynamic data (90) with experimental results.
o = tetragonal PbO i = immunity
c = basic lead carbonate

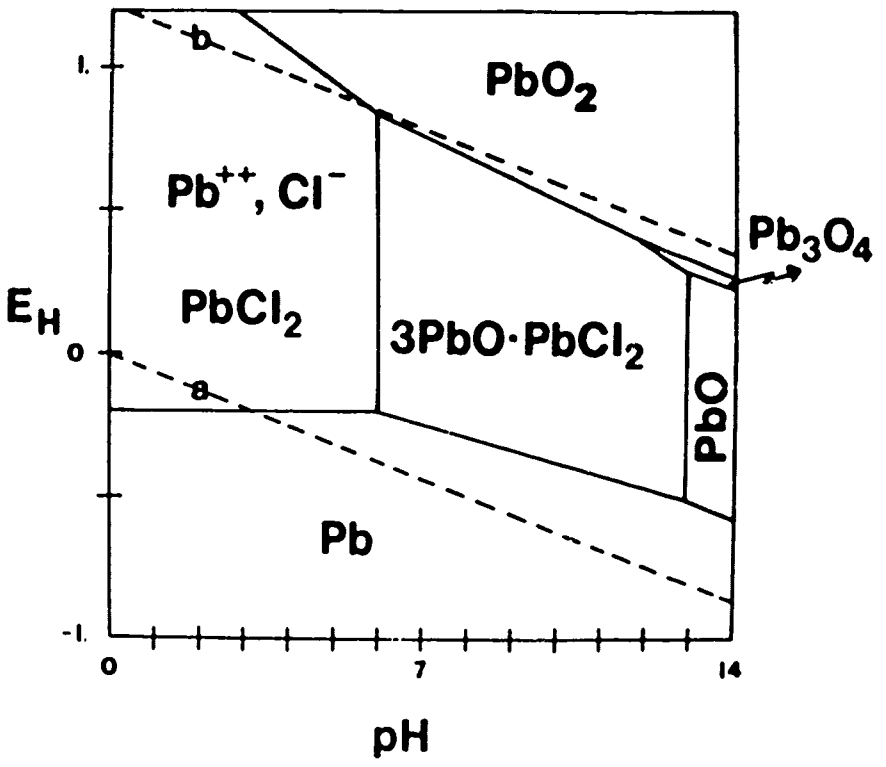

Figure 32. Pourbaix diagram for the lead-water-chloride system (0.1M Cl^-) calculated with recent thermodynamic data (90).

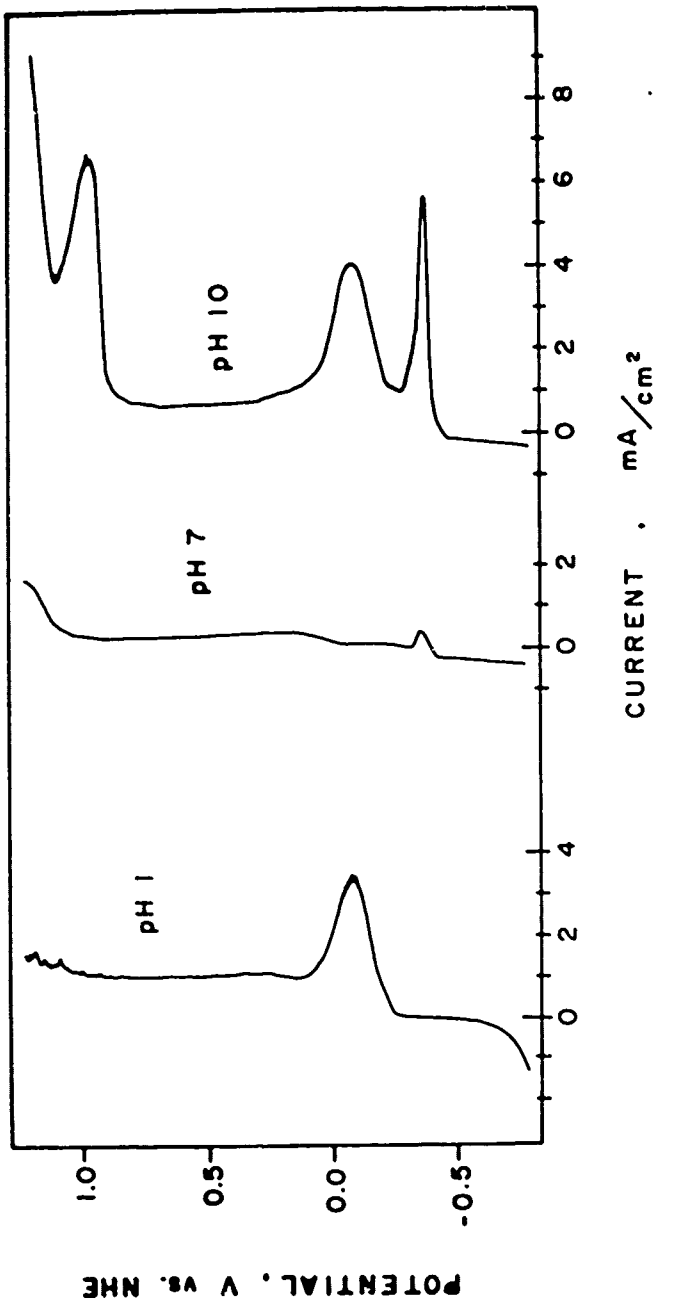

Figure 33. Anodic polarization curves for lead in 0.1M chloride solutions of pH 1, 7, and 10, scan rate 40 mV per min.

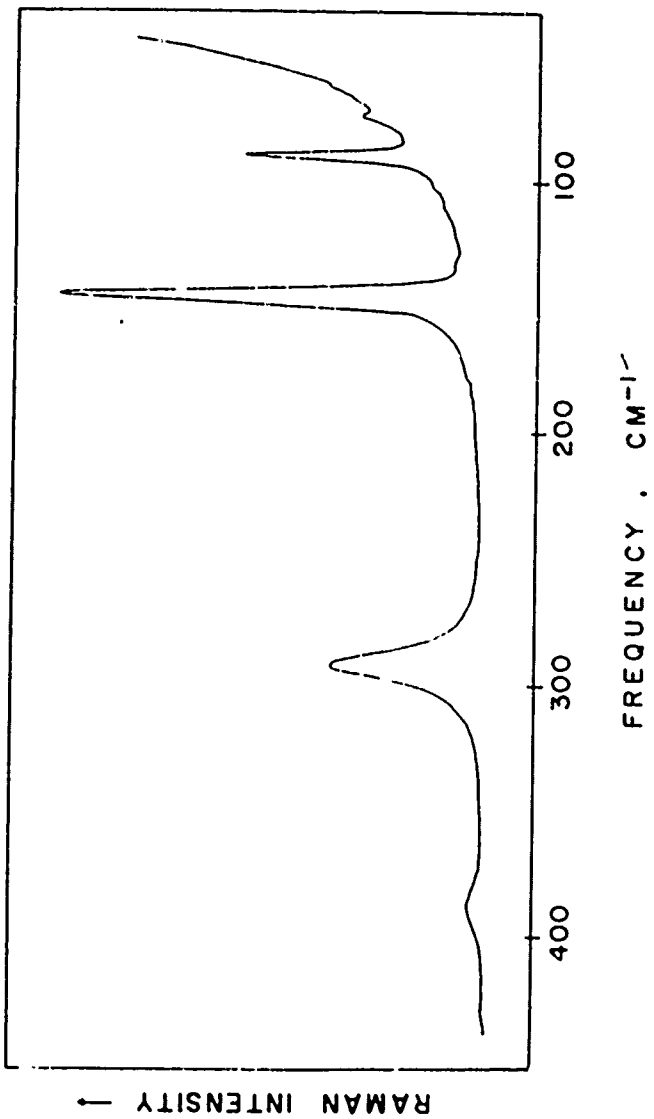

Figure 34. Raman spectrum of orthorhombic PbO on the surface of lead exposed 16.5 hours in 0.1M HCl at -0.46V, washed, and dried.

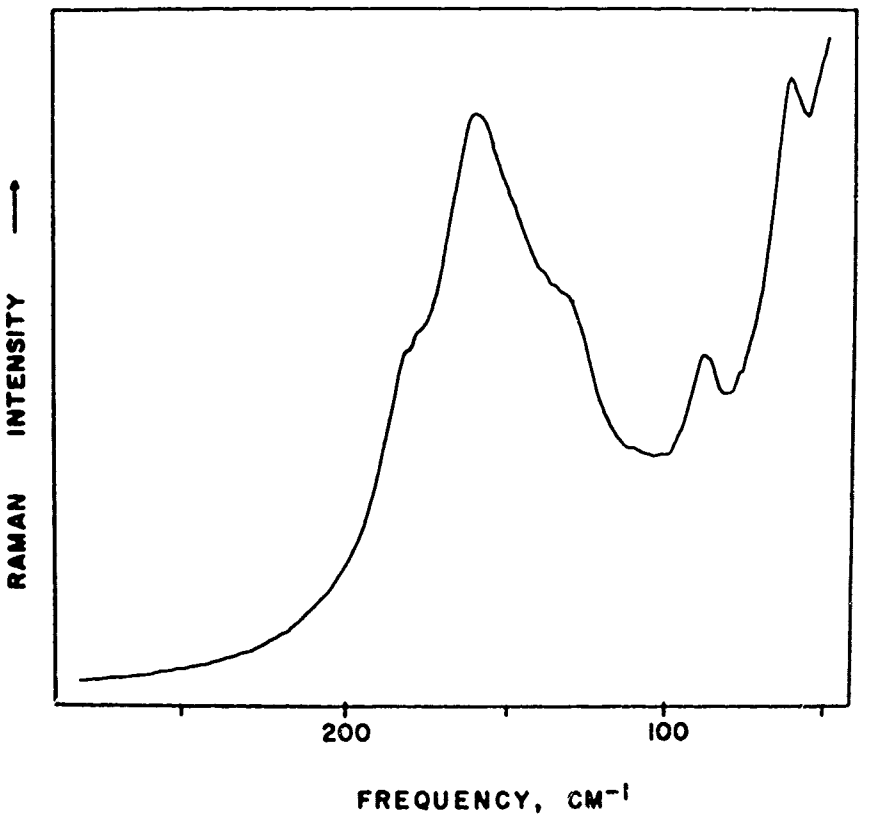

Figure 35. Raman spectrum of the lead chloride surface film on lead after 2.5 hours of exposure to 0.1M HCl at +0.69V.

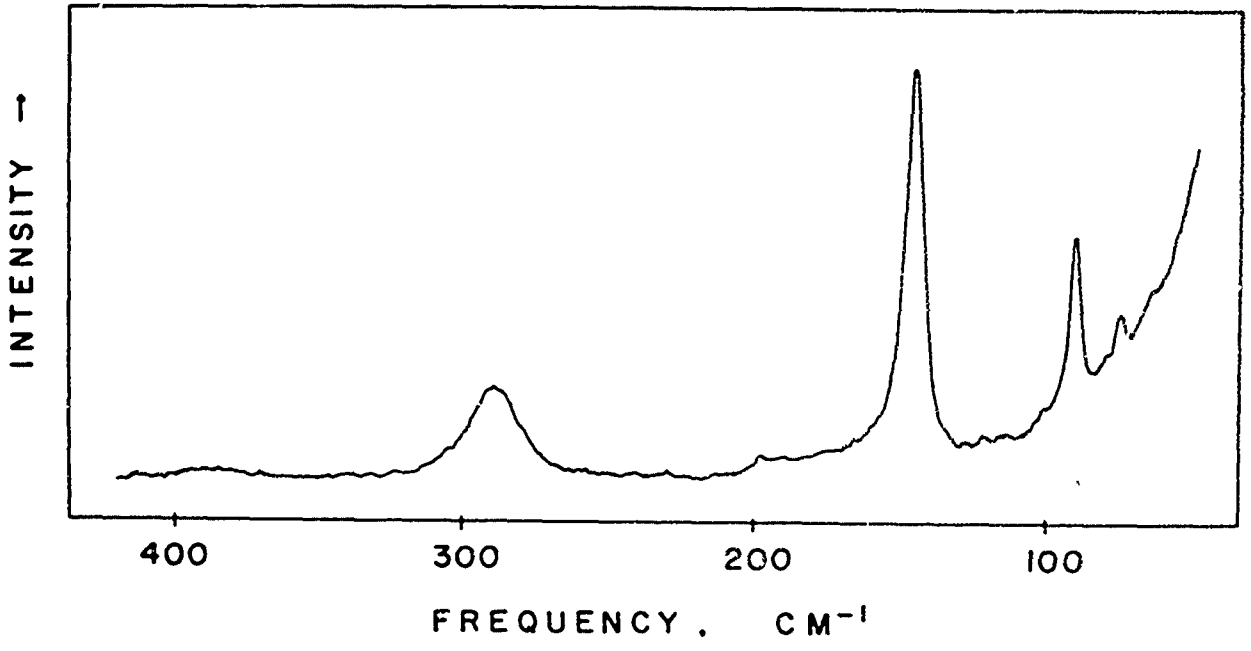

Figure 36. Raman spectrum of orthorhombic PbO from the Pt electrode after oxidation of a lead sample at +1.09V in 0.1M HCl for 17 hours; lead chloride was found on the lead electrode.

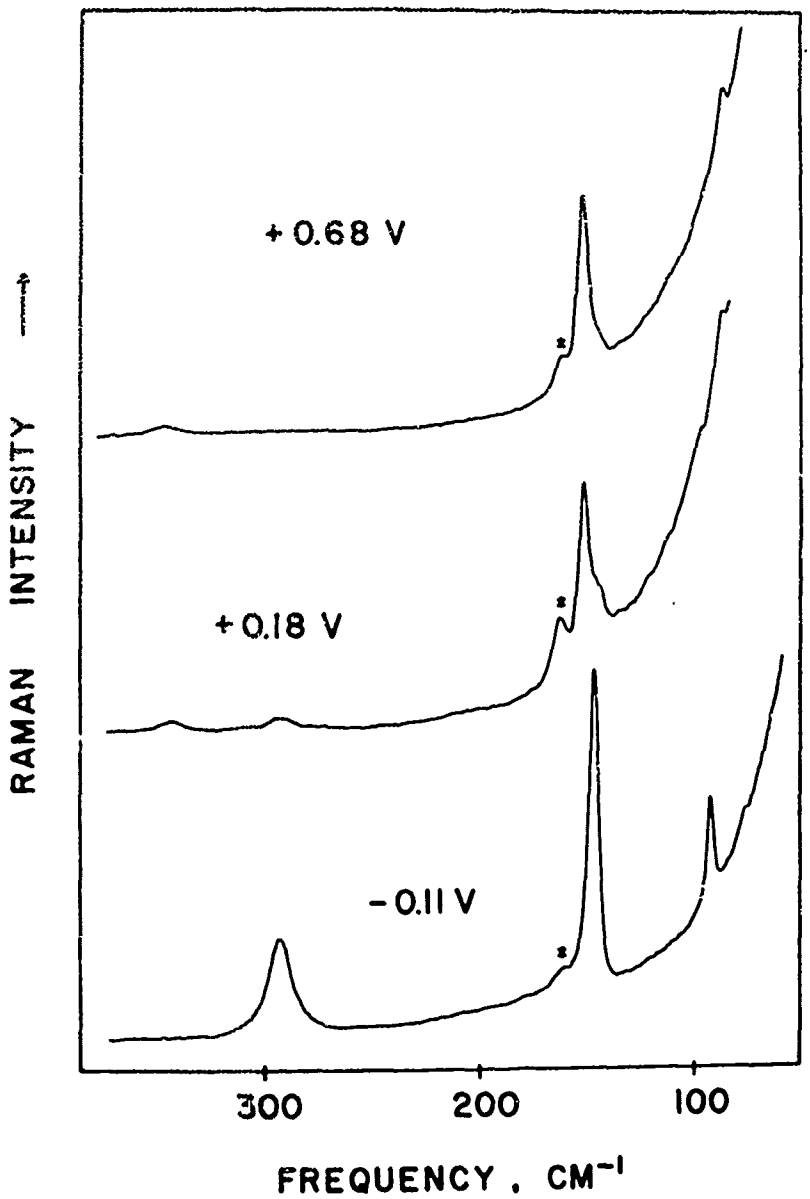

Figure 37. In situ Raman spectra of lead exposed to pH 7, 0.1M chloride solution for 18 hours at +0.68, +0.18, and -0.11V. The spectra indicate tetragonal, tetragonal plus orthorhombic, and orthorhombic PbO films respectively. The feature marked with an asterisk is a grating ghost.

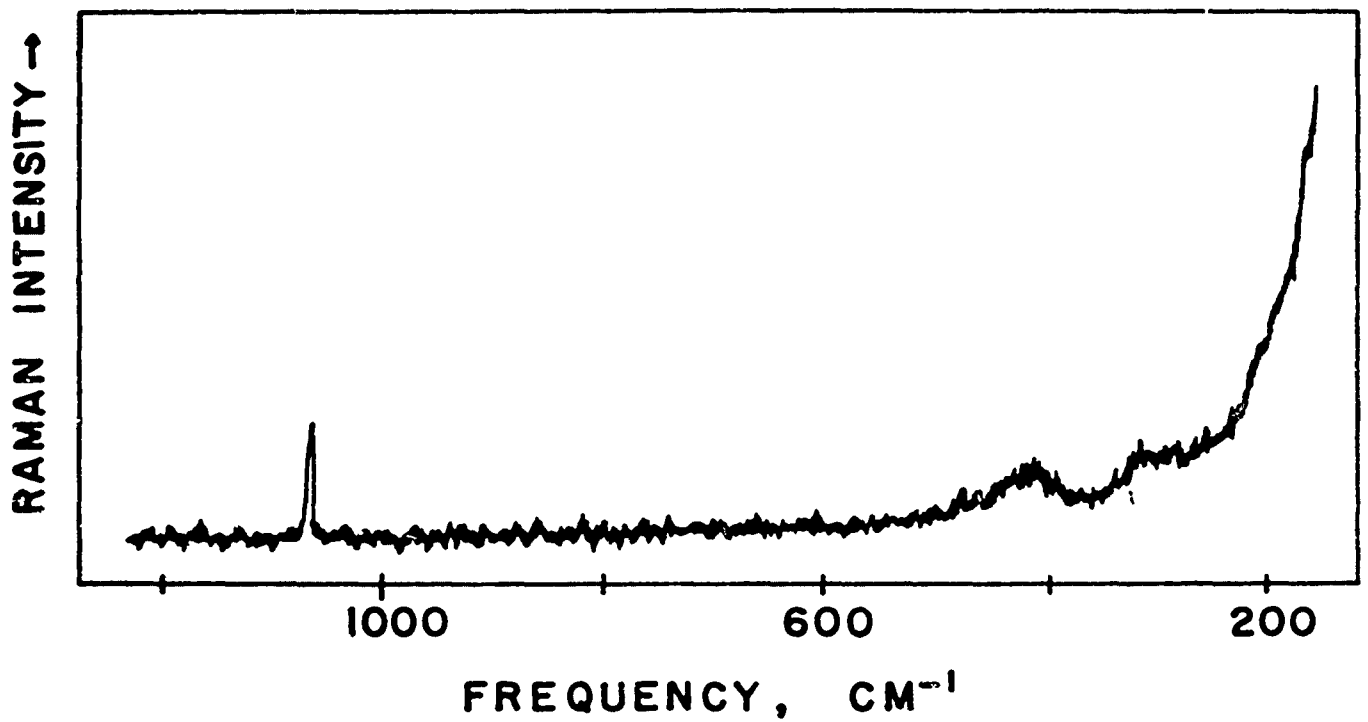

Figure 38. Raman spectrum of the carbonate film formed on lead after 18.5 hours at -0.26V in pH 10, 0.1M chloride solution.

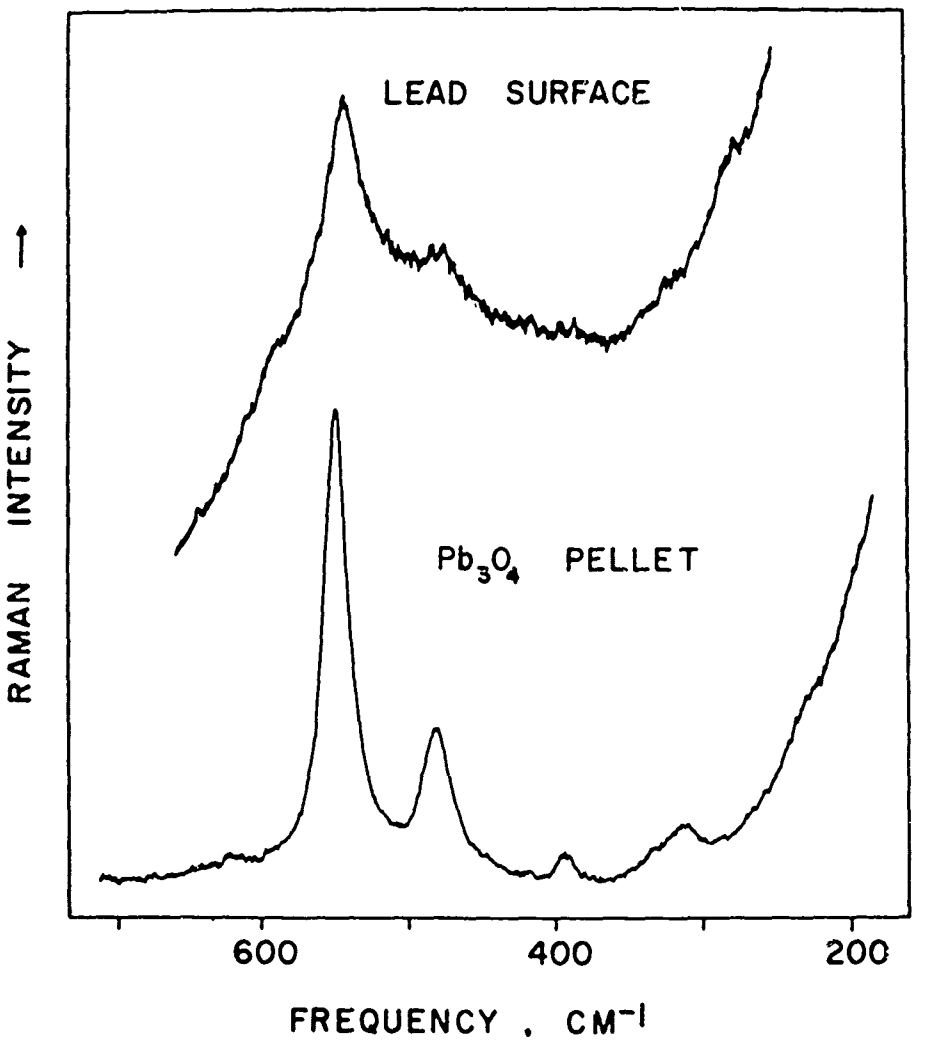

Figure 39. Raman spectra of the surface of lead after exposure in pH 10, 0.1M chloride solution at +1.07V for 18 hours, and of a KBr pellet of Pb_3O_4.

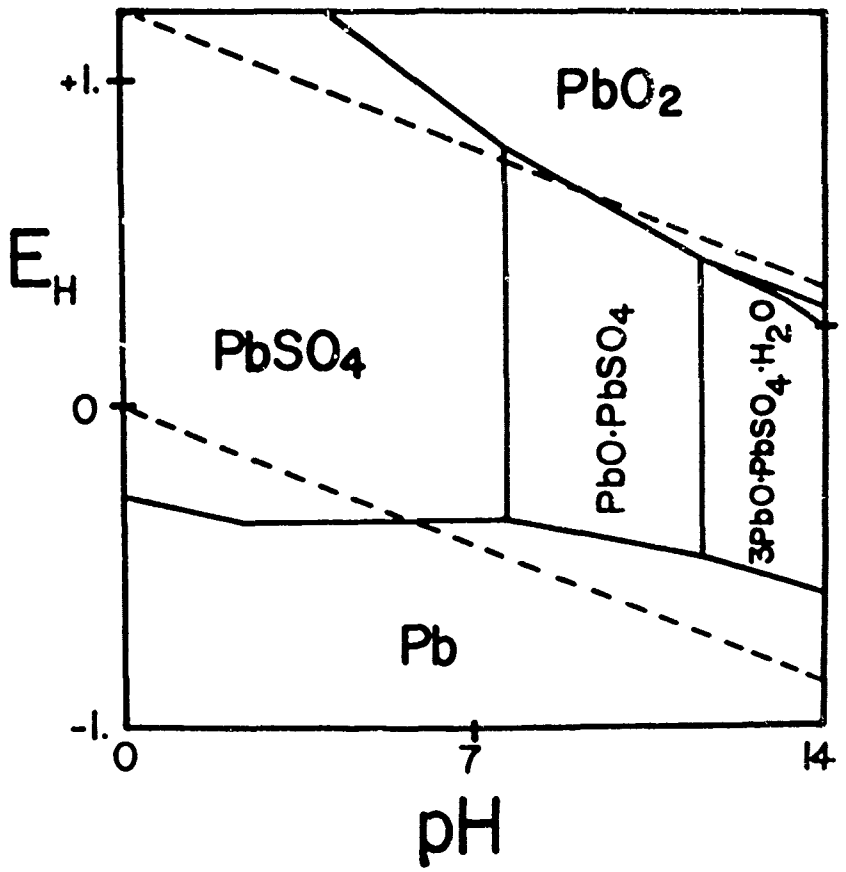

Figure 40. Pourbaix diagram of the lead-water-sulfate system (0.1M sulfate) calculated with recent thermodynamic data (90).

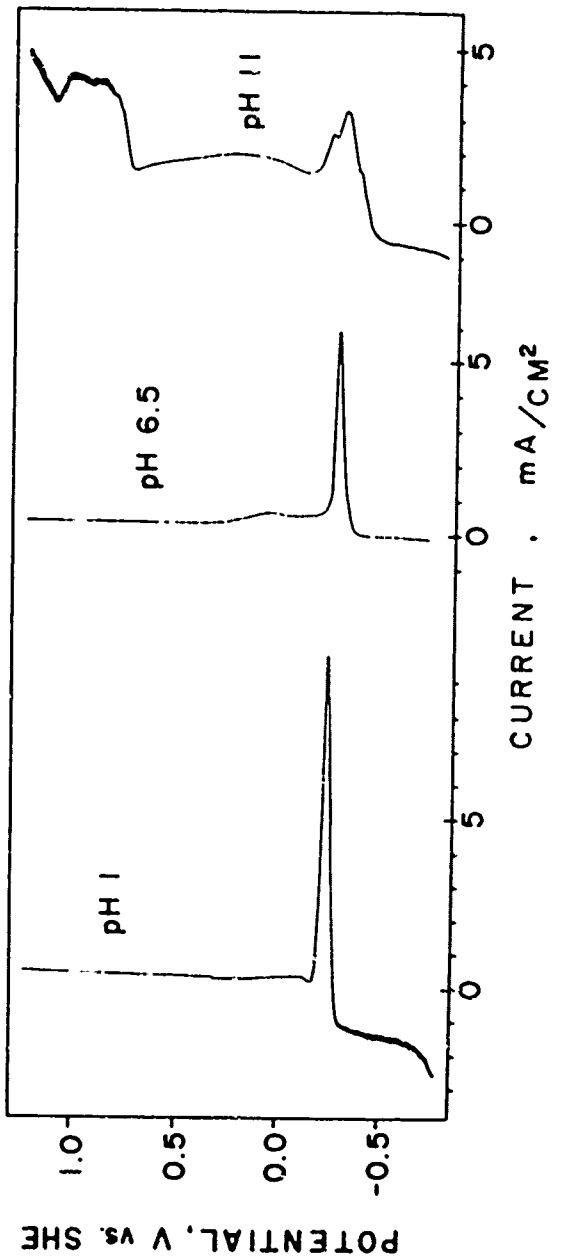

Figure 41. Anodic polarization curves for lead in 0.1M sulfate solutions of pH 1, 6.5, and 11, scan rate 40 mV per min.

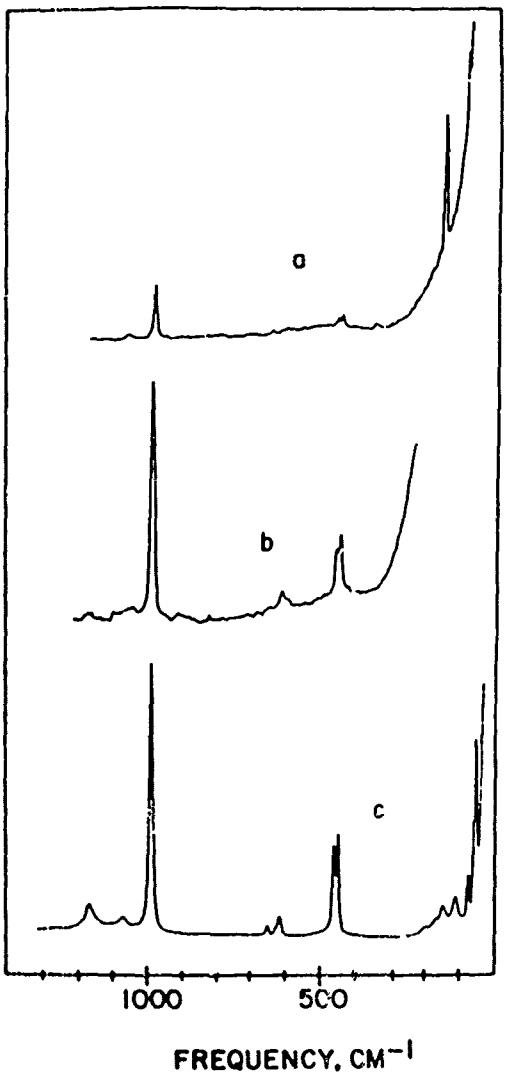

Figure 42. Raman spectra of a) lead in 0.1M sulfuric acid after 20 hours at +0.80V, b) lead in 0.1M sulfuric acid after 18 hours at -0.26V, c) lead sulfate powder.

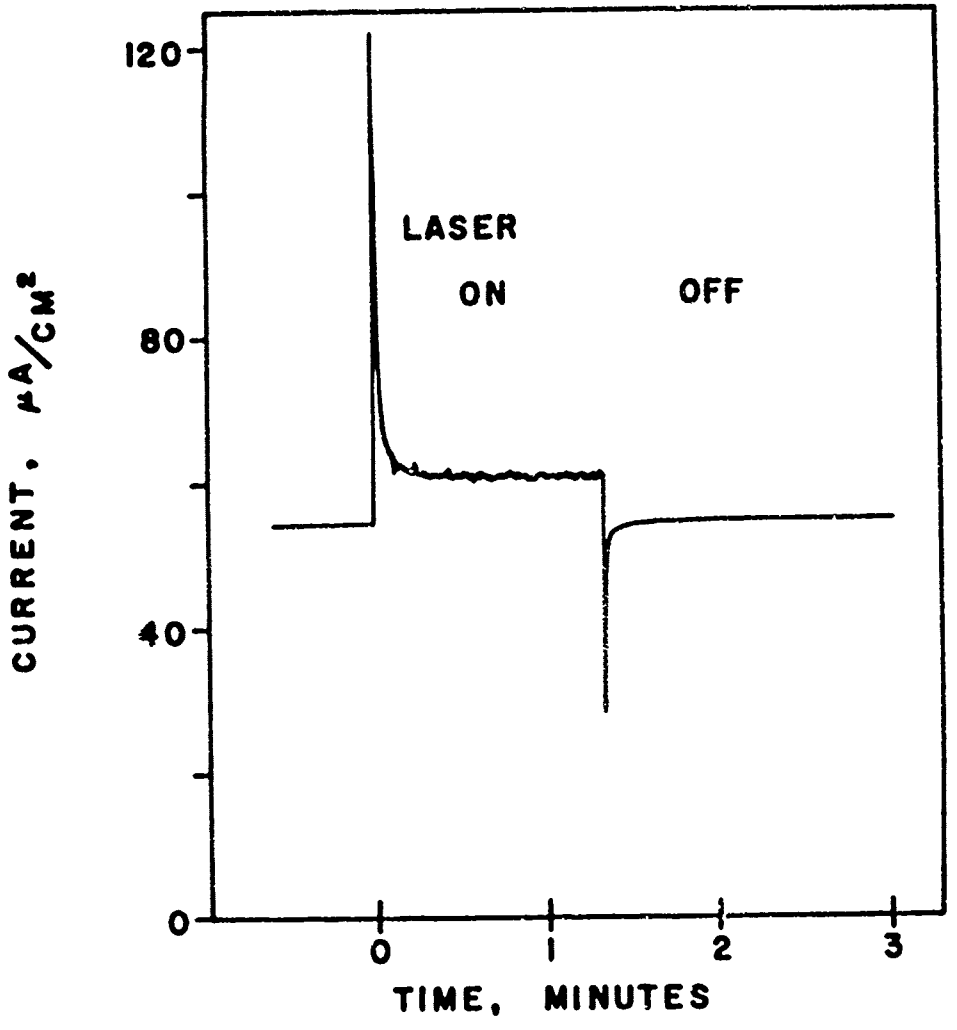

Figure 43. Current behavior of lead oxidized in 0.1M sulfuric acid at +1.24V for 2 hours when exposed to the 488.0 nm. laser line. The sample has a surface covering of tetragonal PbO and lead sulfate.

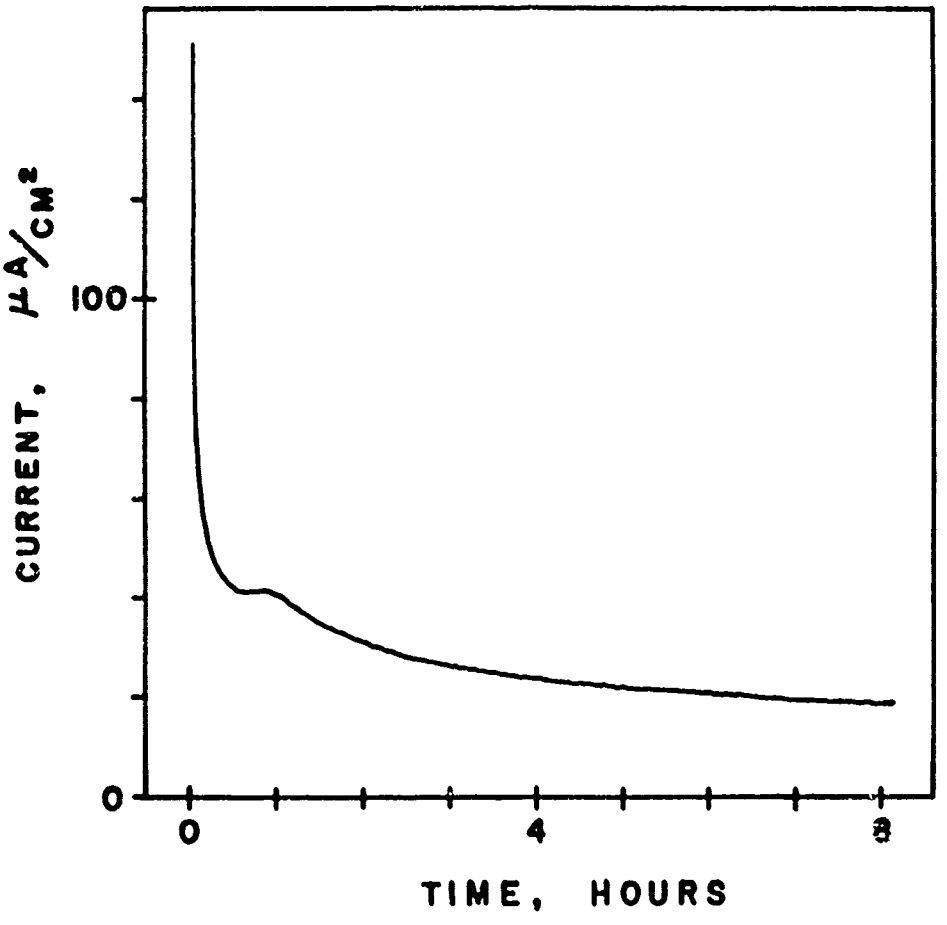

Figure 44. Current vs. time behavior of lead exposed to 0.1M sulfuric acid at +0.48V.

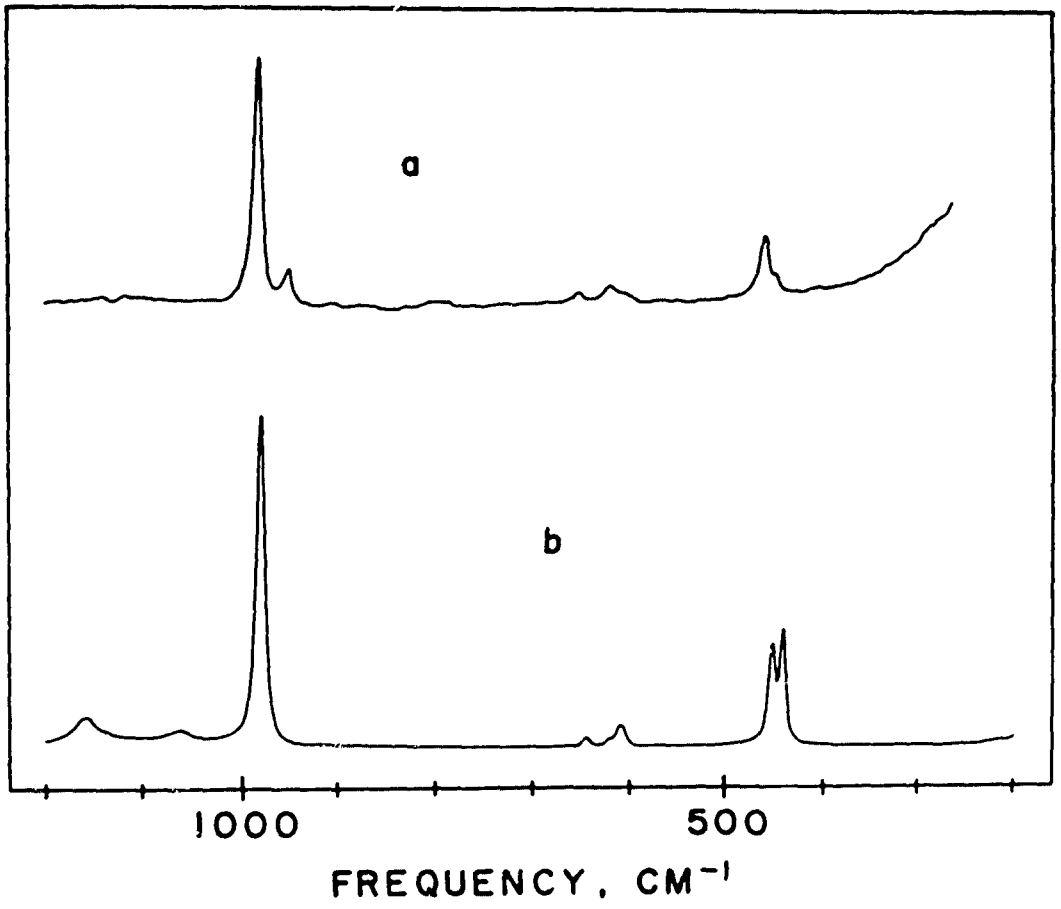

Figure 45. Raman spectra of a) lead sulfate surface film on lead after 19 hours at -0.16V in 0.1M K_2SO_4, b) lead sulfate powder.

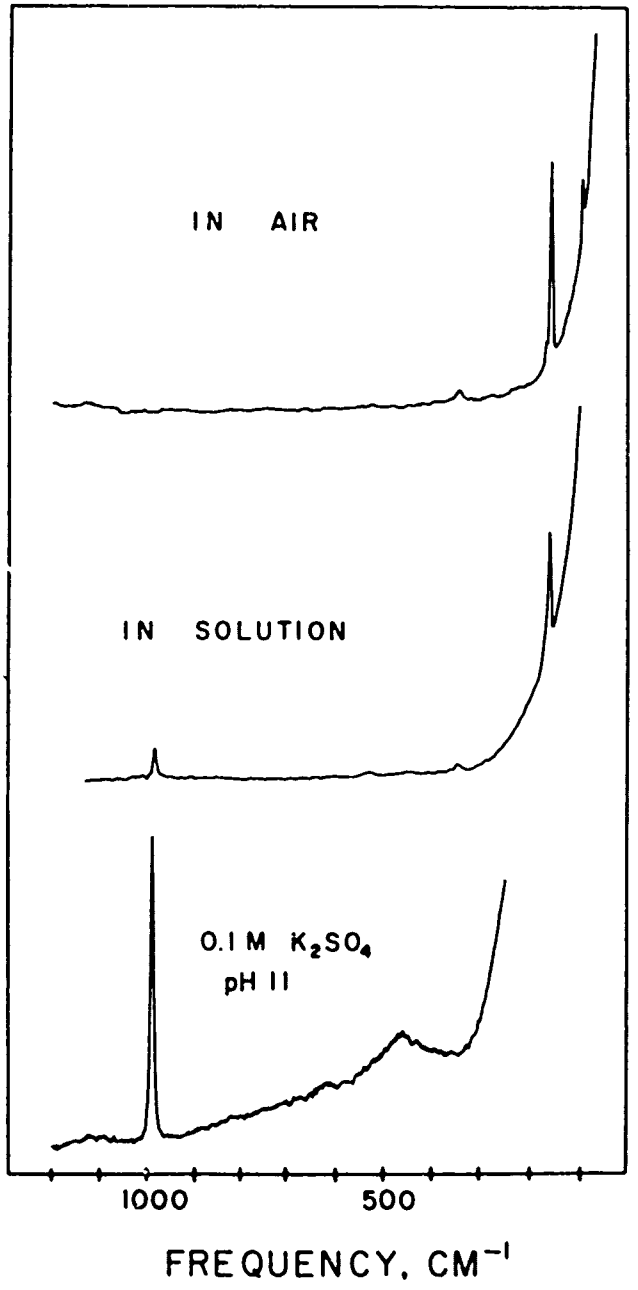

Figure 46. Raman spectra of lead exposed to pH 11 sulfate solution for 18.5 hours at -0.34V recorded with the sample in solution and, after washing, in air; and the Raman spectrum of pH 11, 0.1M sulfate solution.

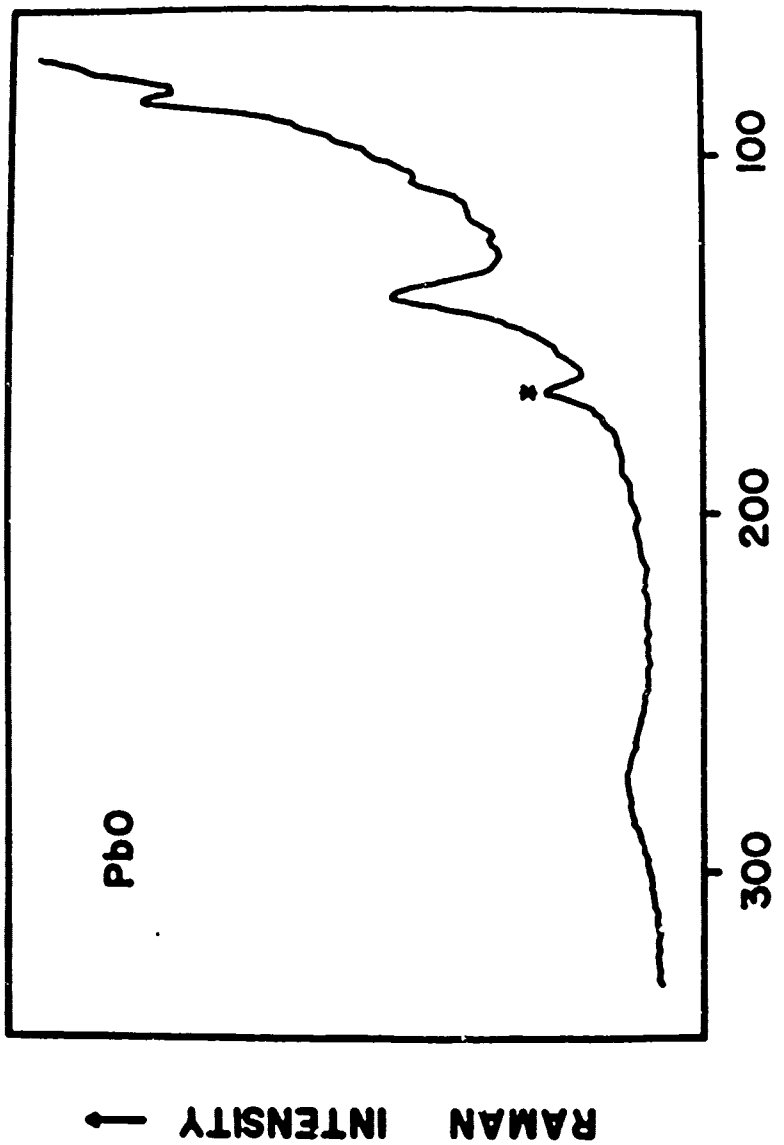

Figure 47. Raman spectrum of a 1620 angstrom thick film of orthorhombic PbO made from a vapor deposited lead sample. A grating ghost is marked with an asterisk.

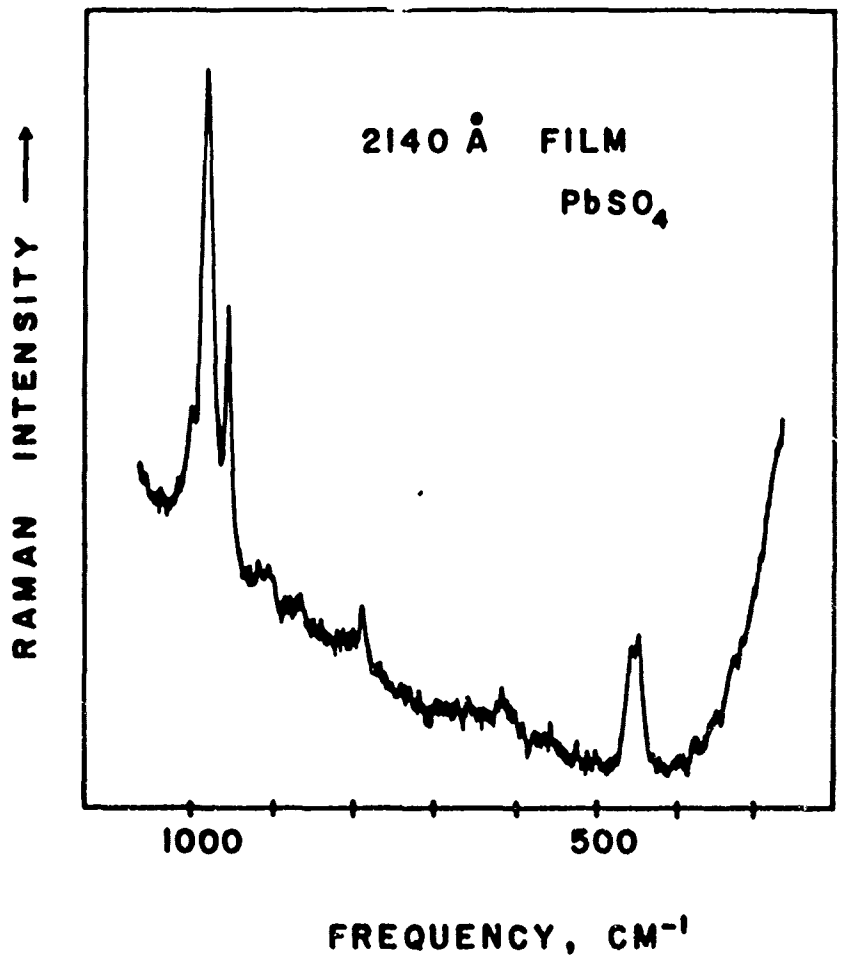

Figure 48. Raman spectrum of a 2140 angstrom thick film of lead sulfate made from a vapor deposited lead sample.

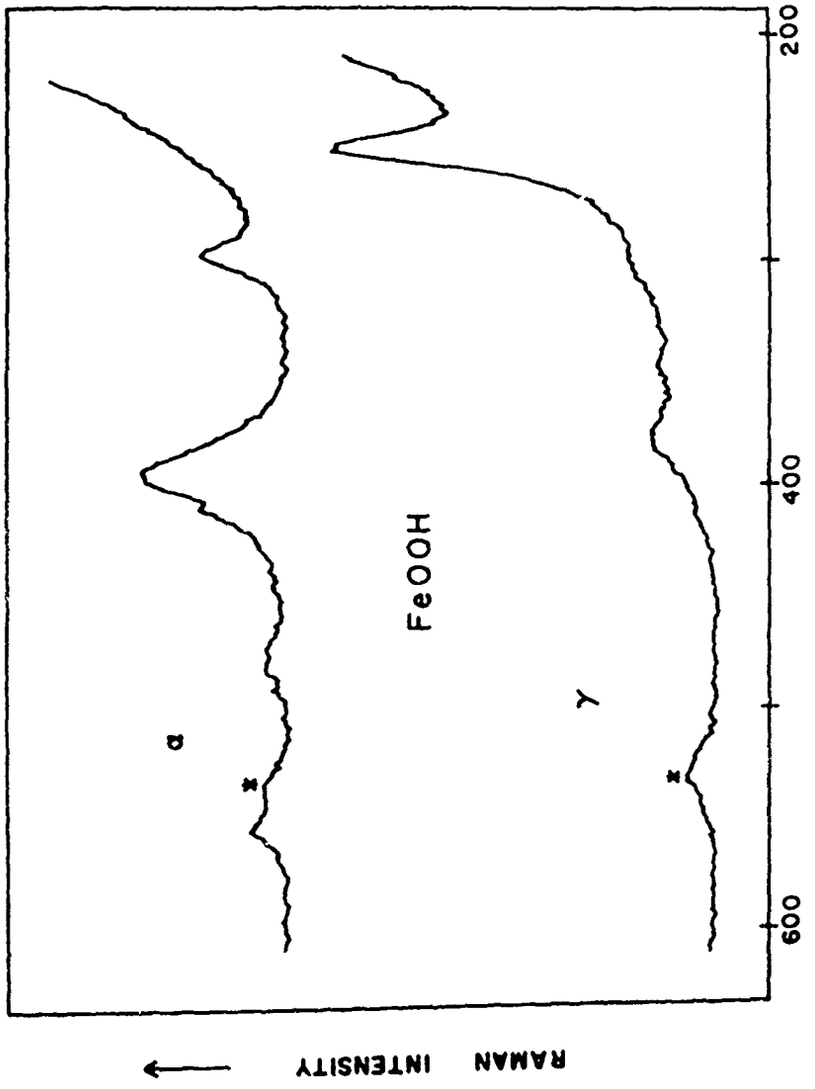

Figure 49. Raman spectra of KBr pellets of two polymorphs of FeOOH. The feature marked with an asterisk is a grating ghost.

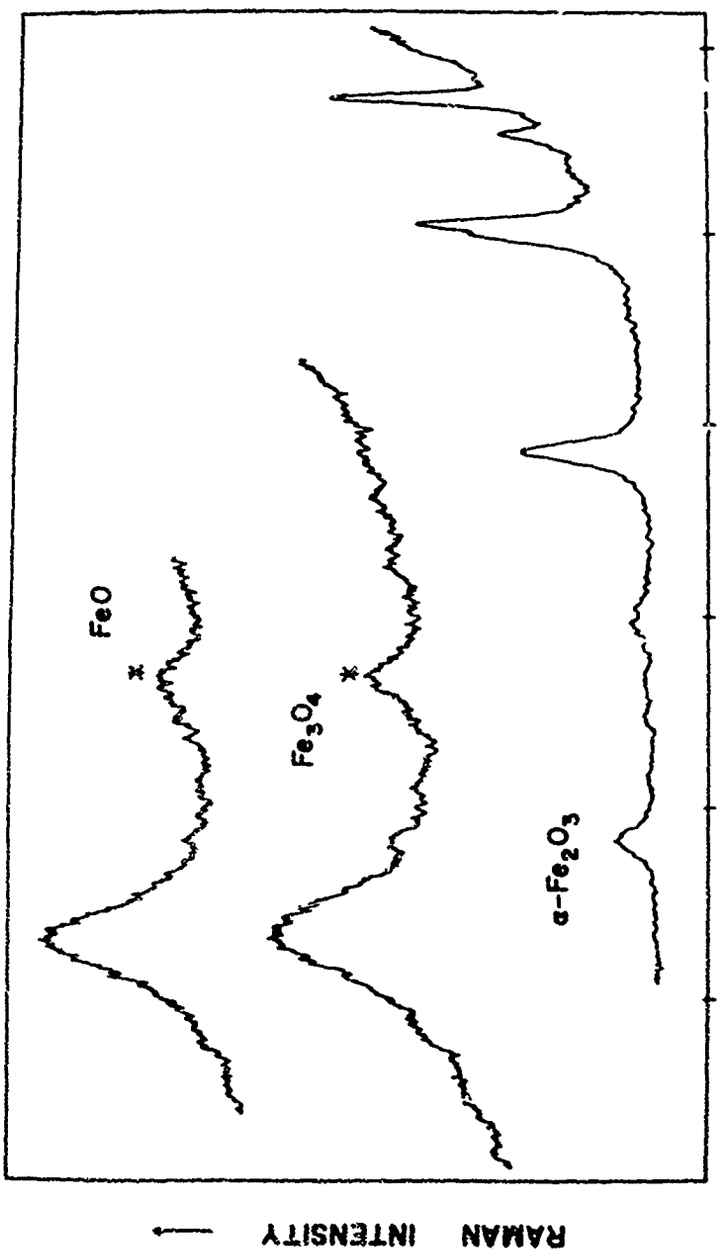

Figure 50. Raman spectra of reagent grade FeO, Fe_3O_4, and the alpha form of Fe_2O_3 in KBr pellets. Grating ghosts are marked with asterisks.

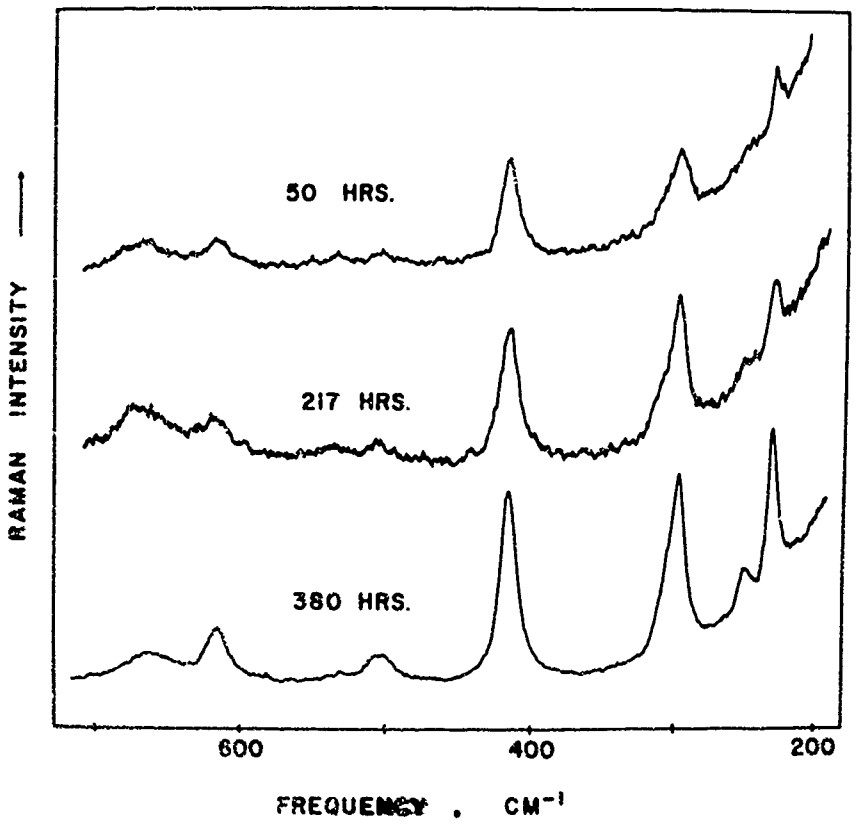

Figure 51. Raman spectra of the surface of Armco iron oxidized in air at 250C for 50, 217, and 380 hours. Full scale on the 50 and 217 hour spectra is 1000 counts/sec., for the 380 hour spectrum it is 3000 counts/sec.

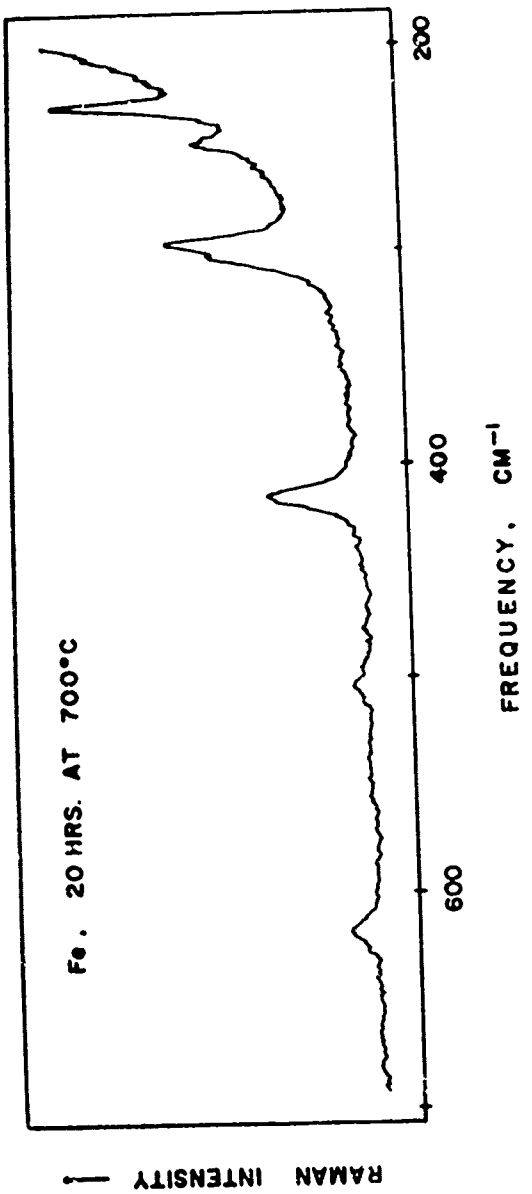

Figure 52. Raman spectrum of Armco iron oxidized in air at 700 C for 20 hours, then cooled quickly with water.

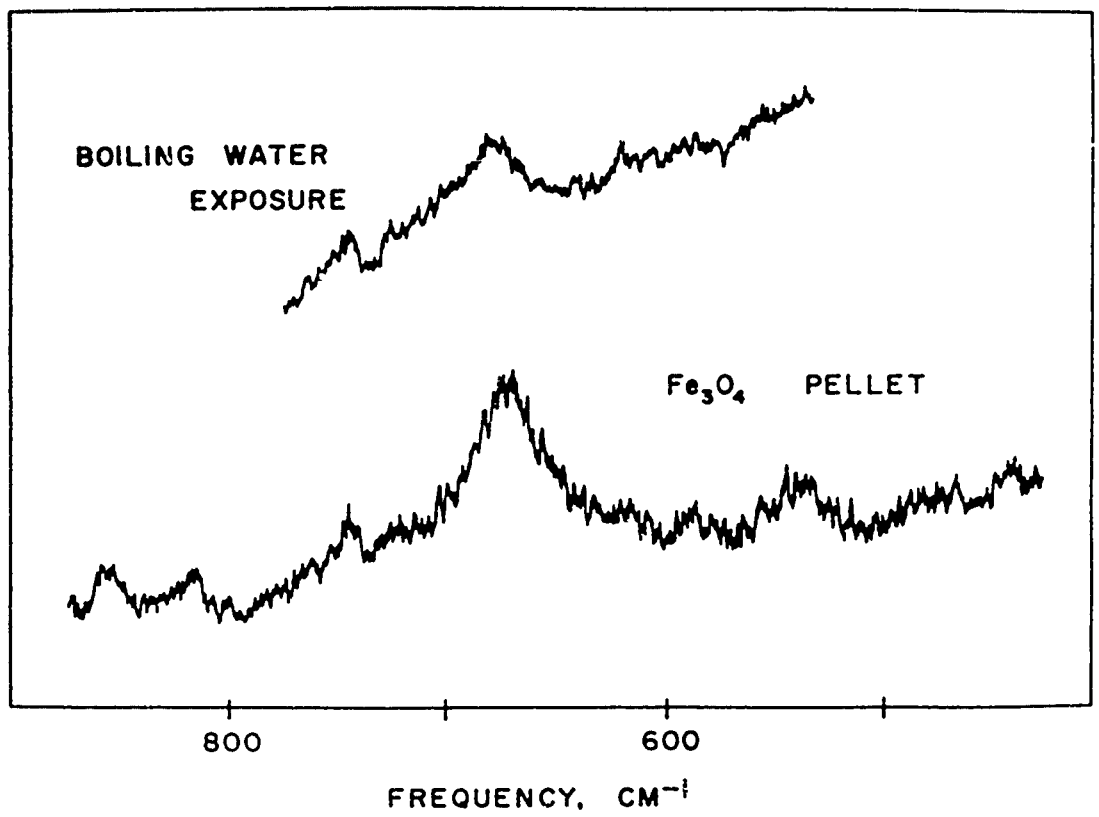

Figure 53. Raman spectra of the surface of an Armco iron sample exposed to boiling 0.01M NaOH solution for 168 hours and of a pellet of Fe_3O_4.

IV. CONCLUSIONS

Raman spectroscopy was demonstrated to be an effective method for in situ analysis of the composition of thin, insoluble surface films formed on lead in aqueous solutions. Simple immersion and controlled potential exposures of clean lead samples formed several different oxidation products which were identified. Spectra of thin surface films (probably as thin as 200 angstroms) were found to be virtually identical to spectra of pure compounds in either loose powder or pellet form. Raman spectra of lead samples immersed in aqueous solutions were identical, although with slightly reduced intensity, to those of the samples when dry.

In situ Raman spectroscopy was used to identify the insoluble oxidation products formed during potentiostatic exposures throughout the different regions of the Pourbaix diagrams calculated for lead in water alone, water with chlorides, and water with sulfates present. The experimental results did not generally agree with thermodynamic predictions. At potentials where lead immunity was predicted experimental findings agreed, but, at higher potentials, where oxidation took place, the products formed showed numerous discrepancies from predictions. In all cases, spectroscopic results and potentiodynamic polarization curves, the two experimental techniques, agreed with each other, but rarely did they agree with calculated

Pourbaix diagrams.

The reasons for differences between experimental and theoretical findings are varied. Effects of the presence of insoluble surface species were not considered in calculating the theoretical diagrams. Thus, the observation of a tetragonal PbO layer beneath a lead sulfate film in sulfuric acid solution could not have been predicted by the calculated diagram. The presence of all anions was not considered. In bicarbonate buffer solutions a carbonate film was detected in the region where immunity was predicted, but the predictions were the result of calculations which did not consider the carbonate ions.

Other shortcomings of the Pourbaix diagrams were pointed out by analyses in chloride solutions which identified orthorhombic PbO at low potentials and tetragonal PbO at higher ones. In potassium sulfate solutions, lead sulfate was observed at some potentials and PbO at others. In both cases no potential dependent reactions between these species were even considered in generating the diagrams.

In general, agreement between the Pourbaix diagrams and experimental results was best for lead exposures in simple solutions, consisting of a very small number of dissolved species. Simple solutions were the closest to the idealized systems used for the thermodynamic calculations. The more complex the solutions became, the less agreement with Pourbaix diagrams was found.

REFERENCES

1) M. Faraday, Experimental Researches in Electricity, vol. II, University of London (1844).

2) R. W. Staehle, Corrosion, 33, 382 (1977).

3) M. G. Fontana and N. D. Greene, Corrosion Engineering, McGraw-Hill, New York (1967).

4) H. H. Uhlig and P. F. King, J. Electrochem. Soc., 106, 1 (1959).

5) V. Brusic, Oxides and Oxide Films, Vol. I, J. W. Diggle, ed., Marcel Dekker, New York (1972).

6) T. P. Hoar, Corrosion Sci., 7, 341 (1967).

7) U. Ebersbach, K. Schwabe, and K. Ritter, Electrochim. Acta, 12, 927 (1967).

8) N. D. Tomashov and Z. P. Vershinina, Electrochim. Acta, 15, 501 (1970).

9) N. Sato, T. Noda, and K. Kudo, Electrochim. Acta, 19, 471 (1974).

10) Lieng-Huang Lee, Characterization of Metal and Polymer Surfaces, Lieng-Huang Lee, ed., Academic Press, New York (1977), vol. I, p.1.

11) Ellipsometry in the Measurement of Surfaces and Thin Films, Symposium Proceedings, Washington, 1963, U. S. Department of Commerce, National Bureau of Standards, Misc. Pub. 256.

12) E. S. Reid, R. P. Cooney, P. J. Hendra, and M. Fleischmann, J. Electroanal. Chem., 80, 405 (1977).

13) D. M. Adams and D. C. Stevens, J. Chem. Soc. Dalton Trans., 11, 1096 (1977).

14) J. D. Donaldson, K. T. Donoghue, and S. D. Ross, Spectrochim Acta, 30A, 1967 (1974).

15) T. Misawa, K. Asami, K. Hashimoto, and S. Shimodaira, Corrosion Sci., 14, 279 (1974).

16) C. L. McBee and J. Kruger, Electrochim. Acta, 17, 1337 (1972).

17) M. Pourbaix and L. R. de Miranda, Passivity and its Breakdown on Iron and Iron Base Alloys, U. S. A. - Japan Seminar, R. W. Staehle and H. Okada, eds., NACE, Houston, 1976, p.47.

18) R. G. Greenler and T. L. Slager, Spectrochim. Acta, 29A, 193 (1973).

19) M. L. Howe. K. L. Watters, and R. G. Greenler, J. Phys. Chem., 80, 382 (1976).

20) T. A. Egerton and A. H. Hardin, Catal. Rev. - Sci. Eng., 11, 71 (1975).

21) R. P. Cooney, G. Curthoys, and Nguyen The Tam, Adv. Catal., 24, 293 (1975).

22) M. Fleischmann, P. J. Hendra, and A. J. McQuillan, Chem. Phys. Lett., 26, 163 (1974).

23) A. J. McQuillan, P. J. Hendra, and M. Fleischmann, J. Electroanal. Chem.,65, 933 (1975).

24) P. L. Paul, A. J. McQuillan, P. J. Hendra, and M. Fleischmann, J. Electroanal. Chem., 66, 248 (1975).

25) M. Fleischmann, P. J. Hendra, A. J. McQuillan, R. L. Paul, and E. S. Reid, J. Raman Spectrosc. ,4, 269 (1976).

26) R. P. Cooney, E. S. Reid, P. J. Hendra, and M. Fleischmann, J. Amer. Chem. Soc., 99, 2002 (1977).

27) R. P. Cooney, M. Fleischmann, and P. J. Hendra, J. C. S. Chem. Comm. (1977), 235.

28) M. G. Albrecht and J. A. Creighton, J. Amer. Chem. Soc., 99, 5215 (1977).

29) D. L. Jeanmaire and R. P. VanDuyne, J. Electroanal. Chem., 84, 1 (1977).

30) T. R. Gilson and P. J. Hendra, Laser Raman Spectroscopy, Wiley - Interscience, New York (1971).

31) M. Tobin, Laser Raman Spectroscopy, Wiley - Interscience, New York (1971).

32) J. A. Koningstein, Introduction to the Theory of the Raman Effect, Reidel, Dordrecht, Holland (1972).

33) A. Anderson, The Raman Effect, Marcel Dekker, New York (1973).

34) N. B. Colthup, L. H. Daly, and S. E. Wilberley, Introduction to Infrared and Raman Spectroscopy, Academic Press, New York (1977).

35) M. Pourbaix, Atlas of Electrochemical Equilibria in Aqueous Solutions, NACE, Houston (1974).

36) K. D. Efrid, Corrosion, 31, 77 (1975).

37) E. D. Verink and T. Lee, Proceedings of the Third International Conference on Marine Corrosion and Fouling, 1972, Gaithersburg, MD.

38) M. Pourbaix, Passivity and its Breakdown on Iron and Iron Base Alloys, U. S. A. - Japan Seminar, R. W. Staehle and H. Okada, eds., NACE, Houston (1976), p.27.

39) P. Parrish, M. S. Thesis, University of Florida, 1970.

40) E. D. Verink and M. Pourbaix, Corrosion, 27, 12 (1971).

41) E. D. Verink and R. H. Heidersbach, Localized Corrosion - Cause of Metal Failure, ASTM STP 516, American Society for Testing and Materials (1972), pp.303-322.

42) R. Turcotte, M. S. Thesis, University of Rhode Island (1977).

43) J. J. Lander, Trans. Electrochem. Soc., 95, 174 (1949).

44) M. Fleischmann and H. R. Thirsk, Trans. Faraday Soc., 51, 71 (1955).

45) S. C. Barnes and R. T. Mathieson, Batteries 2, D. H. Collins, ed., Pergamon, New York (1965).

46) T. F. Sharpe, Encyclopedia of the Electrochemistry of the Elements, A. J. Bard, ed., Marcel Dekker, New York (1973).

47) Lead in Modern Industry, Lead Industries Association, New York (1952).

48) J. Burbank, J. Electrochem. Soc., 103, 87 (1956).

49) J. Burbank, J. Electrochem. Soc., 104 , 693 (1957).

50) D. Pavlov, Electrochim. Acta, 13, 2051 (1968).

51) D. Pavlov, C. N. Poulieff, E. Klaja, and N. Iordanov, J. Electrochem. Soc., 116, 316 (1969).

52) D. Pavlov and N. Iordanov, J. Electrochem. Soc., 117, 1103 (1970).

53) D. Pavlov and R. Popova, Electrochim. Acta, 15, 1483 (1970).

54) D. Pavlov, S. Zanova, and G. Papazov, J. Electrochem. Soc., 124, 1522 (1977).

55) P. Reutschi and B. D. Cahan, J. Electrochem. Soc., 104, 406 (1957).

56) P. Reutschi and R. T. Angstadt, J. Electrochem. Soc., 111, 1323 (1964).

57) P. Reutschi, J. Electrochem. Soc., 120, 331 (1973).

58) A. N. Fleming and J. A. Harrison, Electrochim. Acta, 21, 905 (1976).

59) E. M. L. Valeriote and L. D. Gallop, J. Electrochem. Soc., 124, 370 (1977).

60) E. M. L. Valeriote and L. D. Gallop, J. Electrochem. Soc., 124, 380 (1977).

61) J. Ambrose, R. G. Barradas, K. Belinko, and D. W. Shoesmith, J. Colloid Interface Sci., 47, 441 (1974).

62) R. G. Barradas, K. Belinko, and J. Ambrose, Can. J. Chem., 53, 389 (1975).

63) R. G. Barradas, K. Belinko, and E. Ghibaudi, Can. J. Chem., 53 407 (1975).

64) R. G. Barradas, K. Belinko, and D. W. Shoesmith, Electrochim. Acta, 21, 357 (1976).

65) J. W. Mellor, A Comprehansive Treatise on Inorganic and Theoretical Chemistry, Longmans, Green, and Co., London (1937), vol. VII.

66) K. Appelt, Electrochim. Acta, 13, 1521 (1968).

67) P. Delahay, M. Pourbaix, and P. Van Rysselberghe, J. Electrochem. Soc., 98, 57 (1951).

68) P. Hess, Electrochim. Acta, 12, 161 (1967).

69) J. Burbank, J. Electrochem. Soc., 106, 369 (1959).

70) W. Scheuermann and K. Nakamoto, Appl. Spectrosc., 32, 302 (1978).

71) A. Z. Goldfarb, M. S. Thesis, University of Rhode Island (1978).

72) N. D. Greene, Experimental Electrode Kinetics, Rensselaer Polytechnic Institute, Troy, N. Y. (1965).

73) H. B. Weiser and W. O. Milligan, Chem. Rev., 25, 1 (1939).

74) K. J. Gallagher and D. N. Phillips, Trans. Faraday Soc., 64, 785 (1968).

75) T. Ishikawa and K. Inouye, Bull. Chem. Soc. Japan, 45, 2350 (1972).

76) O. Baudisch and W. H. Albrecht, J. Amer. Chem. Soc., 54, 943 (1932).

77) G. A. Ozin, Can. J. Chem., 48, 2931 (1970).

78) L. A. Isupova and E. V. Sobolev, Zh. Struct. Khim., 9, 324 (1968).

79) P. A. Chen, J. Amer. Ceram. Soc., 57, 275 (1975).

80) E. W. Abel, Comprehensive Inorganic Chemistry, J. C. Bailar, H. J. Emeleus, R. Nyholm, and A. F. Trotman-Dickenson, eds., Pergamon Press, Oxford (1973), vol. 2, p.119.

81) W. Kwestroo and A. Huizing, J. Inorg. Nucl. Chem., 27, 1951 (1965).

82) W. Kwestroo, J. deJonge, and P. H. G. M. Vromans, J. Inorg. Nucl. Chem., 29, 39 (1967).

83) H. Szymanski, ed., Raman Spectroscopy, Plenum Press, New York (1967).

84) S. K. Freeman, Applications of Laser Raman Spectroscopy, Wiley - Interscience, New York (1974).

85) N. T. McDevitt and W. L. Baun, Spectrochim. Acta, 20, 799 (1964).

86) F. Lappe, J. Phys. Chem. Solids, 20, 173 (1961).

87) A. E. Ennos, J. Opt. Soc. Amer., 52, 261 (1962).

88) S. Nomura and N. Ito, Nippon Kinzoku Gakkaishi, 29, 985 (1965).

89) P. A. Wilks, Laboratory Methods in Infrared Spectroscopy, R. G. J. Miller and B. C. Stace, eds., Heyden and Son, London (1972), p.206.

90) D. D. Wagman, W. H. Evans, V. B. Parker, I. Halow, S. M. Bailey, and R. H. Schumm, NBS Technical Note 270-3, U. S. Government Printing Office, 1975.

91) R. L. Cusamano, M. S. Thesis, University of Florida (1971).

92) E. Gileadi, E. Kurowa-Eisner, and J. Penciner, Interfacial Electrochemistry, Addison - Wesley, Reading, Mass. (1975).

93) V. A. Izvozchikov and G. A. Bordovski, Dokl. Akad. Nauk. SSSR, 145, 1253 (1962).

94) H. Bode and E. Voss, Ber. Bunsenges. Phys. Chem., 60, 1053 (1953).

95) G. Charlot and B. Tremillon, Chemical Reactions in Solvents and Melts, Pergamon Press, Oxford (1969), p.389.

96) P. Tsai and R. P. Cooney, J. Chem. Soc. Dalton Trans., 1976, 1631.

97) P. Dawson, M. M. Hargreave, and G. R. Wilkinson, Spectrochim. Acta, 33A, 83 (1977).

98) K. Nakamoto, Infrared Spectra of Inorganic and Coordination Compounds, Wiley - Interscience, New York (1970), p.111.

99) H. W. Billhardt, J. Electrochem. Soc., 117, 690 (1970).

100) C. H. Warren and L. Ramaley, Appl. Opt., 12, 1976 (1973).

101) I. R. Beattie and T. R. Gilson, J. Chem. Soc. A, 1970, 980.

102) J. W. Mellor, op. cit., vol. XIII, p.706.

103) G. W. Poling, J. Electrochem. Soc., 116, 958 (1969).

104) D. E. Davies, U. R. Evans, and J. N. Agar, Proc. Roy. Soc. (A), 225, 443 (1954).

APPENDIX I.

Description of Vibrational Raman Spectroscopy

Vibrational Raman spectroscopy involves transitions between vibrational levels of a molecule or a unit of a crystal lattice. The simplest system to use for a model is a diatomic molecule; only one chemical bond exists between the two atoms, and the only vibration possible is stretching of that bond.

The two lowest vibrational energy levels, the ground state and the first excited state, are the levels of interest. A molecule must always vibrate. The ground state is the lowest energy level it may attain, and it is assigned a vibrational quantum number, V, of zero. The energy of a vibrational state is proportional to the frequency of vibration and related to the vibrational quantum number, i.e.,

$$E = (V + 1/2)\ h\ \nu\ c$$

where h is Planck's constant, c is the speed of light, and ν is the frequency characteristic of that particular vibration. It can be seen that even in the ground state, V=0, each molecule has some vibrational energy.

The two lowest vibrational energy levels, with V=0 and V=1, are shown in Figure 54. Molecules can absorb light by going from the lower to the higher level, or they can emit light by going from the higher to the lower. The energy corresponding to the absorption of a quantum of light is

given by

$$E = E^1 - E^0 = h \nu c$$

A typical transition for a diatomic molecule corresponds to approximately 2000 cm^{-1} and the absorption appears in the infrared region of the electromagnetic spectrum.

An infrared absorption spectrum is obtained by passing infrared radiation through a sample. If the sample molecules have dipole moments (a condition required by quantum mechanics for optical transitions from one vibrational level to another), some of the light will be absorbed at the resonance frequency of the molecule, i.e., the frequency corresponding to a transition between the V=0 and V=1 levels.

Although a diatomic molecule has only one possible vibrational mode, nonlinear polyatomic molecules have 3N-6 (where N is the number of atoms in the molecule) excited levels with V=1. A molecule in the ground vibrational level may be excited to any of the higher levels, each of which corresponds to a different vibrational mode. Each vibration has its own characteristic frequency, ν_i, giving each a different energy, so the infrared absorption spectrum of a polyatomic molecule represents transitions to the V=1 levels of a large number of vibrations. An infrared spectrum may not contain 3N-6 absorption bands, however, since all of the excited states may not be accessible through absorption of infrared radiation.

The transitions responsible for Raman scattering are

transitions between the same vibrational levels but the process is more complicated than simple absorption. A simple picture of some Raman transitions is presented in Figure 55. When the electric vector of an electromagnetic wave interacts with the electrons surrounding a molecule it distorts the electron cloud, causing temporary dipole moments. The sum of the dipole moments induced per unit volume is called the polarization, P, which is related to the electric field strength, E.

$$P = \alpha E$$

The polarizability, α, is related to the dielectric constant of the material. Incident radiation in the visible range, approximately 20,000 cm^{-1}, excites the molecule, inducing a temporary dipole. In a very short time (10^{-14} seconds) the molecule reemits a photon at the same frequency, ν_0, releasing the energy of excitation as Rayleigh scattering, to return to the ground vibrational level. Some photons are emitted at a lower frequency, returning the excited molecule not to the ground state but to the higher vibrational level, V=1. The energy of the photon emitted corresponds to the frequency $\nu_0 - \nu_1$. This type of scattering is called Stokes Raman scattering.

There is a Boltzmann distribution of molecules at all possible vibrational levels. Thus, even at room temperature, there are always some molecules in the V=1 level. These can also be excited by the incident radiation and either return to the V=1 level by emitting a photon at

ν_0 or they may return to the V=0 level by emitting a photon at $\nu_0 + \nu_i$. The latter transitions are referred to as anti-Stokes Raman scattering.

A typical Raman spectrum of a diatomic molecule is shown in the bottom of Figure 55. It is simply a plot of scattered light intensity versus frequency. The intensity of the anti-Stokes Raman bands depends on the magnitude of ν_i, i.e., the greater ν_i, the smaller the number of molecules in the V=1 level to begin with (Boltzmann distribution) and the smaller the intensity of the transition. Normally, because they are much stronger, only the Stokes transitions are used in Raman spectroscopy, i.e., only the left half of the spectrum is used. Furthermore, it is conventional to plot the frequency difference from the excitation frequency, $\nu_0 - (\nu_0 - \nu_i) = \nu_i$, the frequency corresponding to the energy differences between vibrational levels.

As in absorption spectroscopy, for polyatomic molecules transitions to some or all of the possible 3N-6 vibrational levels can take place. For a Raman transition to occur, the geometry of the molecule in the excited state must be such that a change in polarizability has taken place, i.e., the electron density about the molecule must be distorted by the transition. For an absorption of infrared radiation to occur, the geometry of the molecule in the excited state must be such that a change in the dipole moment has taken place. Thus, while both Raman and infrared absorption

spectra provide information about vibrational transitions, the two processes are entirely different, and transitions which show up strongly with one are usually weak with the other. Typically strong infrared bands are due to vibrations of polar bonds such as those involving hydrogen, while strong Raman bands are usually due to species with large numbers of electrons, such as lead compounds.

Since vibrational frequencies are characteristic of the specific type of vibration (bending, stretching, etc.), the type of atoms involved in the bonds, the type of bond, and any other environmental influences on the electrons involved in bonding, spectra are unique to each compound or structure. Every molecule has its own characteristic Raman spectrum which can be used to identify the molecule, specifying not only which compound is present, but also which polymorph of that compound, and possibly identifying any distortion from the normal structure.

In this discussion of Raman spectroscopy a small molecule has been used as an example to make the explanation as simple as possible. For the solid species examined in this research, the spectra are somewhat more complex. In addition to the vibrations of the molecules or very small parts of a crystal, termed the internal vibrations, vibrations of entire molecules or larger units of a crystal, the external, or lattice vibrations, are also observed. Thus, although spectra of solids are more complicated than those of free molecules, the example of a small molecule is

completely valid.

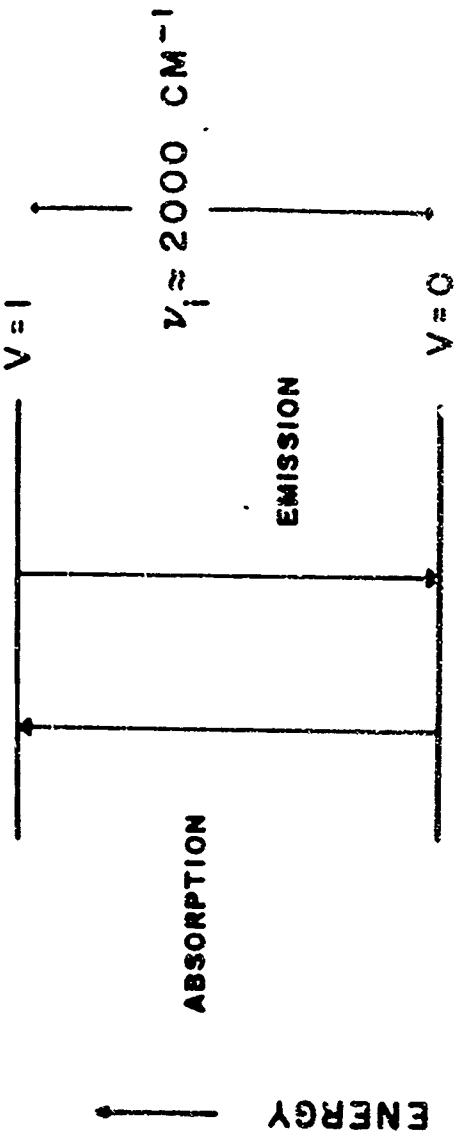

Figure 54. Vibrational energy levels of a diatomic molecule.

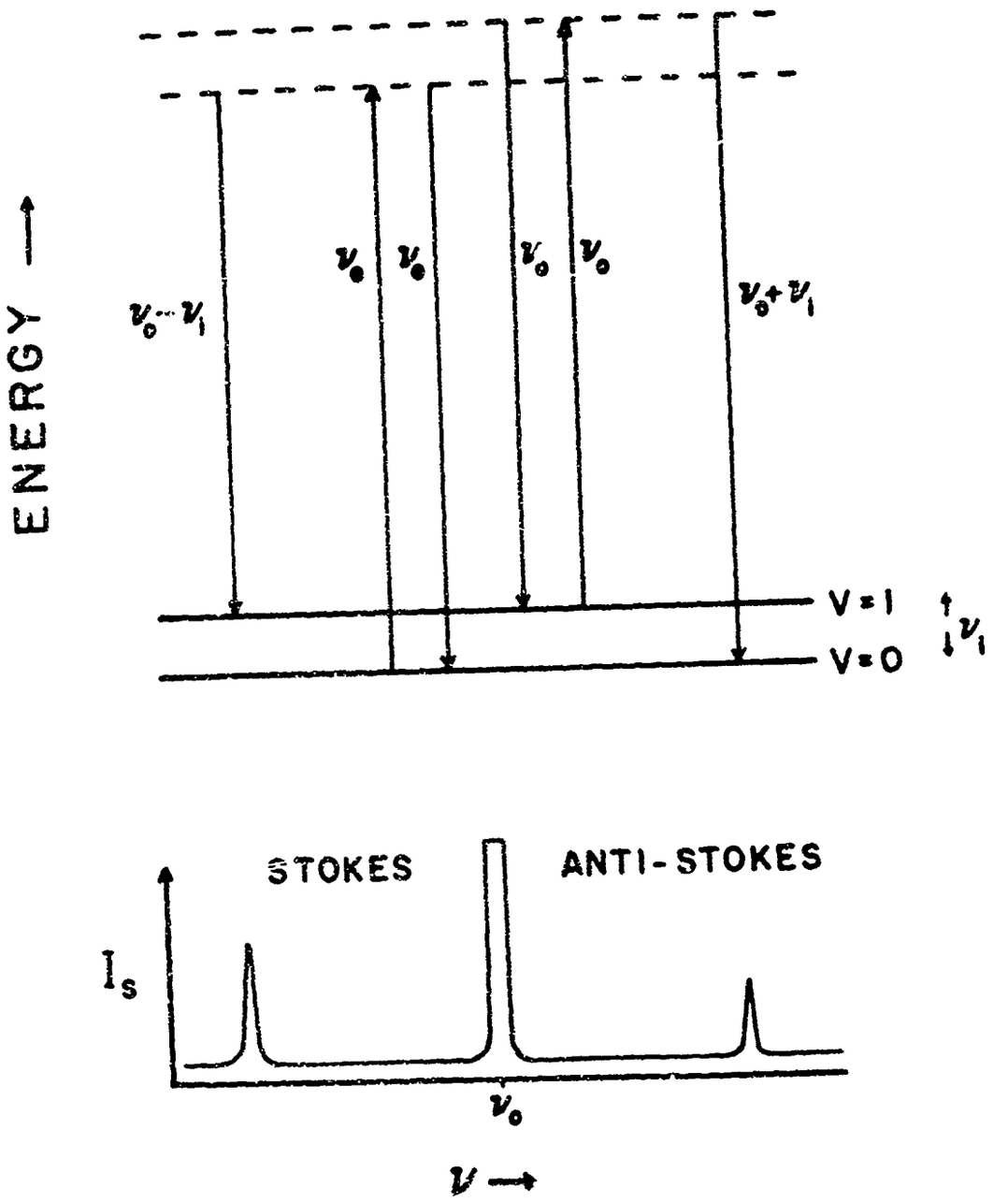

Figure 55. Energy level diagram for a typical vibrational Raman transition and the Raman spectrum resulting from such a transition.

BASIC DISTRIBUTION LIST

Technical and Summary Reports April 1978

Organization	Copies
Defense Documentation Center Cameron Station Alexandria, VA 22314	12
Office of Naval Research Department of the Navy 800 N. Quincy Street Arlington, VA 22217	
ATTN: Code 471	1
Code 102	1
Code 470	1
Commanding Officer Office of Naval Research Branch Office Building 114, Section D 666 Summer Street Boston, MA 02210	1
Commanding Officer Office of Naval Research Branch Office 536 South Clark Street Chicago, IL 60605	1
Office of Naval Research San Francisco Area Office 760 Market Street, Room 447 San Francisco, CA 94102	1
Naval Research Laboratory Washington, DC 20375	
ATTN: Codes 6000	1
6100	1
6300	1
6400	1
2627	1
Naval Air Development Center Code 302 Warminster, PA 18964 ATTN: Mr. F. S. Williams	1

Organization	Copies
Naval Air Propulsion Test Center Trenton, NJ 08628 ATTN: Library	1
Naval Construction Batallion Civil Engineering Laboratory Port Hueneme, CA 93043 ATTN: Materials Division	1
Naval Electronics Laboratory San Diego, CA 92152 ATTN: Electron Materials Sciences Division	1
Naval Missile Center Materials Consultant Code 3312-1 Point Mugu, CA 92041	1
Commanding Officer Naval Surface Weapons Center White Oak Laboratory Silver Spring, MD 20910 ATTN: Library	1
David W. Taylor Naval Ship Research and Development Center Materials Department Annapolis, MD 21402	1
Naval Undersea Center San Diego, CA 92132 ATTN: Library	1
Naval Underwater System Center Newport, RI 02840 ATTN: Library	1
Naval Weapons Center China Lake, CA 93555 ATTN: Library	1
Naval Postgraduate School Monterey, CA 93940 ATTN: Mechanical Engineering Department	1

Organization	Copies
Naval Air Systems Command Washington, DC 20360 ATTN: Codes 52031 52032	1
Naval Sea System Command Washington, DC 20362 ATTN: Code 035	1
Naval Facilities Engineering Command Alexandria, VA 22331 ATTN: Code 03	1
Scientific Advisor Commandant of the Marine Corps Washington, DC 20380 ATTN: Code AX	1
Naval Ship Engineering Center Department of the Navy Washington, DC 20360 ATTN: Code 6101	1
Army Research Office P.O. Box 12211 Triangle Park, NC 27709 ATTN: Metallurgy & Ceramics Program	1
Army Materials and Mechanics Research Center Watertown, MA 02172 ATTN: Research Programs Office	1
Air Force Office of Scientific Research Bldg. 410 Bolling Air Force Base Washington, DC 20332 ATTN: Chemical Science Directorate Electronics & Solid State Sciences Directorate	1 1
Air Force Materials Laboratory Wright-Patterson AFB Dayton, OH 45433	1
Library Building 50, Rm 134 Lawrence Radiation Laboratory Berkeley, CA	1
NASA Headquarters Washington, DC 20546 ATTN: Code RPM	1
NASA Lewis Research Center 21000 Brookpark Road Cleveland, OH 44135 ATTN: Library	1
National Bureau of Standards Washington, DC 20234 ATTN: Metallurgy Division Inorganic Materials Div.	1 1
Director Applied Physics Laboratory University of Washington 1013 Northeast Forthieth Street Seattle, WA 98105	1
Defense Metals and Ceramics Information Center Battelle Memorial Institute 505 King Avenue Columbus, OH 43201	1
Metals and Ceramics Division Oak Ridge National Laboratory P.O. Box X Oak Ridge, TN 37380	1
Los Alamos Scientific Laboratory P.O. Box 1663 Los Alamos, NM 87544 ATTN: Report Librarian	1
Argonne National Laboratory Metallurgy Division P.O. Box 229 Lemont, IL 60439	1
Brookhaven National Laboratory Technical Information Division Upton, Long Island New York 11973 ATTN: Research Library	1
Office of Naval Research Branch Office 1030 East Green Street Pasadena, CA 91106	1

C
April 1978

SUPPLEMENTARY DISTRIBUTION LIST

Technical and Summary Reports

Dr. T. R. Beck
Electrochemical Technology Corporation
10035 31st Avenue, NE
Seattle, Washington 98125

Professor I. M. Bernstein
Carnegie-Mellon University
Schenley Park
Pittsburgh, Pennsylvania 15213

Professor H. K. Birnbaum
University of Illinois
Department of Metallurgy
Urbana, Illinois 61801

Dr. Otto Buck
Rockwell International
1049 Camino Dos Rios
P.O. Box 1085
Thousand Oaks, California 91360

Dr. David L. Davidson
Southwest Research Institute
8500 Culebra Road
P.O. Drawer 28510
San Antonio, Texas 78284

Dr. D. J. Duquette
Department of Metallurgical Engineering
Rensselaer Polytechnic Institute
Troy, New York 12181

Professor R. T. Foley
The American University
Department of Chemistry
Washington, D.C. 20016

Mr. G. A. Gehring
Ocean City Research Corporation
Tennessee Avenue & Beach Thorofare
Ocean City, New Jersey 08226

Dr. J. A. S. Green
Martin Marietta Corporation
1450 South Rolling Road
Baltimore, Maryland 21227

Professor R. H. Heidersbach
University of Rhode Island
Department of Ocean Engineering
Kingston, Rhode Island 02881

Professor H. Herman
State University of New York
Material Sciences Division
Stony Brook, New York 11794

Professor J. P. Hirth
Ohio State University
Metallurgical Engineering
Columbus, Ohio 43210

Dr. D. W. Hoeppner
University of Missouri
College of Engineering
Columbia, Missouri 65201

Dr. E. W. Johnson
Westinghouse Electric Corporation
Research and Development Center
1310 Beulah Road
Pittsburgh, Pennsylvania 15235

Professor R. M. Latanision
Massachusetts Institute of Technology
77 Massachusetts Avenue
Room E19-702
Cambridge, Massachusetts 02139

Dr. F. Mansfeld
Rockwell International Science Center
1049 Camino Dos Rios
P.O. Box 1085
Thousand Oaks, California 91360

Professor A. E. Miller
University of Notre Dame
College of Engineering
Notre Dame, Indiana 46556

C
April 1978

SUPPLEMENTARY DISTRIBUTION LIST
(Continued)

Professor H. W. Pickering
Pennsylvania State University
Department of Material Sciences
University Park, Pennsylvania 16802

Professor R. W. Staehle
Ohio State University
Department of Metallurgical Engineering
Columbus, Ohio 43210

Dr. E. A. Starke, Jr.
Georgia Institute of Technology
School of Chemical Engineering
Atlanta, Georgia 30332

Dr. Barry C. Syrett
Stanford Research Institute
333 Ravenswood Avenue
Menlo Park, California 94025

Dr. R. P. Wei
Lehigh University
Institute for Fracture and
Solid Mechanics
Bethlehem, Pennsylvania 18015

Professor H. G. F. Wilsdorf
University of Virginia
Department of Materials Science
Charlottesville, Virginia 22903

August 1978

SUPPLEMENTARY DISTRIBUTION LIST

Technical and Summary Reports

People and organizations who have requested copies of reports on this research.

Dr. F.P. Mertlas
Department of Energy and Environment
Building 815
Upton, NY 11973

Dr. B. Vyas
Brookhaven National Laboratory
Building 703
Upton, NY 11973

Dr. Henry White
Physics Department
University of Missouri - Columbia
Columbia, MO 65211

Dr. M.J. Graham
National Research Council of Canada
Division of Chemistry
Ottawa, Ontario
Canada K1A OR9

Dr. B.J. Berkowitz
Corporate Research Laboratories
Exxon Research and Engineering Company
P.O. Box 45
Linden, NJ 07036

Dr. S. Gottesfeld
Bell Laboratories
600 Mountain Avenue
Murray Hill, NJ 07974

Dr. Jeff Perkins
Liason Scientist, Metallurgy
Office of Naval Research
Branch Office, London
Box 39
FPO New York 09510

T.E. Evans
Inco Europe, Ltd.
European R & D Centre
Wiggin Street, Birmingham
B160AJ
England

Dr. N. Sato
Faculty of Engineering
Hokkaido University
Kita-Ku, Sapporo, 060
Japan

Dr. K. Sugimoto
Department of Metallurgy
Tohoku University
Aoba, Aramaki, Sendai
Miyagi, 980, Japan

Distribution List - ONR

Martin W. Kendig
Corrosion Science Group
Department of Nuclear Energy
Brookhaven National Laboratory
Upton, NY 11973

A.S. (Bert) Krisher
Engineering Fellow
Materials Technology
Monsanto
Corporate Engineering Department
Monsanto Company
800 N. Lindbergh Boulevard
St. Louis, Missouri 63166

Tom E. Furtak
Leader, Electrochemistry Group
Solid State Physics Division
Ames Laboratory
U.S. Department of Energy
Iowa State University
Ames, Iowa 50011

Alan G. Miller, Ph.D.
Analytical Specialist Engineer
Boeing Materials Technology
Boeing Commercial Airplane Co.
P.O. Box 3707
MS 73-43
Seattle, WA 98124